Regulation of Dlg-containing adhesion complexes during epithelial and synaptic plasticity in *Drosophila*

by

Simon Ji Hau Wang

B.Sc., Simon Fraser University, 2004

THESIS SUBMITTED IN PARTIAL FULFILLMENT

OF THE REQUIREMENTS FOR THE DEGREE OF

DOCTOR OF PHILOSOPHY

in the

Department of Molecular Biology and Biochemistry

Faculty of Science

SIMON FRASER UNIVERSITY

Spring 2013

Approval

Name:	**Simon Ji Hau Wang**
Degree:	**Doctor of Philosophy**
Title of Thesis:	***Regulation of Dlg-containing adhesion complexes during epithelial and synaptic plasticity in Drosophila***
Examining Committee:	**Chair:** Dr. Michel Leroux Professor

Dr. Nicholas Harden
Senior Supervisor
Professor

Dr. Nancy Hawkins
Supervisor
Associate Professor

Dr. Charles Krieger
Supervisor
Associate Professor

Dr. Esther Verheyen
Supervisor
Professor

Dr. Bruce Brandhorst
Internal Examiner
Professor
Dept. of Molecular Biology and Biochemistry
Simon Fraser University

Dr. J. Roger Jacobs
External Examiner
Professor
Dept. of Biology
McMaster University

by video conference (Hamilton, ON)

Date Defended/Approved: February 28th, 2013

Partial Copyright Licence

Abstract

Discs large (Dlg) is a multi-PDZ domain-containing protein belonging to the MAGUK superfamily of scaffolding proteins. In epithelia, Dlg serves as an apicobasal polarity determinant, where its disruption leads to tumor formation. Dlg also plays roles in maintaining synaptic structure and function, and has been implicated in neurodegeneration. Thus, understanding Dlg regulation can provide insights into human diseases including cancers and neurological disorders. In this thesis, we characterize novel Dlg regulators during epithelial and synaptic plasticity events in *Drosophila* development through two separate but overlapping projects.

Project 1: Dorsal closure, which is a wound healing model, occurs when a hole in the embryonic epidermis is closed due to surrounding epidermal flanks that migrate towards each other over the amnioserosa occupying the hole. During migration, the leading edges of the epidermal cells abutting the hole exhibit a breakdown in apicobasal polarity as adhesions are severed with the amnioserosa. At the end of migration, however, apicobasal polarity is re-established as adhesions must form between the opposing epidermal flanks in order to seal the hole shut. Mammalian studies indicate that the Dlg-containing Scribble complex recruits p21-activated kinases (Paks), effectors for Rho GTPase signalling, to the leading edge during cell migration. We show that this interaction can act in the opposite direction as Paks can recruit the Scribble complex back to the leading edge upon dorsal closure completion. We propose that the bidirectional relationship between Paks and Dlg may allow epithelia to toggle between migratory and adhered states.

Project 2: Previous studies have shown that adducin, a membrane cytoskeletal protein that regulates actin, is hyperphosphorylated in spinal cord tissue taken from patients who died with the motor neuron disease, Amyotrophic Lateral Sclerosis. To further explore the roles of adducin in the nervous system, we decided to study the *Drosophila*

orthologue encoded by *hu-li tai shao* (*hts*). We show that Hts regulates larval neuromuscular junction morphogenesis by controlling Dlg postsynaptic targeting via indirect phosphorylation. This process is partially supressed when Hts phosphorylation in the MARCKS domain is blocked. We propose that Hts is a signalling-responsive cytoskeletal protein that contributes to synaptic growth through Dlg-mediated adhesion.

Keywords: p21-activated kinases (Paks); Hu-li tai shao (Hts); Discs large (Dlg); dorsal closure; larval neuromuscular junction; epithelial and synaptic plasticity

For my dad, mom and sister.

You were all right.

But dogs can look up!

Acknowledgements

I could not have completed my thesis without the help and support of the many people I have had the privilege of getting to know during my graduate studies, to only some of whom it is possible to give particular mention here – sorry in advance if I have inadvertently omitted anyone.

First and foremost, I would like to express my sheer gratitude to my supervisor, Dr. Nicholas Harden, for his guidance, encouragement and patience. I am fortunate to have trained under someone whose door was always open. Nick has also taught me invaluable lessons about the ins and outs of academic research during our many bus rides together on the not so reliable '143'. I doubt that I will ever be able to convey my appreciation to him fully.

Many thanks to my supervisory committee members – Dr. Charles Krieger, Dr. Esther Verheyen and Dr. Nancy Hawkins – for their encouraging words and thoughtful criticisms. I am grateful to Charles for being a wonderful ''co-supervisor'' who introduced our lab to a great project. I am indebted to Esther for giving me my start in academic research. I am appreciative of Nancy's passion for science which I found extremely motivating, especially in a field that can be trying at times. Thanks also goes to my examining committee members – Dr. J. Roger Jacobs (the external examiner), Dr. Bruce Brandhorst (the internal examiner), and Dr. Michel Leroux (the chair) – for taking time out of their busy schedules to evaluate my thesis. A special nod goes to Roger for agreeing to be on my examining committee during his sabbatical.

I would like to thank my wonderful labmates, past and present, for their constant support and friendship. They include: my Hardenite comrades – Xi Chen, David Cheng, Michael Chou, Kevin Dong, Sharayu Jangam and my lab sister, Dr. Stephanie Vlachos; the Kriegerites – Vincent Chui, Hae-yoon Kim, Mandeep Rao, Jing Yang, Nicole Yoo and Clare Zheng; and the lone Parkhousian and my partner in crime – Mannan

Wang. I am especially grateful to Dr. Ryan Conder and Dr. Weiping Shen for their guidance, and Byoungjoo Yoo for all of her help. I would also like to thank our fellow Drosophilists, the Verheyen and Honda labs, specifically Jessica Blaquiere, Dr. Lorena Braid, Dr. Kristi Charish, Joanna Chen, Desiree Essen, Graham Hallson, Dr. Barry Honda, Dr. Wendy Lee, Dr. Maryam Rahnama, Dr. Don Sinclair, Sharan Swarup and Dr. Monika Syrzycka. I am particularly thankful to Dr. Ariel Zeng for her kindness and generosity.

A special and sincere thanks goes to Amy Tsai, a former research assistant under Charles Krieger. Words cannot express how much I appreciate everything you have done during the four years we have worked together. In particular, thank you so much for your countless hours of dissecting larval body walls – I hope your neck is better. I am very lucky to have met you and miss seeing you in the lab.

Throughout my graduate studies, I have had the pleasure of working with some great undergraduate students. They include Alex Butskiy, Monica Chung, Ehsan Fadaei, Bayan Farshi, Merry Gong, Nikola Lazic, Deborah Lee, Jeehwa Lee, Sandy Lou, Mila Lukic, Richard Ly, Shoko Nakano, Sonia Paul, Eunju Rhee, Amanda Ribeiro, Hila Roshanravan, Terence Tang and Jamie Wright. Thank you all for your patience and hard work.

Penultimately, I thank our many collaborators, in particular Dr. Sami Bahri, Dr. Wade Parkhouse and Dr. Bryan Stewart. I thank the fly community for their feedback on our work and the sharing of reagents. I also thank the following people: Dr. Tim Heslip and Dr. Christine Carson for guidance in confocal microscopy; Apollos Kim, Dr. Neil Dobson and Duncan Napier for technical support; Dr. Dee Brink for training in larval body wall dissections; and Mimi Fourie, Nancy Suda and Joanie Wolfe for help in preparing this thesis. This work was funded by the Canadian Institutes of Health Research (CIHR) and the Natural Sciences and Engineering Research Council (NSERC). I am extremely appreciative to have received internal support from the Weyerhaeuser Molecular Biology Graduate Scholarship, the David L. Baillie Graduate Fellowship in Molecular and Cellular Biology, the Hemingway Nelson Architects Graduate Scholarship,

the President's Ph.D. Research Stipend and the Department of Molecular Biology and Biochemistry Graduate Fellowship.

Finally, I would like to thank my parents, Christopher and Eliza, and my sister, Audrey, for allowing me to realize my own potential. All the support they have provided me over the years was the greatest gift anyone has ever given me. Thank you so much.

Table of Contents

List of Figures

List of Acronyms

Add	adducin
AID	autoinhibitory domain
AJ	adherens junction
ALS	amyotrophic lateral sclerosis
Arm	Armadillo
AS	amnioserosa
Baz	Bazooka
CaMKII	Calcium/calmodulin-dependent protein kinase
CeAj	*C. elegans* apical junction
Cora	Coracle
Crb	Crumbs
CRIB	Cdc42/Rac interacting binding
CSP	Cysteine string protein
DE-Cad	DE-Cadherin
Dlg	Discs large
DME	dorsal-most epidermal
Drpr	Draper
DV	dorsal vessel
E	epidermis
EMT	epithelial-mesenchymal transition
F-actin	filamentous actin
Fas2	Fasciclin 2
Fas3	Fasciclin 3
GAP	GTPase activating protein
GEF	guanine nucleotide exchange factor
GMR	Glass multimer reporter
Grh	Grainy head
GS	gene search

GUK	guanylate kinase
H	head
Hts	Hu-li tai shao
ITG	integrin
LE	leading edge
Lgl	Lethal giant larvae
LRR	leucine-rich repeat
MAGUK	membrane-associated guanylate kinase
MARCKS	myristoylated alanine-rich C kinase substrate
MARK	microtubule affinity regulating kinase
MET	mesenchymal-epithelial transition
Mys	Myospheroid
N	neck
NCAM	neural cell adhesion molecule
NES	nuclear export signal
NLS	nuclear localization signal
NMJ	neuromuscular junction
p-Dlg	phosphorylated Dlg
Pak	p21-activated kinase
Pak3	p21-activated kinase 3
PAR-1	Partitioning defective 1
PDZ	PSD95/DLG/ZO-1
PIP_2	phosphatidylinositol 4,5-bisphosphate
Pix	Pak-interacting exchange factor
PKA	Protein kinase A
PKC	Protein kinase C
pY	phospho-tyrosine
RC	ring canal
Rok	Rho-kinase
Scrib	Scribble

SH3	Src homology 3
SJ	septate junction
SOD1	superoxide dismustase 1
T	tail
TJ	tight junction
VM	ventral midline

Preface

During my doctorate studies under Dr. Nicholas Harden in the Department of Molecular Biology and Biochemistry up at Simon Fraser University, I worked on two projects that involved studying cell plasticity – i.e. the ability of cells to alter both their shape and their interactions with other cells. One of my projects investigated the roles of p21-activated kinases (Paks) in epithelial plasticity using the leading edge membrane of dorsal-most epidermal (DME) cells during dorsal closure as a model. My other project, which was done in collaboration with Dr. Charles Krieger from the Department of Biomedical Physiology and Kinesiology, characterized the roles of Hu-li tai shao (Hts) in synaptic plasticity using the developing neuromuscular junction (NMJ) of third instar larvae. Although the projects seemed unrelated at first, I determined that both center around mediating the membrane localization of protein complexes containing Discs large (Dlg) (see diagram below). In this thesis, I will present my work on the Paks in the first chapter, then Hts in the second chapter. In the third and final chapter, I will conclude the thesis by discussing how the findings in one project may provide important and relevant insights to the other.

1. Characterizing the roles of p21-activated kinases in epithelial apicobasal polarity during dorsal closure

1.1. Introduction

1.1.1. Dorsal closure

Several metazoan developmental processes involve the coming together of epithelial sheets such as epiboly and neural tube closure in vertebrates, ventral enclosure in *Caenorhabditis elegans* and dorsal closure in *Drosophila melanogaster*. However, dorsal closure is by far the most characterized due to the advanced genetic and developmental biological techniques available to Drosophilists (reviewed in Harden, 2002; reviewed in Jacinto et al., 2002a; reviewed in Gorfinkiel et al., 2011). Since many of the proteins that regulate other epithelial spreading and fusion events have also been implicated in dorsal closure, studying dorsal closure can help researchers better understand how embryos develop in general (reviewed in Harden, 2002; reviewed in Martin and Wood, 2002; reviewed in Lawrence and Morel, 2003). More importantly, dorsal closure is of great medical interest as it is a model for wound healing and may lead to new treatments to help those with compromised healing such as burn victims and sufferers of persistent skin lesions due to diabetes (reviewed in Martin and Parkhurst, 2004; reviewed in Redd et al., 2004; reviewed in Belacortu and Paricio, 2011). In addition, dorsal closure may provide critical insights concerning birth defects that result from failed epithelial fusions such as cleft palate, spina bifida and anencephaly.

Dorsal closure is the last major morphogenetic event of *Drosophila* embryogenesis that occurs between stages 12 to 15, i.e. approximately eight to 13 hours after egg laying (see Movie 1 in the attached CD-ROM) (reviewed in Harden, 2002;

reviewed in Jacinto et al., 2002a). Following germband retraction, a hole is left in the dorsal epidermis of the embryo (Figure 1A). The hole is occupied by an extraembryonic tissue called the amnioserosa which consists of large, squamous epithelial cells that cover and contain the underlying yolk sac. Dorsal closure occurs when the epidermal flanks that surround both sides of the hole stretch dorsally up and over the amnioserosa towards each other (Figure 1B,C). The advancing flanks eventually meet at the dorsal midline and fuse together, closing the hole to form a continuous epidermis (Figure 1D). As a consequence, the amnioserosa is internalized and degraded. If dorsal closure fails to complete, the embryo will die since there is no epidermis where the hole is to secrete a cuticle which is necessary for insect life. This makes identifying genes required for the process simple as mutations in these genes can result in a visible dorsal hole in the embryonic cuticle (reviewed in Harden, 2002).

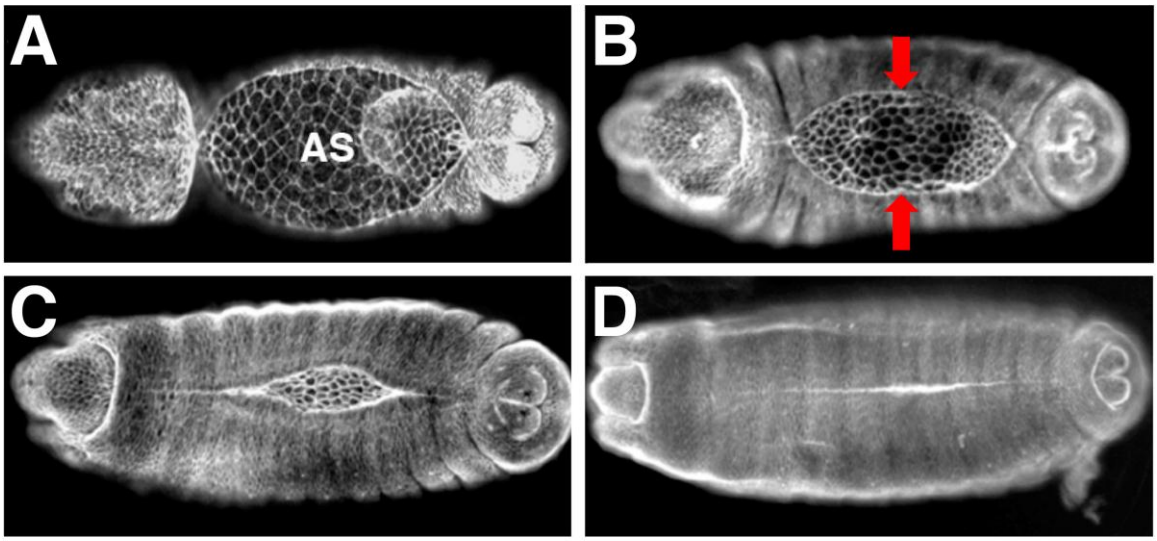
A
AS
B
C
D

FIGURE 1 Dorsal closure of the *Drosophila* embryo.

(A-D) Dorsal views of progressively older embryos throughout dorsal closure. The embryos are stained with an anti-phospho-tyrosine antibody which marks cell membranes. (A) Following germband retraction, a hole is left in the dorsal epidermis of the embryo which is occupied by the amnioserosa. (B-C) Dorsal closure occurs when the epidermal flanks that surround both sides of the hole stretch dorsally up and over the amnioserosa towards each other (see red arrows). (D) The advancing flanks eventually meet at the dorsal midline and fuse together, closing the hole shut to form a continuous epidermis. As a result, the amnioserosa is internalized and degraded. Note that the figure was modified from Harden et al., 2002. AS = amnioserosa.

During dorsal closure, the first row of epidermal cells that directly abut the hole, known as the **dorsal-most epidermal** (**DME**) cells, become planar polarized with regards to the actin cytoskeleton at the leading edge, i.e. the side that faces the amnioserosa (see Figure 4A,C) (reviewed in Harden, 2002; reviewed in Jacinto et al., 2002a; Kaltschmidt et al., 2002; reviewed in Harris et al., 2009). Accumulation of **filamentous actin** (**F-actin**) and non-muscle myosin II along the leading edge of each DME cell forms a contractile ring around the dorsal hole. The contractile ring constricts the DME cells along the anterior-posterior axis, consequently causing elongation in the dorsal-ventral direction. Elongation of the more ventral rows of epidermal cells is believed to be a passive response to the pulling action provided by the DME cells. Thus, the net result is dorsal-ward migration of the epidermis over the amnioserosa in a process that has been likened to a ''purse string''. In addition to the contractile ring apparatus, the leading edge of each DME cell also contains filopodial and lamellipodial protrusions (Jacinto et al., 2000; Jacinto et al., 2002b; Millard and Martin, 2008). These actin-based structures help zip the opposing epidermal flanks together, and are also involved in ensuring the correct alignment of the embryonic segments as the hole closes. Several studies indicate that the amnioserosa also plays an active role in dorsal closure, i.e. the tissue is not simply compressed by the migrating epidermal flanks (reviewed in Harden, 2002; Zahedi et al., 2008; reviewed in Heisenberg, 2009; Shen et al., 2013). However, the role of the amnioserosa during dorsal closure will not be discussed in this thesis.

1.1.2. Epithelial apicobasal polarity and intercellular junctions

Epithelia, such as the *Drosophila* embryonic epidermis, act as barriers that line and partition the body into morphologically and physiologically distinct compartments. Several different types of epithelia exist to fulfill specific cellular needs and functions which can include protection and sensory reception, in addition to absorption, diffusion, filtration, secretion and excretion of various substances. The structural and functional

properties of epithelia depend on apicobasal polarity, where epithelial cell membranes along the apical-basal axis are divided into three general domains that differ in protein and lipid composition (Figure 2) (reviewed in Tepass et al., 2001). The apical domain faces either the external environment or a lumen, the basal domain faces the interstitial space of the body and is anchored to an extracellular matrix, and the lateral domains face and are adhered to neighboring epithelial cells within the sheet. Epithelial apicobasal polarity is essential for maintaining tissue integrity and, consequently, defects in apicobasal polarity are associated with numerous human pathologies such as cancer (reviewed in Wodarz and Nathke, 2007; reviewed in Bergstralh and St Johnston, 2012; reviewed in Ellenbroek et al., 2012). Since work in *Drosophila* has identified several important regulators of apicobasal polarity which are evolutionarily conserved, studying how apicobasal polarity is established and maintained in *Drosophila* epithelial cells can provide critical insights into the process of malignant transformation.

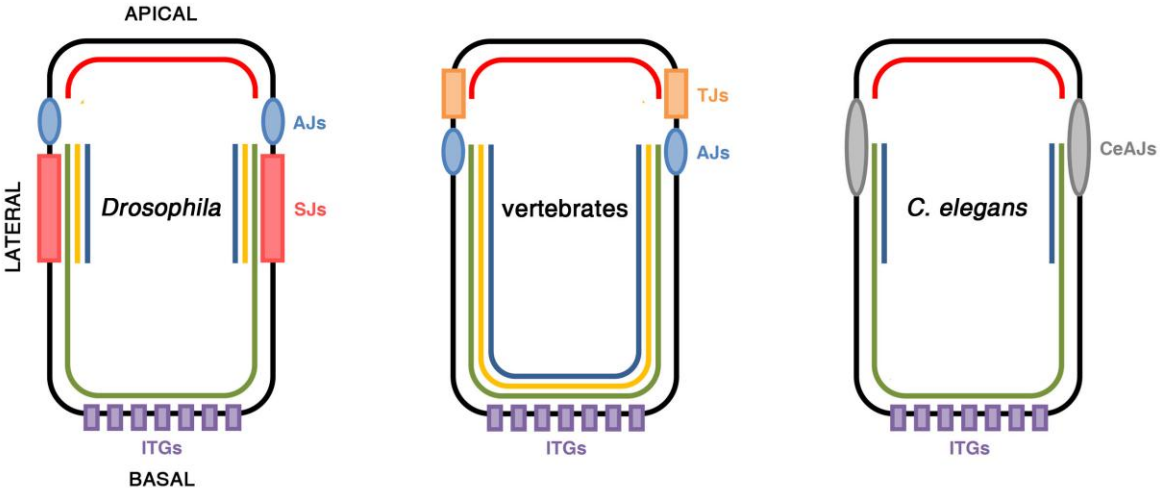

Discs large (Dlg)	Dlg1 / hDlg / SAP97	DLG-1
Scribble (Scrib)	Scrb1	LET-413
Lethal giant larvae (Lgl)	Lgl1 Lgl2	
Crumbs (Crb) Bazooka (Baz)	Crb1 Crb2 Crb3 Par3	CRB-1 PAR-3

FIGURE 2 Epithelial apicobasal polarity in *Drosophila*, vertebrates and *C. elegans*.

Schematic diagram comparing apicobasal polarity in *Drosophila*, vertebrate and *C. elegans* epithelial cells. *Drosophila* epithelial cells contain an apicolateral belt of adherens junctions (shown in blue) and basolateral septate junctions (shown in pink). In contrast, vertebrate epithelial cells contain tight junctions (shown in orange) that lie apical to the adherens junctions. *C. elegans* epithelial cells contain a single type of junction at the apicolateral membrane known as apical junctions (shown in grey) that share similar properties to both the adherens and tight junctions. In *Drosophila*, the distribution of Dlg, Scrib and Lgl overlaps with septate junctions. However, Lgl is more broadly distributed throughout the basolateral region in comparison to Dlg and Scrib. Vertebrate homologues of Dlg (i.e. Dlg1), Scrib (i.e. Scrb1) and Lgl (i.e. Lgl1 and Lgl2) localize throughout the basolateral region and to adherens junctions, but not to tight junctions. In *C. elegans*, the homologues of Dlg (i.e. DLG-1) and Scrib (i.e. LET-413) both overlap with apical junctions. However, LET-413 is also present throughout the basolateral region. The distribution of apical polarity determinants, e.g. the Crb and Baz/PAR-3 complexes, in addition to basally localized integrin junctions (shown in purple), are also presented. Note that the figure was modeled after Yamanaka and Ohno, 2008. AJs = adherens junctions, SJs = septate junctions, TJs = tight junctions, CeAjs = C. elegans apical junctions, ITGs = integrins.

Epithelial apicobasal polarity is characterized in part by asymmetrically distributed intercellular junctions along the apicobasal axis (reviewed in Tepass et al., 2001; reviewed in Gibson and Perrimon, 2003; reviewed in Yamanaka and Ohno, 2008). Intercellular junctions have many functions in epithelia such as adhesion between neighbouring cells within the sheet, and formation of permeability barriers that prevent both paracellular diffusion of solutes in between cells and intramembrane diffusion of macromolecules along the apicobasal axis. In *Drosophila*, epithelial cells contain an apicolateral belt of adherens junctions, known as the zonula adherens, and basolateral septate junctions (Figure 2) (reviewed in Tepass et al., 2001). Vertebrate epithelial cells, on the other hand, lack septate junctions and instead contain functionally analogous but molecularly distinct tight junctions that lie apical, not basal, to the adherens junctions (Figure 2) (reviewed in Shin et al., 2006). In *C. elegans*, epithelial cells contain only a single type of junction at the apicolateral membrane, known as the apical junction, which has similar properties to both the adherens and tight junctions (Figure 2) (reviewed in Labouesse, 2006). Other types of intercellular junctions that can be found in animal epithelia are the desmosomes and gap junctions. However, as *Drosophila* epithelial cells do not contain desmosomes and the role of gap junctions in epithelial differentiation is poorly understood, they will not be further commented upon in this thesis (reviewed in Tepass et al., 2001).

Adherens junctions are important apicolateral adhesion and signalling centers that play multiple roles in development and tissue homeostasis such as initialization and stabilization of cell-cell adhesion, regulation of the actin cytoskeleton, intracellular signalling and transcriptional control (reviewed in Harris and Tepass, 2010; reviewed in Harris, 2012). Adherens junctions connect the actin cytoskeletons of neighbouring epithelial cells together by means of the cadherin-catenin complex which is composed of the following core proteins: E-Cadherin or Shotgun/**DE-Cadherin** (**DE-Cad**) in *Drosophila*, α-catenin, β-catenin or **Armadillo** (**Arm**) in *Drosophila*, and p120-catenin (reviewed in Harris, 2012). A generally accepted model is that E-cadherin, a

transmembrane protein that engages in homotypic interactions between adjacent cells through its extracellular domains, binds to both β-catenin and p120-catenin via its intracellular domains. β-catenin can bind to α-catenin which in turn binds to actin filaments, thereby forming a link between the adherens junctions and the actin cytoskeleton. Interestingly, monomeric α-catenin, which can bind to β-catenin, preferentially associates with adherens junctions whereas dimeric α-catenin, which cannot bind to β-catenin, preferentially associates with actin and suppresses Arp2/3 complex-mediated actin branching (Pokutta and Weis, 2000; Drees et al., 2005; Yamada et al., 2005). Thus, it has been proposed that α-catenin can act as a molecular switch to regulate actin polymerization though the exact mechanism remains unclear (reviewed in Hartsock and Nelson, 2008; reviewed in Harris and Tepass, 2010). In addition to its roles in cell-cell adhesion, adherens junctions also regulate signal transduction as β-catenin is a key effector for the canonical Wnt pathway where it mediates the transcription of target genes that control cell fate decisions in many tissues (Zeng at al., 2008; reviewed in Valenta et al., 2012).

Septate junctions are basolateral intercellular junctions in invertebrate epithelia including cell-cell adhesion and the formaion of permeability barriers that prevent both paracellular diffusion of solutes in between cells and intramembrane diffusion of macromolecules along the apicobasal axis (reviewed in Tepass et al., 2001). Although no systematic attempt has been made as of yet to characterize the molecular make-up of the septate junction, individual studies have led to the identification of numerous transmembrane and scaffolding proteins that are required for septate junction formation (reviewed in Banerjee et al., 2006). These include Neurexin IV, **Coracle** (**Cora**), Contactin, Neuroglian, Na^+K^+ ATPase, Gliotactin, Sinuous, Megatrachea, Lachesin and **Fasciclin 3** (**Fas3**). Mutational analysis of most of these proteins revealed disruptions of the transepithelial seal via dye or ion permeation assays, thus highlighting their role in barrier formation. As mentioned previously, vertebrate epithelial cells do not have septate junctions, instead containing functionally analogous but molecularly

distinct tight junctions which lie apical, not basal, to the adherens junctions (reviewed in Shin et al., 2006). Initially, septate junctions were believed to be unique to invertebrates. However, it is now apparent that within the vertebrate nervous system a molecularly and functionally analogous septate junction exists in myelinated neurons at either end of each node of Ranvier (reviewed in Tepass et al., 2001).

Another adhesion complex found predominately at the basal membrane of animal epithelial cells are the integrins (Figure 2) (reviewed in Takada et al., 2007). Integrins are transmembrane receptors that link the extracellular matrix of the basement membrane to the actin cytoskeleton, thus attaching the cells to their surrounding environment. They also play important roles in cell migration and signal transduction that affects many different cellular processes including growth, division, survival, differentiation and apoptosis. Integrins function as obligate heterodimers consisting of two distinct chains, called the α and β subunits. In humans, eighteen α and eight β subunits have been characterized, generating 24 heterodimers. The *Drosophila* genome encodes only five α and two β subunits. The five α subunits are αPS1/Multiple edematous wings, αPS2/Inflated, αPS3/Scab, αPS4/CG16827 and αPS5/CG5372. The two β subunits are βPS/**Myospheroid** (**Mys**), which is ubiquitously expressed, and βv, which is restricted to the midgut endoderm.

1.1.3. The Scribble complex, an apicobasal polarity determinant

Despite the differences in the types and distribution of intercellular junctions found in *Drosophila* and vertebrate epithelial cells, three conserved protein complexes act in cooperation to establish apicobasal polarity: the **Crumbs** (**Crb**) complex (composed of Crb, Sdt and Dlt), the **Bazooka** (**Baz**)/PAR-3 complex (composed of Baz, PAR-6 and aPKC) and the **Scribble** (**Scrib**) complex (composed of Scrib, Lgl and Dlg) (reviewed in Tepass et al. 2001). In *Drosophila*, the Crb and Baz/PAR-3 complexes associate with the apical-apicolateral membrane whereas the Scrib complex is restricted to the basolateral membrane where it overlaps with the septate junctions (see Figure 2).

Due to our interests with the Scrib complex member, Dlg, during larval neuromuscular junction development (see the next chapter), we focus solely on the Scrib complex, in particular Dlg, in this thesis.

Discs large (**Dlg**) is the founding member of a family of scaffolding proteins known as the **membrane-associated guanylate kinases** (**MAGUKs**) (reviewed in Tepass et al., 2001; reviewed in Humbert et al., 2003; reviewed in Yamanaka and Ohno, 2008; reviewed in Roberts et al., 2012; reviewed in Elsum et al., 2012). Members of this family are defined by a basic core of three different protein interaction modules: the **PSD95/DLG/ZO-1** (**PDZ**) domain, the **Src homology 3** (**SH3**) domain and the enzymatically inert **guanylate kinase** (**GUK**) domain (Figure 3). The domain organization of the MAGUKs enables them to function as scaffolds that orchestrate the assembly of large protein compleses at specific sites within the cell, including at the plasma membrane. Unlike the single Dlg gene found in *Drosophila*, four Dlg genes have been identified in mammals: DLG1 (hDLG, SAP97), DLG2 (chapsyn-110, PSD-93), DLG3 (NE-DLG, SAP102) and DLG4 (PSD-95, SAP90). Dlg was initially identified as a tumour supressor where *dlg* mutants display excessive overproliferation and neoplastic transformation of epithelial cells within imaginal discs.

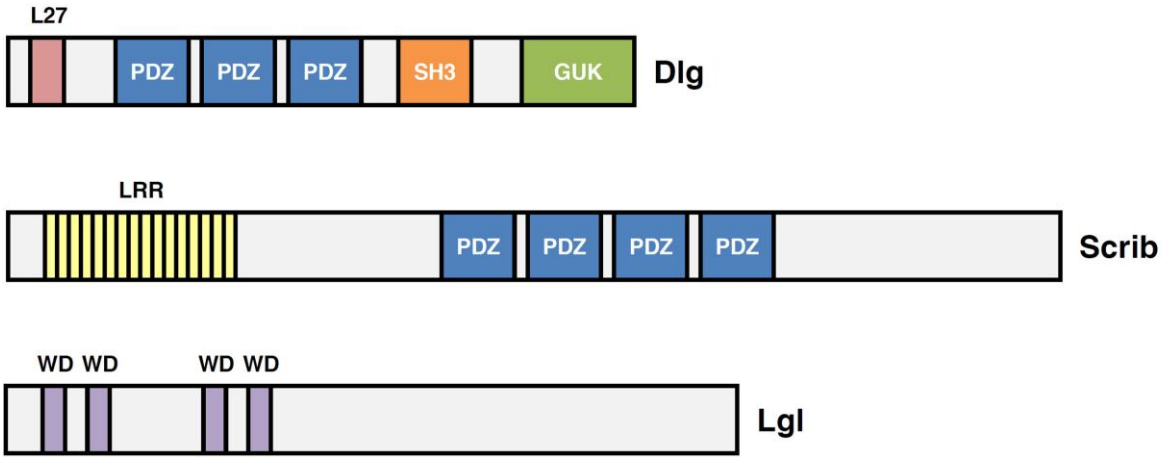
L27
PDZ
PDZ
PDZ
SH3
GUK
Dlg
LRR
PDZ
PDZ
PDZ
PDZ
Scrib
WD WD
WD WD
Lgl

FIGURE 3 Domain organization of the Scrib complex proteins.

Schematic diagram of the domain organization of Dlg, Scrib and Lgl (not to scale). Dlg contains three PDZ domains (shown in blue), an SH3 domain (shown in orange) and an enzymatically inert GUK domain (shown in green). DlgS97, a neuronal-specific isoform of Dlg, contains an additional L27 domain (shown in pink). Scrib contains 16 LRR domains (shown in yellow) and four PDZ domains. Lgl contains at least four WD40 repeats (shown in purple). Note that the figure was modeled after Yamanaka and Ohno, 2008.

Scrib and **Lethal giant larvae** (**Lgl**) are cytoplasmic proteins associated with the basolateral membrane that, along with Dlg, cooperatively establish epithelial apicobasal polarity (see Figure 2) (reviewed in Tepass et al., 2001; reviewed in Humbert et al., 2003; reviewed in Yamanaka and Ohno, 2008; reviewed in Roberts et al., 2012; reviewed in Elsum et al., 2012). Scrib is a member of the LAP family bearing 16 N-terminal **leucine-rich repeats** (**LRRs**) and four PDZ domains (Figure 3). Lgl, on the other hand, is a WD40 repeat protein that can associate with non-muscle myosin II (Figure 3). Mutations in the Scrib complex proteins results in various defects in apicobasal polarity including the loss of septate junctions and the mis-positioning of the adherens junctions. In addition, apically localized proteins, such as the Crb and Baz/PAR-3 complex proteins, are no longer confined to their apical membrane domains and spread basally.

1.1.4. The leading edge membrane of DME cells during dorsal closure: a model for epithelial plasticity

Epithelial plasticity refers to the ability of epithelial cells to alter both their shape and their interactions with other epithelial cells, and occurs during **epithelial-mesenchymal transitions** (**EMTs**) and **mesenchymal-epithelial transitions** (**METs**) (reviewed in Nieto, 2011). EMTs are characterized, in part, by the complete loss of apicobasal polarity and cell-cell adhesion in epithelial cells as they acquire mesenchymal-like properties and exit the epithelium. In contrast, METs are characterized, in part, by the establishment of apicobasal polarity and cell-cell adhesion in mesenchymal cells as they acquire epithelial-like properties and integrate into the epithelium. EMTs and METs occur throughout development and organogenesis, but are relatively limited in the adult organism, occurring during wound healing and regenerative repair. Improper regulation of EMTs and METs can have disastrous consequences as they can promote carcinoma invasion and metastasis, as well as tissue fibrosis. Therefore, understanding how apicobasal polarity is regulated during epithelial plasticity is of great medical interest.

In addition to becoming planar polarized, the leading edge membrane of DME cells undergo dynamic changes in apicobasal polarity and cell-cell adhesion throughout dorsal closure (Figure 4A,C). Prior to the start of dorsal closure, the Scrib and Baz/PAR-3 complexes are initially present on all sides of the DME cells, including at the leading edge membrane (Figure 4D) (Gorfinkiel and Arias, 2007; Bahri et al., 2010; David et al., 2010; Laplante and Nilson, 2011). To date, the status of the Crb complex during the early stages of dorsal closure has not been evaluated. As dorsal closure proceeds, all three apicobasal polarity complexes are missing at the leading edge membrane, but are still present on the other sides of the DME cells, as well as throughout the rest of the epidermis (Figure 4E-G) (Arquier et al., 2001; Kaltschmidt et al., 2002; Morel and Arias, 2004; Gorfinkiel and Arias, 2007; Bahri et al., 2010; David et al., 2010; Laplante and Nilson, 2011; Pickering et al., 2013). Additionally, the adherens junctions and proteins that make up the septate junction, i.e. NrxIV, Cora and Fas3, are also disrupted at just the leading edge membrane of DME cells as adhesions between the DME cells and the amnioserosa are severed to promote migration (Figure 4K,L) (Fehon et al., 1994; Arquier et al., 2001; Grevengoed et al., 2001; Kaltschmidt et al., 2002; Morel and Arias, 2004; Gorfinkiel and Arias, 2007; Bahri et al., 2010). Since DME cells only lose apicobasal polarity and cell-cell adhesion at the leading edge membrane, they remain attached to the rest of the epidermis. Upon dorsal closure completion, all three apicobasal polarity complexes are restored at the leading edge membrane as opposing DME cells meet at the dorsal midline (Figure 4H-J) (Kaltschmidt et al., 2002; Bahri et al., 2010; Laplante and Nilson, 2011). Furthermore, the adherens and septate junctions are formed between DME cells on opposing epidermal flanks at the dorsal midline in order to fuse them together (Figure 4K,L) (Gorfinkiel and Martinez-Arias, 2007; Bahri et al., 2010). Unlike EMTs and METs where apicobasal polarity and cell-cell adhesion are regulated on all sides of the cell, polarity and adhesion are regulated only at the leading edge membrane of DME cells during dorsal closure. We propose that this membrane can be used as a model for epithelial plasticity as it displays EMT-like characteristics during dorsal closure

and MET-like characteristics at the end of dorsal closure in terms of apicobasal polarity and cell-cell adhesion regulation.

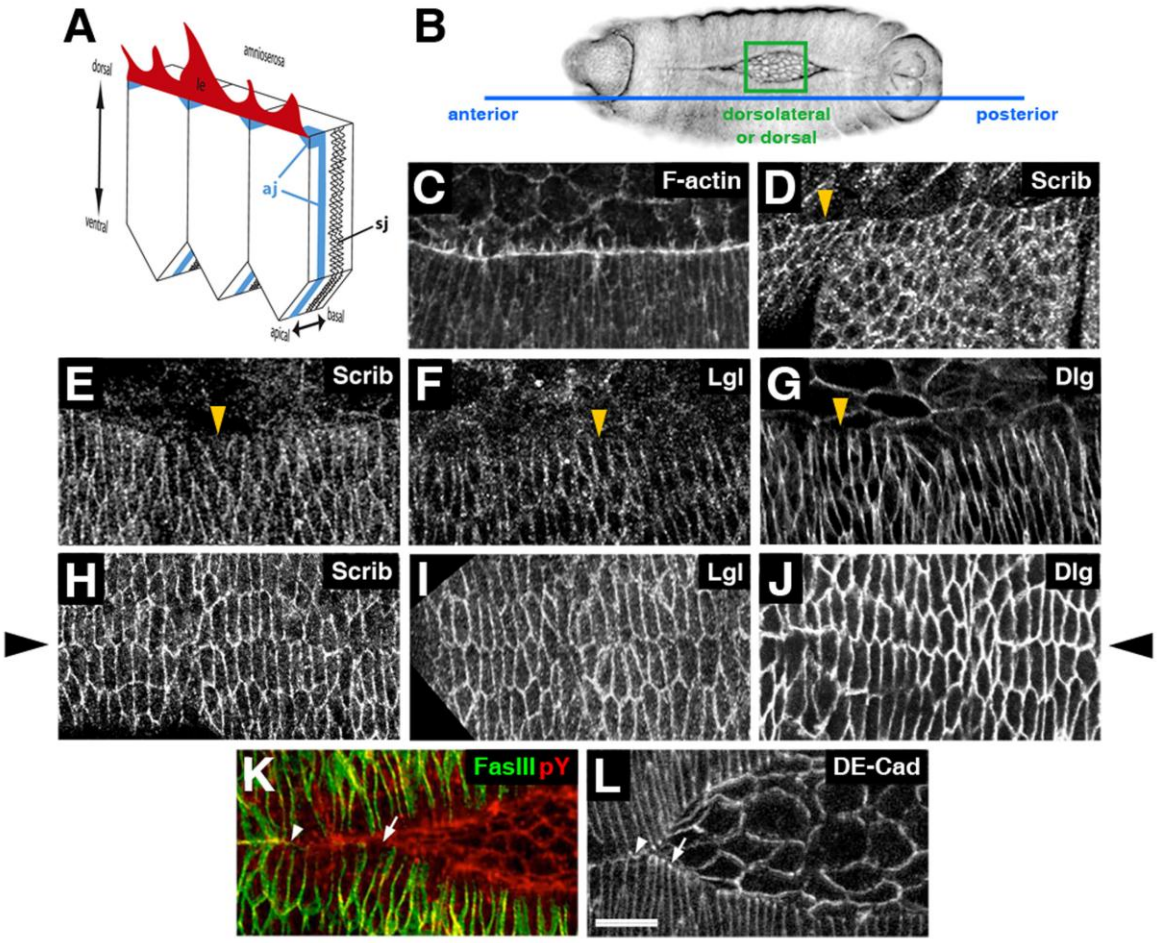
A
dorsal
ventral
amnioserosa
le
aj
sj
apical
basal
B
anterior
dorsolateral
or dorsal
posterior
C
F-actin
D
Scrib
E
Scrib
F
Lgl
G
Dlg
H
Scrib
I
Lgl
J
Dlg
K
FasIII pY
L
DE-Cad

FIGURE 4 Regulation of apicobasal polarity at the leading edge membrane of DME cells during dorsal closure.

(A) Schematic diagram showing the apicobasal axis of DME cells during dorsal closure. Adherens junctions are shown in blue whereas septate junctions are shown as black wavy lines. The leading edge membrane contains actin-based protrusions in the form of filopodia and lamellipodia shown in red, and lacks adherens and septate junctions at this stage. Note that the illustration was done by Dr. Harden. **(B)** Diagram showing the two main embryonic planes of view, i.e. dorsolateral and dorsal, used throughout this thesis. **(C-G)** Confocal fluorescence images (merged stacks) showing dorsolateral views of fixed wild-type embryos during early to mid dorsal closure, focusing on the boundary between the dorsal epidermis and amnioserosa. The amnioserosa is always on the top in each panel. Embryos were stained with either phalloidin (C) which labels F-actin, or antibodies against Scrib (D,E), Lgl (F) or Dlg (G). (C) F-actin accumulates along the leading edge of DME cells during dorsal closure. Filopodia and lamellipodia can be seen protruding from the leading edge. (D) Prior to the start of dorsal closure, the Scrib complex protein, Scrib, is initially present at the leading edge membrane of DME cells (see yellow arrowhead). (E-G) As dorsal closure proceeds, however, the Scrib complex proteins, Scrib, Lgl and Dlg, are all missing at the leading edge membrane (see yellow arrowheads), giving the DME cells an ''open-ended'' appearance. **(H-J)** Dorsal views of wild-type embryos at the end of dorsal closure, focusing straight down on the dorsal midline which is denoted by black arrowheads. Embryos were stained with anti-Scrib (H), anti-Lgl (I) or anti-Dlg (J) antibodies. Upon dorsal closure completion, the Scrib complex proteins are all restored at the leading edge membrane after opposing DME cells meet at the dorsal midline. **(K,L)** Dorsal views of wild-type embryos during dorsal closure, focusing straight down on the dorsal hole. Embryos were stained with antibodies against the septate junction protein, Fas3 (K), or the adherens junction protein, DE-Cad (L). Both the septate and adherens junction proteins are missing at the leading edge membrane of DME cells during dorsal closure (see white arrows), but are formed between opposing DME cells at the dorsal midline upon dorsal closure completion (see white arrowheads). Note that the embryo in panel K is also stained with an antibody against the cell marker, phospho-tyrosine. le = leading edge, aj = adherens junction, sj = septate junction, pY = phospho-tyrosine. Scale bar in panel L represents 10µm (C-L).

1.1.5. p21-activated kinases

The Rho family of GTPases are members of the Ras superfamily of small monomeric GTP-binding proteins that are conserved in all eukaryotic organisms (reviewed in Jaffe and Hall, 2005). Members of the Rho GTPase family have been shown to regulate many aspects of intracellular actin dynamics. The most extensively characterized members are Rho, Rac and Cdc42. Rho GTPases cycle between two conformational states: a GDP-bound inactive state and a GTP-bound active state. Interconversion between these two states is controlled by **guanine nucleotide exchange factors** (**GEFs**), which activate Rho GTPases by promoting the exchange of GDP for GTP, and **GTPase activating proteins** (**GAPs**), which inactivate Rho GTPases by promoting the exchange of GTP for GDP. In the activated GTP-bound state, RhoGTPases interact with downstream effector molecules to elicit their cellular response. Of the many effector proteins that bind to activated Rac and Cdc42, the **p21-activated kinases** (**Paks**) are among the best characterized.

Paks are a family of conserved serine/threonine kinases that participate in many cellular processes (reviewed in Bokoch, 2003). Mammalian Paks are divided into two subfamilies, termed Group I and Group II, based on sequence conservation, domain organization and mode of regulation. Group I Paks contain an N-terminal regulatory region, consisting of a **Cdc42/Rac interacting binding** (**CRIB**) domain which overlaps with an **autoinhibitory domain** (**AID**), and a highly conserved C-terminal kinase domain (see Figure 8A). In its inactive state, Group I Paks exist as a homodimer in a ''head-to-tail'' conformation. That is, the kinase domain of one protein interacts with the AID of the other, thus suppressing each other's kinase activity. When Rac or Cdc42 are activated, they bind to the CRIB domains causing the two Pak proteins in the homodimer to dissociate from one another. Pak then undergoes autophosphorylation to become activated, and can phosphorylate downstream substrates. Group II Paks do not possess a well-defined AID and are regulated in a different, and not well characterized, manner. In mammals, the Group I Paks consist of Paks 1-3 whereas the Group II Paks consist of

Pak 4-6. In *Drosophila*, there are two known Group I Paks, Pak and Pak3, but only one Group II Pak, Mushroom bodies tiny.

Dr. Harden has previously shown that Pak accumulates along the leading edge of DME cells during dorsal closure (Figure 5) (Harden et al., 1996). Loss of Pak function during dorsal closure leads to a disruption of the leading edge cytoskeleton which is required for the migration of the epidermal flanks over the amnioserosa (Conder et al., 2004). In addition, Pak kinase activity in the amnioserosa is required for correct morphogenesis of the epidermis, and may be a component of the signalling known to occur between these two tissues (Conder et al., 2004).

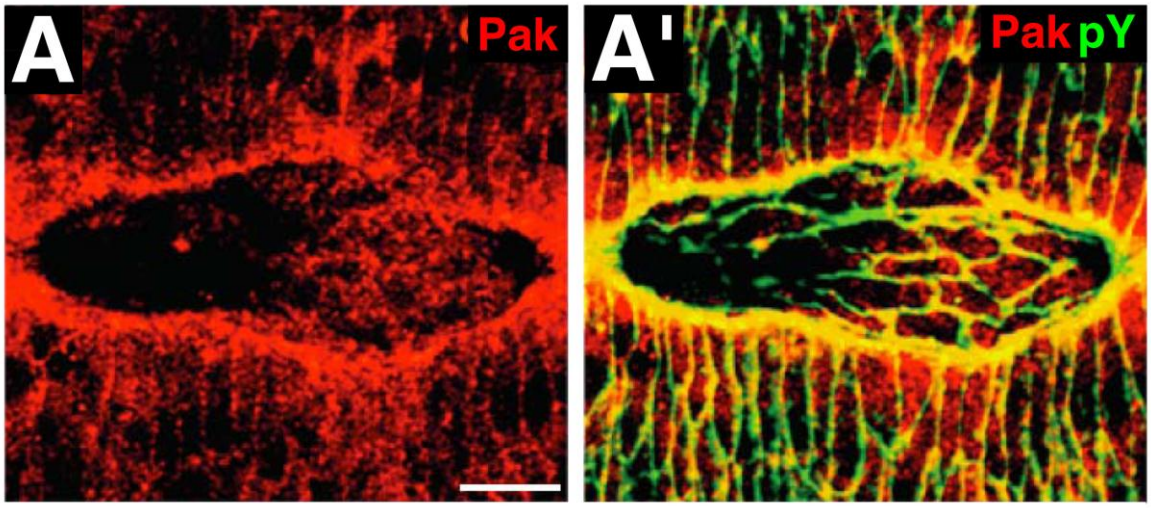
A
Pak
A'
Pak pY

FIGURE 5 Pak distribution during dorsal closure.

(A-A') Dorsal view of a wild-type embryo during dorsal closure stained with Pak and anti-phospho-tyrosine antibodies. The anti-phospho-tyrosine antibody marks cell membranes. Pak accumulates along the leading edge of DME cells during dorsal closure. pY = phospho-tyrosine.

1.2. Objective

Prior to the start of dorsal closure, the Scrib complex is present at the leading edge membrane of DME cells. However, as dorsal closure proceeds and the epidermis starts to migrate over the amnioserosa, the Scrib complex is subsequently missing at the leading edge. Upon dorsal closure completion when the opposing epidermal flanks meet and adhere to each other, the Scrib complex is once again restored at the leading edge. Such dynamic regulation of apicobasal polarity at the leading edge membrane of DME cells is reminiscent of EMTs and METs, and we propose that this membrane can serve as a model to study such processes.

We wondered if Pak is involved in regulating apicobasal polarity during dorsal closure, particularly at the leading edge membrane of DME cells. Previous studies in our lab have shown that Pak promotes apicobasal polarization of the follicular epithelium, which is derived from an MET event, during oogenesis (Conder et al., 2007). Furthermore, Pak accumulates at the leading edge during dorsal closure (Harden et al., 1996). In this chapter, we investigate whether Pak is required for restoring apicobasal polarity at the leading edge membrane upon dorsal closure completion.

1.3. Materials and Methods

Recipes for reagents shown in bold can be found in Appendix B – Recipes.

1.3.1. Fly Stocks

Flies were maintained under standard conditions at 25°C unless otherwise stated (Ashburner and Roote, 2007). w^{1118} was used as a wild-type control unless otherwise stated. The following lines were ordered from the Bloomington *Drosophila* Stock Center (Indiana University, Indiana): w^{1118} (3605), $cora^{14}$ (9099) (Lamb et al., 1998), *prd-Gal4* (1947), *Df(1)JA27/FM7c, kr-Gal4, UAS-GFP* (5193), *In(2LR)Gla/CyO, twi-Gal4, UAS-GFP*

(6662) and *Dr^{Mio}/TM3, twi-Gal4, UAS-GFP* (6663). The following lines were kindly provided by other research groups: *pak^{14}* from Dr. Barry Dickson (Research Institute of Molecular Pathology, Austria) (Newsome et al., 2000a; Newsome et al., 2000b), *EP(3)1191* from Dr. Huey Hing (The College at Brockport, New York) (Spradling et al., 1999), *mys^{G1}* from the late Dr. Danny Brower (Jannuzi et al., 2002), *UAS-dlgA-GFP* from Dr. Ulrich Thomas (Leibniz Institute for Neurobiology, Germany) (Koh et al., 1999), *UAS-scrib-GFP* from Dr. David Bilder (University of California, Berkeley, California) (Zeitler et al., 2004), *ptc-Gal4* from Dr. Elisabeth Knust (Max Planck Institute of Molecular Cell Biology and Genetics, Germany) and *m4-Gal4* from Dr. John Roote (University of Cambridge, England).

The following lines were made by our collaborators: *pak3^{ex27a}*, *pak3^{ex76a}* and *UAS-pak3-GFP* made by Dr. Sami Bahri (Institute of Molecular and Cell Biology, Singapore) (described in Bahri et al., 2010) and *UAS-pak-GFP* from Dr. Stepan Sigrist (Freie Universitat Berlin, Germany) (described in Rasse et al., 2005).

1.3.2. Cuticle Preparation

Cuticle preparations were performed as previously described but with some modifications (Stern and Sucina, 2011). Cages and plates were incubated at 25°C unless otherwise stated. Experiments and their controls were always done at the same time under identical conditions.

Flies placed in cages, made from 100mL tricornered plastic beakers with small holes poked in them, were allowed to lay eggs on **grape juice agar plates** with **yeast paste** for 24 hours. The flies were then removed and the plates were aged for an additional 48 hours. Progeny ranging in age from 48 to 72 hours after egg laying were collected in baskets (see Stern and Sucina, 2011) and dechorionated in **50% bleach** for three minutes. The progeny were then washed in 0.01% Triton X-100 (diluted from Sigma-Aldrich – T8787) three times for a minimum of 30 seconds each and mounted

onto slides with **Hoyer's medium**. Weights were added to flatten the samples and the slides were incubated at 65°C for three days, or until all soft tissue was digested leaving behind only cleared cuticle. Embryonic phenotypes were scored on a Nikon TMS inverted phase contrast microscope with a minimum sample size of 250 progeny. Representative phenotypes were imaged on a Zeiss Axioplan 2 microscope with Openlab software, and the images were processed using Adobe Photoshop CS5.

1.3.3. Embryo Fixation

Embryo fixations were performed as previously described but with some modifications (Rothwell and Sullivan, 2007a; Rothwell and Sullivan, 2007b; Rothwell and Sullivan, 2007c). Cages were incubated at 25°C unless otherwise stated. Experiments and their controls were always done at the same time under identical conditions.

Flies placed in cages, made from 100mL tricornered plastic beakers with small holes poked in them, were allowed to lay eggs on **grape juice agar plates** with **yeast paste** for 16 hours. Embryos ranging in age from 0 to 16 hours after egg laying were collected in baskets (see Stern and Sucina, 2011) and dechorionated in **50% bleach** for three minutes. The embryos were then washed in 0.01% Triton X-100 (diluted from Sigma-Aldrich – T8787) three times for a minimum of 30 seconds each. To remove the vitelline membrane, the embryos were transferred to 20mL glass scintillation vials containing a devitellinization mixture composed of two phases: a bottom aqueous layer consisting of 5mL of **4% paraformaldehyde** and a top organic layer consisting of 5mL of heptane (Caledon Laboratories – 5400-1). The embryos were then shaken vigorously for 25 minutes. After shaking, the bottom paraformaldehyde layer was removed and replaced with 5mL of methanol (Caledon Laboratories – 6700-1). The embryos were then shaken for an additional minute causing properly devitellinized, and thus fixed, embryos to sink to the bottom methanol layer. The top heptane layer, along with improperly devitellinized embryos, were discarded. Fixed embryos were stored in

methanol at -20°C until ready for staining. Note that embryos were typically stained within one month of fixation.

1.3.4. Immunohistochemistry

Immunostaining of embryos was performed as previously described but with some modifications (Swedlow, 2011). Experiments and their controls were always done at the same time under identical conditions. All steps were performed at room temperature unless otherwise stated.

Fixed embryos in methanol were first washed with **PBT** three times for ten minutes each, and then blocked with **1% BSA** for one hour. The samples were next incubated with primary antibodies overnight at 4°C (see a list of the primary antibodies used in this study in the next paragraph). Following three washes with PBT for ten minutes each, the samples were incubated with fluorescently-conjugated secondary antibodies for two hours (see a list of the secondary antibodies used in this study in the next paragraph). As the fluorophores are light sensitive, the samples were protected from light for the remainder of the protocol. After incubation with the secondary antibodies, the samples were then washed with PBT three times for ten minutes each, and subsequently equilibrated with VECTASHIELD Mounting Medium (Vector Laboratories – H-1000) overnight at 4°C. The samples were mounted onto platform slides, consisting of 22×22mm cover slips adhered onto microscope slides with clear nail polish, and stored at -20°C until ready for imaging. Samples were imaged as merged stacks on either a Zeiss LSM 410 laser scanning confocal microscope with Zeiss LSM software or a Nikon A1R laser scanning confocal microscope with NIS-Elements software. Note that experiments and their controls were always imaged on the same day under identical acquisition settings. All images were processed with Adobe Photoshop CS5.

The following primary antibodies were used: 1:2000 rabbit anti-Pak (Harden et al., 1996), 1:1000 mouse anti-Pak3 made by Dr. Sami Bahri (described in Bahri et al., 2010), 1:10 mouse anti-Dlg (Developmental Studies Hybridoma Bank – 4F3) (Parnas et al., 2001), 1:500 guinea pig anti-Scrib from Dr. David Bilder (University of California, Berkeley, California) (Zeitler et al., 2004), 1:100 rabbit anti-Lgl from Dr. Jurgen Knoblich (Institute of Molecular Biotechnology, Vienna) (Betschinger et al., 2003), 1:100 mouse anti-Fas3 (Developmental Studies Hybridoma Bank – 7G10) (Patel et al., 1987), 1:2000 guinea pig anti-Cora from Dr. Richard Fehon (University of Chicago, Illinois) (Fehon et al., 1994), rat anti-DE-Cad (Developmental Studies Hybridoma Bank – DCAD2) (Oda et al., 1994), mouse anti-βPS-integrin (Developmental Studies Hybridoma Bank – CF.6G11) (Brower et al., 1984) (1:2), 1:500 mouse anti-GFP (Sigma-Aldrich – G6539) and 1:200 rabbit anti-GFP (Sigma-Aldrich – G1544). The following secondary antibodies were used: Fluorescein-labeled horse anti-mouse (Vector Laboratories – FI-2000), Texas Red-labeled horse anti-mouse (Vector Laboratories – TI-2000), Fluorescein-labeled goat anti-rabbit (Vector Laboratories – FI-1000), Texas Red-labeled goat anti-rabbit (Vector Laboratories – TI-1000), Fluorescein-labeled anti-rat, Texas Red-labeled anti-rat, Fluorescein-labeled anti-guinea pig and Texas Red-labeled anti-guinea pig. Both primary and secondary antibodies were diluted in 1% BSA. All secondary antibodies were used at a 1:200 dilution.

1.3.5. Live Imaging

Live imaging of embryos was performed as previously described but with some modifications (Reed et al., 2009; Parton et al., 2010). Cages were incubated at 25°C unless otherwise stated.

Flies placed in cages, made from 100mL tricornered plastic beakers with small holes poked in them, were allowed to lay eggs on **grape juice agar plates** with **yeast paste** for 12 hours. Embryos ranging in age from 0 to 12 hours after egg laying were collected in baskets (see Stern and Sucina, 2011) and dechorionated in **50% bleach**, sans

detergent, for three minutes. The embryos were then washed with water three times for a minimum of 30 seconds each and mounted onto a chamber (see next paragraph for details) with Halocarbon oil (LabScientific – FLY-7000). Stage 14 and 15 embryos expressing GFP-tagged proteins were imaged as merged stacks on a Quorum WaveFX spinning disc confocal microscope with Volocity software. All movies were processed using Adobe Photoshop CS5 and ImageJ.

The jerry-rigged chamber consisted of a plastic 60×15mm Petri dish with a rectangular opening, less than 22×40mm in dimension, cut out of the bottom. A gas-permeable membrane (YSI Life Sciences – 5793) was placed over the opening and held down with Scotch double-sided tape. Halocarbon oil was then applied onto the membrane. After the dechorionated embryos were transferred into the oil with a paintbrush, a 22×40mm coverslip was placed on top and secured with Scotch double-sided tape. Note that the membrane, oil and cover slip were all added to the outside, not the inside, of the dish.

1.3.6. Co-immunoprecipitation

Co-immunoprecipitations were performed as previously described but with some modifications (Bahri et al., 2010). Experiments and their controls were always done at the same time under identical conditions. All steps were performed at room temperature unless otherwise stated.

Stocks and crosses were raised at 25°C unless otherwise stated. Whole adult flies, either 100 wild-type females or 30 transgenic females, were homogenized by hand with a pestle in 500µL of **Lysis Buffer I** on ice. The lysate was then centrifuged at 13000rpm for ten minutes at 4°C. The pellet was discarded and the extract was stored at -80°C until ready for immunoprecipitation.

All steps regarding protein immunoprecipitation were performed at 4°C. For each extract, two 100µL aliquots of 50% Protein G Agarose slurry (Santa Cruz Biotechnology – sc-2002) were centrifuged at 13000rpm for five minutes, after which the supernatants were discarded. The beads were subsequently washed with **PBS** for five minutes, and then centrifuged at 13000rpm for five minutes. The supernatants were discarded and two more PBS washes were performed. After the final washes were removed, one of the aliquots of beads was incubated with 5µL of antibody in 300µL of Lysis Buffer I overnight (see a list of the antibodies used in this study in the last paragraph of this section). The other aliquot of beads was incubated with an equal volume of normal IgG serum, and served as a negative control (see a list of the normal IgG sera used in this study in the last paragraph of this section). The beads were next centrifuged at 13000rpm for five minutes, after which the supernatants were discarded. The beads were subsequently washed with Lysis Buffer I for ten minutes, and then centrifuged at 13000rpm for five minutes. The supernatants were discarded and two more Lysis Buffer I washes were performed. After the final washes were removed, the whole adult fly extract (described in the previous paragraph) was equally split amongst the two aliquots of beads and incubated for two hours. The beads were next centrifuged at 13000rpm for five minutes, after which the supernatants were discarded. The beads were subsequently washed with **Lysis Buffer II** for ten minutes, and then centrifuged at 13000rpm for five minutes. The supernatants were discarded and two more Lysis Buffer II washes were performed. After the final washes were removed, loading dye (Thermo Fisher Scientific – 39000) was added and the samples were stored at -20°C until ready for SDS-PAGE.

After boiling for ten minutes, the samples were loaded onto an 8% discontinuous SDS-PAGE gel (see Simpson, 2006) along with a prestained ladder (Bio-Rad – 161-0318). The samples were run at 100V in **Running Buffer** until the dye front migrated to the end of the gel, and then were transferred onto a nitrocellulose membrane (Bio-Rad – 162-

0115) at 15V with **Transfer Buffer** for one hour using a semi-dry transfer apparatus. The membranes were stored in **TBS** at 4°C until ready for immunoblotting.

The membranes were first washed with **TBST** three times for ten minutes each, and then blocked with **5% BSA** or **5% Milk** for one hour. The membranes were next incubated with a primary antibody overnight at 4°C (see a list of the primary antibodies in the next paragraph). Following two washes with TBST and two blocks with **2.5% BSA** or **2.5% Milk** for ten minutes each, the membranes were incubated with an HRP-conjugated secondary antibody for two hours (see a list of the secondary antibodies in the next paragraph). The membranes were then washed with TBST four times for 15 minutes each. Detection was accomplished with the BM Chemiluminescence Western Blotting Peroxidase Substrate (Roche Applied Science – 11500694001). Maximum sensitivity film (Cedarlane – CLMS810) was exposed from anywhere between 5 seconds to one hour, depending on the strength of the signal, and developed. If multiple blottings of a single membrane were required, the membrane was stripped with **Stripping Solution** two times for 30 minutes each at 50°C.

The following antibodies were used for immunoprecipitation: rabbit anti-Pak (Harden et al., 1996), mouse anti-Pak3 (Bahri et al., 2010) and rabbit anti-GFP (Sigma-Aldrich – G1544). The following normal IgG sera were used for immunoprecipitation: normal mouse IgG (Santa Cruz Biotechnology – sc-2025) and normal rabbit IgG (Santa Cruz Biotechnology – sc-2027). The following primary antibodies were used for immunoblotting: 1:5000 rabbit anti-Pak (Harden et al., 1996), 1:5000 mouse anti-Pak3 (Bahri et al., 2010) and 1:1000 rabbit anti-GFP (Sigma-Aldrich – G1544). The following secondary antibodies, which were all diluted to 1:2000, were used for immunoblotting: Peroxidase-labeled horse anti-mouse (Vector Laboratories – PI-2000) and Peroxidase-labeled goat anti-rabbit (Vector Laboratories – PI-1000). Primary and secondary antibodies were diluted in either 2.5% BSA or 2.5% Milk. Milk was only used for Pak and Pak3 blotting.

1.3.7. Molecular Subcloning

Subcloning was performed as outlined in the ''Subcloning Notebook'' (Promega) but with some modifications. Recipes for reagents are described in the ''Bench Guide'' (QIAGEN). The following cDNA clones were used: *LD20767* (Canadian *Drosophila* Microarray Centre) (Rubin et al., 2000), *LD10376* (Berkeley *Drosophila* Genome Project) (Rubin et al., 2000), *RE02389* (Berkeley *Drosophila* Genome Project) (Stapleton et al., 2002), *LD06034* (Canadian *Drosophila* Microarray Centre) (Stapleton et al., 2002) and *RE30311* (Berkeley *Drosophila* Genome Project) (Rubin et al., 2000).

The coding region from each cDNA clone was PCR amplified using the Phusion High-Fidelity PCR Kit (New England Biolabs – M0531S). Forward and reverse primers, which were made by Invitrogen, contained EcoRI and XhoI adapter sites respectively (see a list of the primers in Appendix C). Following PCR amplification, the PCR product was purified using the QIAquick PCR Purification Kit (QIAGEN – 28106). The purified PCR product was next digested with EcoRI (Thermo Fisher Scientific – FD0274) and XhoI (Thermo Fisher Scientific – FD0694) for three hours at 37°C, and then purified using the QIAquick PCR Purification Kit. The digested PCR product was ligated in frame into the pGEX-4T-1 vector (GE Healthcare – 27-4580-01) with T4 DNA Ligase (Invitrogen – 15224017), using a 6:1 molar ratio of insert to 50ng of vector, for 24 hours at 14°C. Afterwards, the ligation reaction was transformed into DH5α competent cells (Invitrogen – 18265-017), which were subsequently streaked onto LB-amp plates (see the ''Bench Guide'' from QIAGEN) and incubated overnight at 37°C. Single colonies that formed on the plates were then inoculated in LB-amp broth (see the ''Bench Guide'' from QIAGEN) and incubated for 18 hours at 37°C with shaking. Plasmid DNA was isolated using the QIAprep Spin Miniprep Kit (QIAGEN – 27106) and screened for the presence of the insert by EcoRI/XhoI test digestions. Putative positive clones were further confirmed through sequencing using GENEWIZ (see a list of the sequencing primers in Appendix C).

1.4. Results

Some of the work from this section was published in ''The leading edge during dorsal closure as a model for epithelial plasticity: Pak is required for recruitment of the Scribble complex and septate junction formation'' by Sami Bahri, Simon Wang, Ryan Conder, Juliana Choy, Stephanie Vlachos, Kevin Dong, Carlos Merino, Stephan Sigrist, Cristina Molnar, Xiaohang Yang, Edward Manser and Nicholas Harden (Development 2010; 137:2023-32). Dr. Sami Bahri and I contributed equally to this publication. Note that work done by others is credited throughout the text.

1.4.1. Pak is a component of the Scrib complex

We wondered if Pak is involved in regulating apicobasal polarity in the embryonic epidermis, particularly at the leading edge membrane of DME cells during dorsal closure, given several lines of supporting evidence. Most notably, previous studies in our lab have shown that Pak promotes apicobasal polarization of the follicular epithelium, which is derived from an MET event, during oogenesis (reviewed in Wu et al., 2008; Conder et al., 2007). As mentioned previously, the leading edge membrane of DME cells during dorsal closure exhibits MET-like behaviour. Furthermore, Pak accumulates along the leading edge membrane as dorsal closure progresses (see Figure 5) (Harden et al., 1996). We confirmed this transient distribution pattern, which was originally reported in fixed embryos, through live image analysis of embryos expressing Pak-GFP in the epidermis with the segmental *prd-Gal4* driver using the UAS-Gal4 system (Figure 6A-C) (see Movie 2 in the attached CD-ROM) (reviewed in Duffy, 2002; Bahri et al., 2010). One reason for Pak's localized accumulation during dorsal closure is to maintain the integrity of the leading edge cytoskeleton which is required for the migration of the epidermal flanks over the amnioserosa (Conder et al., 2004). Another possible reason is that its presence may be needed for restoring apicobasal polarity at the leading edge membranes of opposing DME cells when they meet at the dorsal midline upon dorsal closure completion.

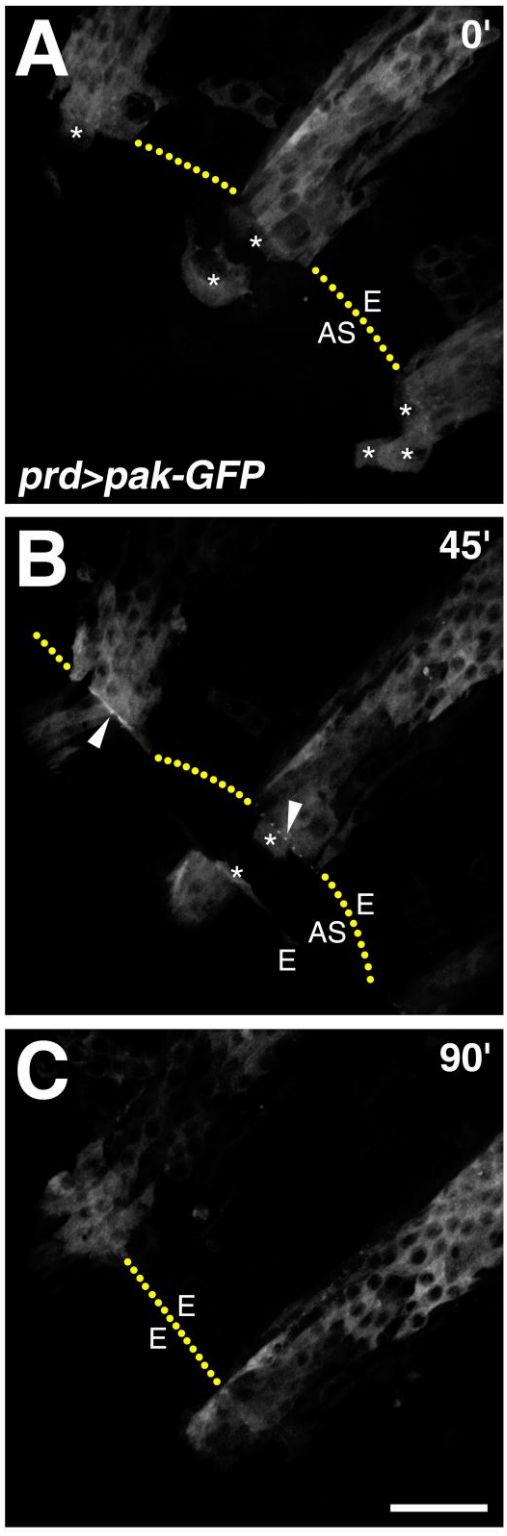
A
0'
E
AS
prd>pak-GFP
B
45'
E
AS
E
C
90'
E
E

FIGURE 6 Live image analysis of Pak-GFP distribution during dorsal closure.

(A-C) Live imaging of an embryo expressing *UAS-pak-GFP* with *prd-Gal4* during dorsal closure. For the orientation of the embryo, refer to the yellow dotted lines that mark the leading edge of one of the epidermal flanks. Gal4, and consequently Pak-GFP, is expressed under the *prd* promoter in odd-numbered embryonic epidermal segments that extend into the amnioserosa (GFP positive amnioserosa cells are marked with asterisks). Images were processed from stills taken from Movie 2 (see the attached CD-ROM). (A,B) Pak-GFP progressively accumulates along the leading edge of DME cells during dorsal closure. Compare early (A) to mid (B) stages of dorsal closure (see white arrowheads). (C) Upon dorsal closure completion, the accumulation of Pak-GFP at the leading edge is lost after opposing DME cells meet at the dorsal midline. Scale bar in panel C represents 25µm (A-C). E = epidermis, AS = amnioserosa.

We addressed whether Pak can regulate apicobasal polarity during dorsal closure by first determining if Pak co-localizes with the Scrib complex in the embryonic epidermis, as the mammalian Paks have been previously reported to interact with Scrib (Nola et al., 2008). This was accomplished by co-staining stage 14 and 15 wild-type embryos with antibodies against Pak and the Scrib complex protein, Dlg. The Pak antibody targets N-terminal sequences whereas the Dlg antibody targets the second PDZ domain (Harden et al., 1996; Parnas et al., 2001). In a cross-sectional view of a row of neighbouring DME cells during dorsal closure, Pak overlapped with Dlg along the lateral membrane, though Pak was also present throughout the cytoplasm (Figure 7B-B'') (Bahri et al., 2010). Furthermore, cross-sectional views of the leading edge membranes of opposing DME cells at the dorsal midline also showed that Pak overlapped with Dlg once Dlg was restored upon dorsal closure completion (Figure 7C-D''). These results show that the localizations of Pak and the Scrib complex overlap along the lateral membrane of embryonic epidermal cells, including at the leading edge of DME cells, during dorsal closure.

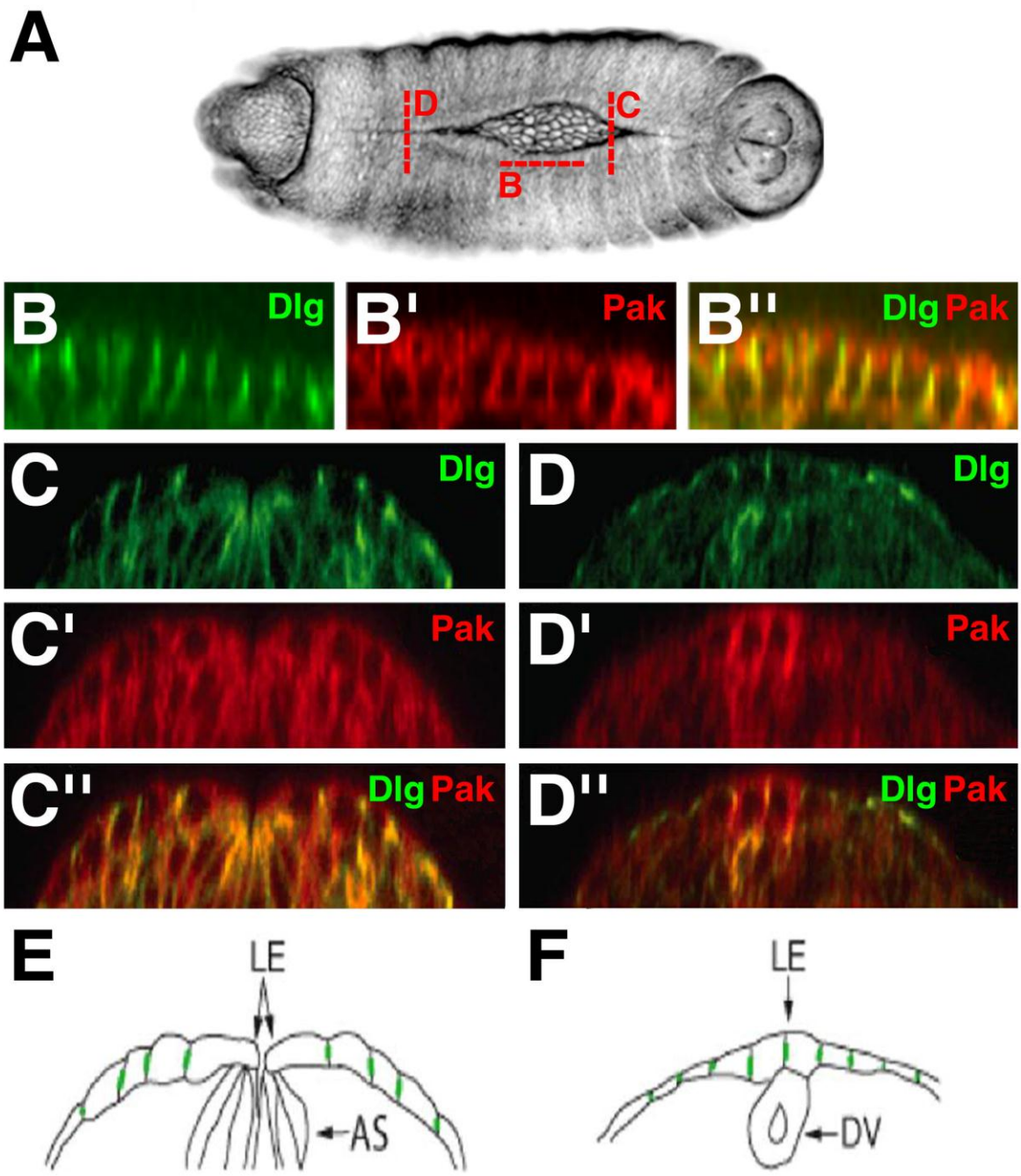
A
D
C
B
B
Dlg
B'
Pak
B''
Dlg Pak
C
Dlg
D
Dlg
C'
Pak
D'
Pak
C''
Dlg Pak
D''
Dlg Pak
E
LE
AS
F
LE
DV

FIGURE 7 Pak distribution along the lateral membrane of embryonic epidermal cells overlaps with the Scrib complex.

(A) Diagram showing where the optical cross-sections were taken in order to view the apicobasal axis. **(B-D'')** Cross-sectional views of stage 14 (B-C'') and 15 (D-D'') wild-type embryos co-stained with antibodies against Pak and the Scrib complex protein, Dlg. (B-B'') Cross-sectional view of a row of neighbouring DME cells during dorsal closure (see line B in panel A). Pak overlaps with Dlg along the lateral membrane, though Pak is also present throughout the cytoplasm. (C-C'') Cross-sectional view of the leading edge membranes of opposing DME cells during dorsal closure (see line C in panel A). Pak does not overlap with Dlg at the leading edge membrane, as Dlg has yet to be restored. (D-D'') Cross-sectional view of the leading edge membranes of opposing DME cells at the end of dorsal closure (see line D in panel A). Pak overlaps with Dlg at the leading edge membrane, as Dlg is restored. **(E-F)** Schematic diagrams of panels C (E) and D (F), with Dlg shown in green. Note that the illustrations were done by Dr. Harden. LE = leading edge, AS = amnioserosa, DV = dorsal vessel.

We next determined whether Pak is a component of the Scrib complex through co-immunoprecipitation assays. Previous studies done in collaboration with Dr. Ryan Conder, a former Ph.D. student under Dr. Harden, have shown that Pak can form a complex with both Scrib and Lgl (see the thesis entitled ''The role of p21-activated kinase in *Drosophila* development'' which was submitted to the SFU Library in 2007) (Bahri et al., 2010). We assessed whether Pak can also form a complex with Dlg by performing similar experiments. We ubiquitously expressed the *UAS-pak-GFP* transgene with the heat-shock inducible driver, *m4-Gal4*, by raising the flies at 29°C. From whole adult fly lysates, GFP immunoprecipitates blotted for Dlg revealed no Dlg immunoreactive bands (data not shown). Likewise, reciprocal assays involving a *UAS-dlgA-GFP* transgene, which encodes for the predominant Dlg isoform present in epithelia, revealed no Pak immunoreactive bands when GFP immunoprecipitates were blotted for Pak (data not shown) (Woods and Bryant, 1991; Woods et al., 1996; Koh et al., 1999; Mendoza et al., 2003). Although I was not able to co-immunoprecipitate Pak and Dlg, our lab has collectively shown that Pak can form a complex with select Scrib complex members in these particular assays, indicating further that Pak associates with apicobasal polarity determinants.

1.4.2. Pak3 is present in the embryonic epidermis and, like Pak, is also a component of the Scrib complex

We wanted to test whether Pak is involved in restoring apicobasal polarity to the leading edge membrane of DME cells at the end of dorsal closure through mutant analysis. Unfortunately, *pak* zygotic mutants die relatively late in the *Drosophila* life cycle as pharate adults, i.e. the stage before the adult fly emerges from the pupal case (Hing et al., 1999). We wondered if *pak* zygotic mutants were able to survive past embryogenesis due to maternal contributions. Although a maternal and zygotic loss of *pak*, created through germline clones, does indeed cause various embryonic defects including dorsal holes, these embryos fail to complete dorsal closure precluding any evaluation of Pak function specifically at the end of dorsal closure (Conder et al., 2004).

Another possible reason as to why zygotic *pak* mutants survive embryogenesis is that Pak may be functionally redundant with the other *Drosophila* Group I Pak, Pak3 (Dan et al., 2001; Mentzel and Raabe, 2005). We therefore decided to characterize *pak3* during dorsal closure. When we began our study, *pak3* was not characterized *in vivo*. However, a recent study has shown that Pak3 localizes to the leading edge of induced wounds in the epidermis of third instar larvae where it mediates Rac1-induced organization of actin and myosin during wound closure (Baek et al., 2012).

Pak and Pak3 show high structural homology with 35.4% identity and 47.9% similarity overall, and 63.4% identity and 79.9% similarity within the kinase domain (Mentzel and Raabe, 2005). Alternative splicing produces two different Pak3 protein isoforms: Pak3-A (64kDa) and Pak3-B (46kDa) (Bahri et al., 2010). Unlike Pak and Pak3-A, Pak3-B is missing a proline-rich region between the CRIB/AID and kinase domains which is required for binding to the Rho-GEF **Pak-interacting exchange factor** (**Pix**) in mammals (Figure 8A) (Manser et al., 1998; Bahri et al., 2010).

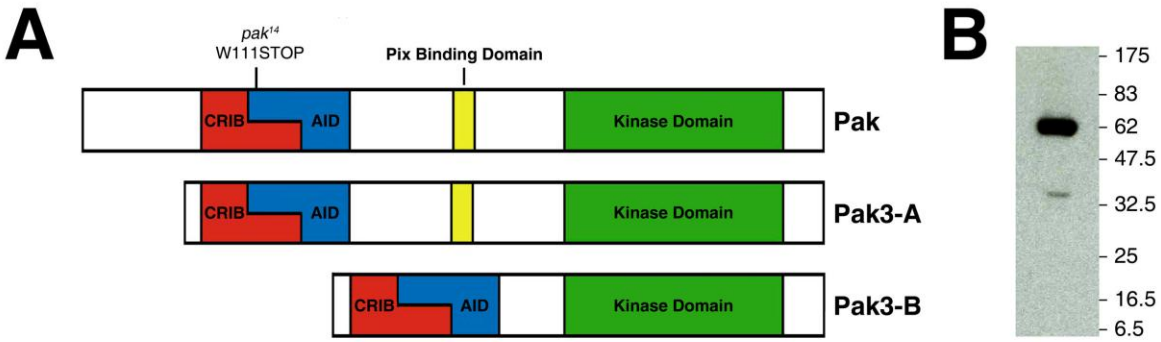
A
pak14
W111STOP
Pix Binding Domain
CRIB
AID
Kinase Domain
Pak
Pak3-A
Pak3-B
B
175
83
62
47.5
32.5
25
16.5
6.5

FIGURE 8 Pak3 is present during embryonic development.

(A) Schematic diagram showing the domain organization of Pak and the two Pak3 isoforms, Pak3-A and Pak3-B (not to scale). Unlike Pak (76kDa) and Pak3-A (64kDa), Pak3-B (46kDa) is missing a region between the CRIB/AID and kinase domains which is required for binding to the GEF, Pix, in mammals. The *pak*^{14} mutation, which is used throughout this study, is also shown. *pak*^{14} encodes for a truncated Pak protein with no kinase activity due to the presence of a premature stop codon in the CRIB/AID domain. Note that the illustrations were done by Dr. Harden. **(B)** Western blot analysis of total protein lysates from embryos ranging in age from 0-24 hours after egg laying. When blotted with the anti-Pak3 antibody, two bands are detected. The larger, stronger band is consistent with the size of Pak3-A, whereas the smaller, much fainter band is probably Pak3-B but it migrated below the predicted size.

We assessed whether Pak3 is present during embryogenesis through Western blot analysis. An anti-Pak3 polyclonal antibody in mouse was made against the 300 amino acids of the N-terminus by our collaborator, Dr. Sami Bari (Institute of Molecular and Cell Biology, Singapore) (Bahri et al., 2010). In total protein lysates of embryos ranging in age from 0-24 hours after egg laying, the antibody detected two bands (Figure 8B) (Bahri et al., 2010). The larger, stronger band was consistent with the size of Pak3-A, whereas the smaller, much fainter band was probably Pak3-B but it migrated below the predicted size. Based on this result, we show that Pak3 is present during embryonic development and that Pak3-A is the predominant isoform.

We next assessed the distribution of Pak3 proteins during dorsal closure in comparison to Pak by co-staining stage 14 wild-type embryos with antibodies against both Group I Paks. Pak3 was present throughout the embryonic epidermis, with Pak3 immunoreactive signal being detected at the cell membrane and in the cytoplasm (Figure 9A-A''; see Figure 10B) (Bahri et al., 2010). During dorsal closure, both Pak and Pak3 were enriched in the dorsal epidermis surrounding the amnioserosa (Harden et al., 1996; Bahri et al., 2010). However, Pak3 did not accumulate specifically along the leading edge of DME cells as Pak does. Furthermore, only Pak is elevated in cells that flank the transverse infoldings of the embryo known as segment border cells (Harden et al., 1996; Bahri et al., 2010).

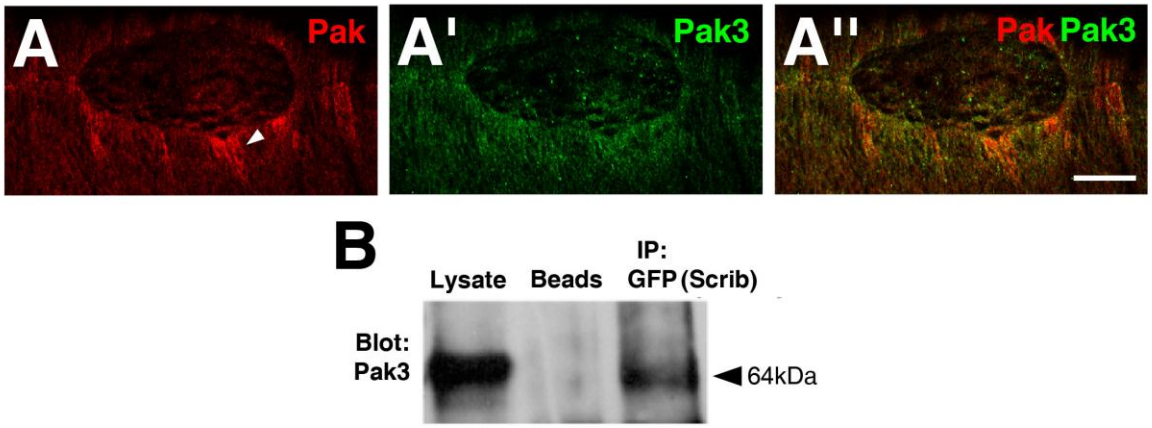
A
Pak
A'
Pak3
A''
Pak Pak3
B
Lysate
Beads
IP:
GFP (Scrib)
Blot:
Pak3
64kDa

FIGURE 9 Pak3 is present in the embryonic epidermis, and is a component of the Scrib complex.

(A-A'') Dorsolateral view of a stage 14 wild-type embryo co-stained with antibodies against Pak3 and Pak. Similar to Pak, Pak3 is present thro.ughout the embryonic epidermis, with immunoreactive signal detected at the cell membrane and in the cytoplasm. During dorsal closure, both Pak and Pak3 are enriched in the dorsal epidermis surrounding the amnioserosa. However, Pak3 does not accumulate specifically along the leading edge of DME cells. In addition, only Pak is elevated in cells that flank the segment borders (see white arrowhead). **(B)** Co-immunoprecipitation assays between Pak3 and Scrib. *UAS-scrib-GFP* was ubiquitously expressed with *m4-Gal4* by raising the flies at 29°C. From whole adult fly lysates, GFP immunoprecipitates blotted for Pak3 reveal an immunoreactive band representing Pak3-A. Pak3 was not pulled down in our negative control assays involving IgG (''Beads''). Scale bar in panel A'' represents 25µm (A-A'').

We were curious about whether the enrichment of Pak3 in the dorsal epidermis signifies a role in the restoration of apicobasal polarity to the leading edge membrane of DME cells at the end of dorsal closure. Based on the literature, though, Pak3 may more likely be required for maintaining the leading edge cytoskeleton (Mentzel and Raabe, 2005; Baek et al., 2012). Nonetheless, we assessed if Pak3 can also associate with the Scrib complex by performing co-immunoprecipitation assays. We ubiquitously expressed a *UAS-pak3-GFP* transgene, which was also made by Dr. Bahri, with the *m4-Gal4* heat-shock driver by raising the flies at 29°C (Bahri et al, 2010). From whole adult fly extracts, GFP immunoprecipitates blotted for Scrib revealed no immunoreactive bands that corresponded to Scrib (data not shown) (Zeitler et al., 2004). However, reciprocal assays involving a *UAS-scrib-GFP* transgene revealed a Pak3 immunoreactive band representing Pak3-A in GFP immunoprecipitates (Figure 9B) (Zeitler et al., 2004; Bahri et al., 2010). Similar experiments were performed between Pak3 and the Dlg isoform present in epithelia, but Pak3 and DlgA did not co-immunoprecipitate in these assays (data not shown) (Koh et al., 1999). We could not test for the presence of Lgl in Pak3-GFP immunoprecipitates as we no longer had any anti-Lgl antibody left. Unfortunately, the group that originally made the antibody no longer had a stock of it, though they are in the midst of making more (Betschinger et al., 2003). We did, however, recently obtain Myc-tagged *lgl* transgenes which will allow us to test whether Pak3 can be detected in Myc immunoprecipitates in the near future (Betschinger et al., 2003). From these results, we show that Pak3 can form a complex with select Scrib complex members in these particular assays, indicating that Pak3 can also associate with apicobasal polarity determinants.

1.4.3. Pak and Pak3 genetically interact during dorsal closure

When we began our studies, there were not many *pak3* mutations available. Through imprecise excision of the P element insertion, *EP(3)1191*, which lies 67 base pairs downstream of the *pak3* transcription start point, two new *pak3* alleles were

created by Dr. Bahri: *pak3*^{27A} and *pak3*^{76A} (Figure 10A) (Spradling et al., 1999; Bahri et al., 2010). The *pak3*^{27a} and *pak3*^{76a} alleles contain deletions that remove the first 325 and 148 codons of Pak3-A respectively (Bahri et al., 2010). When stained with the anti-Pak3 antibody, both *pak3*^{27a} and *pak3*^{76a} mutant embryos lacked any detectable Pak3 immunoreactive signal in comparison to wild-type suggesting that both alleles are null mutations (data not shown and Figure 10B,C) (Bahri et al., 2010). These results also show that the anti-Pak3 antibody is specific to Pak3 and does not cross-react with Pak. As both alleles are similar in nature, we arbitrarily chose to analyze further the *pak3*^{76a} allele in our studies.

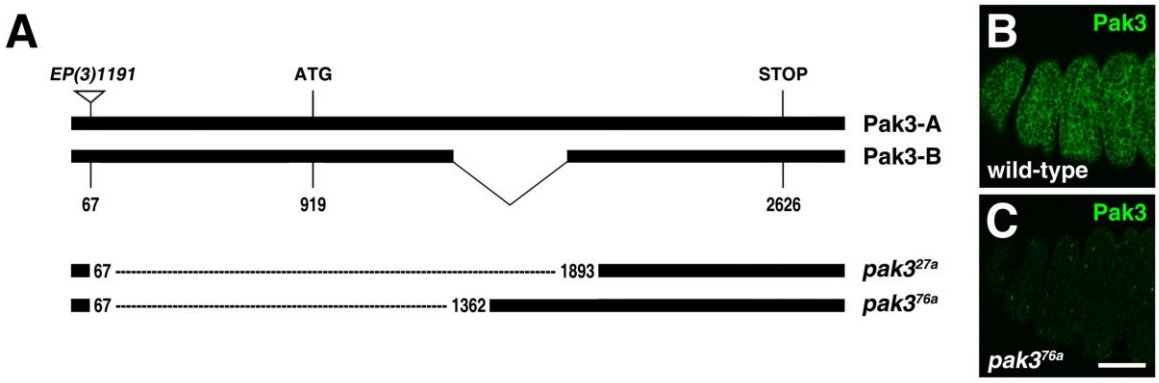
A
EP(3)1191
ATG
STOP
Pak3-A
Pak3-B
67
919
2626
67
1893
pak3^27a
67
1362
pak3^76a
B
Pak3
wild-type
C
Pak3
pak3^76a

FIGURE 10 *pak3* mutations created through imprecise P element excisions.

(A) Schematic diagram of wild-type and mutant *pak3* transcripts (not to scale). The P element insertion, *EP(3)1191*, lies 67 base pairs downstream of the transcription start site (see white triangle). Through imprecise excisions, two *pak3* alleles were created: $pak3^{27a}$ *and* $pak3^{76a}$. The $pak3^{27a}$ and $pak3^{76a}$ alleles contain deletions that remove the first 325 and 148 codons of Pak3-A respectively (see dotted lines). Numbers indicate nucleotide position corresponding to the Pak3-A transcript. Note that the illustrations were done by Dr. Harden. **(B-C)** Comparative analysis of wild-type (B) and $pak3^{76a}$ mutant (C) embryos stained with the anti-Pak3 antibody. $pak3^{76a}$ mutant embryos lack detectable Pak3 immunoreactive signal in the embryonic epidermis compared to wild-type. Scale bar in panel C represents 50µm (B-C).

We determined whether the two Group I Paks in *Drosophila* have redundant roles during dorsal closure by comparing *pak3* single mutants to *pak* and *pak3* double mutants using embryonic cuticle preparations. *pak* and *pak3* double mutants were created by Dr. Conder who recombined $pak3^{76a}$ with pak^{14}, an allele which encodes for a truncated Pak protein with no kinase activity due to the presence of a premature stop codon in the CRIB/AID domain (see Figure 8A) (Newsome et al., 2000). Whether in $pak3^{76a}$ single mutants, embryos homozygous mutant for one gene and heterozygous mutant for the other, or $pak^{14}pak3^{76a}$ double mutants, the same embryonic defects were observed (see Figure 11B-D for representative images) (Bahri et al., 2010). These included anterior holes which represent defects in head involution, in addition to dorsal holes and puckers which represent defects in dorsal closure. Interestingly, $pak3^{76a}$ single mutants showed a similar frequency of dorsal closure defects in comparison to $pak^{14}pak3^{76a}$ double mutants (Figure 11E). This suggests that Pak3 plays a more siginificant role in dorsal closure than Pak. However, Pak3 may also have less of a maternal contribution compared to Pak, thus possibly explaining why $pak3^{76a}$ mutants die at a higher frequency during embryonic development than pak^{14} mutants. That being said, we provide evidence that Pak and Pak3 genetically interact during dorsal closure as $pak^{14}pak3^{76a}/pak^{14}$ mutants showed an increased frequency of dorsal closure defects when compared to pak^{14} mutants (Figure 11E). Additionally, ubiquitous expression of a *UAS-pak* transgene with *hs-Gal4* by incubating the embryos at 29°C effectively suppressed the $pak^{14}pak3^{76a}$-associated defects observed in the dorsal cuticle, though it was less effective at rescuing the anterior holes (Figure 11E; data not shown) (Bahri et al., 2010). Our results indicate that Pak and Pak3 genetically interact during dorsal closure, though the nature of this interaction remains unkown.

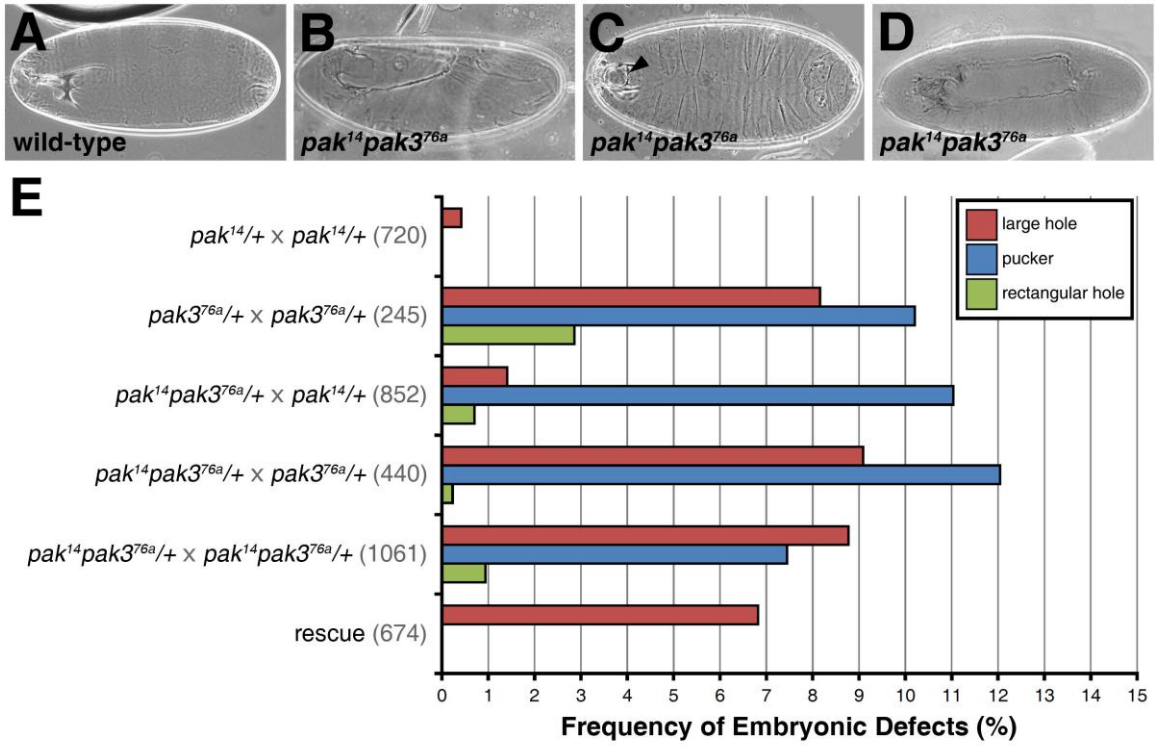
A
wild-type
B
pak14pak3 76a
C
pak14pak3 76a
D
pak14pak3 76a
E
pak14/+ x pak14/+ (720)
pak3 76a/+ x pak3 76a/+ (245)
pak14pak3 76a/+ x pak14/+ (852)
pak14pak3 76a/+ x pak3 76a/+ (440)
pak14pak3 76a/+ x pak14pak3 76a/+ (1061)
rescue (674)
large hole
pucker
rectangular hole
0 1 2 3 4 5 6 7 8 9 10 11 12 13 14 15
Frequency of Embryonic Defects (%)

FIGURE 11 Pak and Pak3 genetically interact during dorsal closure.

(A-D) Representative embryonic cuticle defects typically observed in *pak* and *pak3* single and double mutants. Compared to the wild-type embryonic cuticle (A), the most prevalent phenotypes were defects in the dorsal cuticle including large holes (B), puckers (C) and rectangular openings (D). Most mutant embryos also exhibited an additional anterior hole (see black arrowhead in panel C). **(E)** Quantification of embryos with dorsal closure defects consisting either of large holes, puckers or rectangular openings. Progeny were examined from stocks and crosses bearing pak^{14} and $pak3^{76a}$ mutations, and are listed to the left of each bar of the graph. Numerical values in brackets denote the total number of progeny counted. The rescue involved ubiquitous expression of a *UAS-pak* transgene with *hs-Gal4* in $pak^{14}pak3^{76a}$ double mutant embryos raised at 29°C. These results collectively show that Pak and Pak3 genetically interact during embryonic development.

1.4.4. Pak and Pak3 are required for Scrib complex recruitment and septate junction formation at the leading edge membrane of DME cells upon dorsal closure completion

We further examined the dorsal closure defects observed in our cuticle preparations by staining $pak^{14}pak3^{76a}$ mutant embryos with antibodies against Scrib, Lgl and Dlg in order to assess the status of the Scrib complex at the leading edge membrane of DME cells upon dorsal closure completion. We decided not to look at embryos with large dorsal holes, as dorsal closure had probably not progressed due to actin cytoskeletal defects. Instead, we focused on embryos that likely corresponded to the puckered cuticle phenotype, as these embryos potentially had defects late in dorsal closure. In these particular embryos, the epidermal flanks appeared to have come together at the dorsal midline, but Scrib, Lgl and Dlg all failed to be restored at the leading edge membrane of DME cells in contrast to similarly staged wild-type embryos (Figure 12A-F) (Bahri et al., 2010). Disruption of Scrib complex recruitment strongly suggested that septate junctions were not being formed at the dorsal midline. This was confirmed by Dr. Harden with the use of antibodies against the septate junction proteins, Cora and FasIII (data not shown) (Bahri et al., 2010). Interestingly, the effects of the *pak* and *pak3* mutations were restricted to the leading edge membrane of the DME cells, as there were no disruptions observed in Scrib complex localization and septate junction formation along the other membranes of the DME cells, as well as throughout the rest of the epidermis. Work done by Dr. Stephanie Vlachos, a former Ph.D. student under Dr. Harden, has shown that the localization of the Scrib complex is also disrupted in *pak* somatic clones in the follicular epithelium (see the thesis entitled ''Characterization of the p21-activated kinase Pak during *Drosophila* oogenesis'' which was submitted to the SFU Library in 2012) (Bahri et al., 2010). Collectively, our results suggest that Pak and Pak3 regulate apicobasal polarity only in membranes undergoing MET, or MET-like, events. We conclude that Pak and Pak3 are required for Scrib complex restoration and septate junction formation specifically at the leading edge

membrane of DME cells upon dorsal closure completion. Note that we did not evaluate the status of the Crb and Baz/Par-3 complexes.

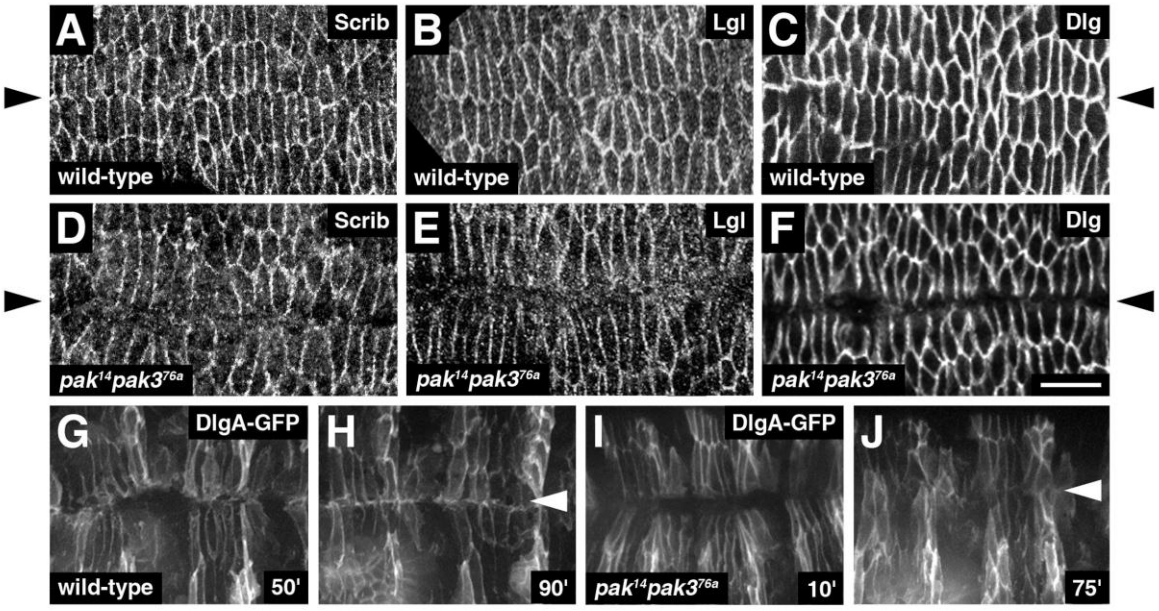
A
Scrib
wild-type
B
Lgl
wild-type
C
Dlg
wild-type
D
Scrib
pak14pak376a
E
Lgl
pak14pak376a
F
Dlg
pak14pak376a
G
DlgA-GFP
wild-type
50'
H
90'
I
DlgA-GFP
pak14pak376a
10'
J
75'

FIGURE 12 Pak and Pak3 recruit the Scrib complex to the leading edge membrane of DME cells at the end of dorsal closure.

(A-F) Dorsal views of stage 15 wild-type (A-C) and *pak*^{14}*pak3*^{76a} mutant (D-F) embryos stained with antibodies against Scrib (A,D), Lgl (B,E) and Dlg (C,F). In *pak*^{14}*pak3*^{76a} mutant embryos, the epidermal flanks appear to meet at the dorsal midline, but Scrib, Lgl and Dlg are not restored at the leading edge membrane of DME cells in contrast to similarly staged wild-type embryos. Dorsal midlines are denoted with black arrowheads. **(G-J)** Live image analysis of wild-type (G-H) and *pak*^{14}*pak3*^{76a} mutant (I-J) embryos expressing *UAS-dlgA-GFP* with *ptc-Gal4* during dorsal closure. (G-H) In a wild-type background, DlgA-GFP is missing at the leading edge membrane of DME cells during dorsal closure. Upon dorsal closure completion, DlgA-GFP is restored at the dorsal midline (see white arrowhead). (I-J) In a *pak*^{14}*pak3*^{76a} mutant background, however, DlgA-GFP is not observed at the dorsal midline (see white arrowhead), even though the dorsal hole has completely closed and the opposing epidermal flanks are clearly in contact with each other. Images were processed from stills taken from Movies 3 and 4 (see the attached CD-ROM). Scale bar in panel F represents 10µm (A-F).

Our initial impression was that the epidermal flanks in these *pak*^{14}*pak3*^{76a} mutant embryos stop just short of making contact with each other, thus leaving behind an open cleft. This may provide a plausible explanation as to why we did not observe Scrib complex recruitment at the leading edge membrane of DME cells, as dorsal closure may not have actually proceeded to completion. However, we provide three key results that strongly indicate that the epidermal flanks are indeed in contact with each other. First, most of the late dorsal closure defects that were observed in our cuticle preparations corresponded to a puckered phenotype in the dorsal cuticle that contained no apparent hole or slit (see Figure 11C) (Bahri et al., 2010). Second, the dorsal vessel in these mutant embryos had developed normally (Figure 13B) (Bahri et al., 2010). During dorsal closure, two rows of cardioblast and pericardial cells, which flank both sides of the dorsal hole, migrate towards each other along with the overlying epidermis (Figure 13A) (reviewed in Tao and Schulz, 2007). These cells meet and fuse at the dorsal midline upon dorsal closure completion, thus forming a four-row cellular structure, which can be observed in *pak*^{14}*pak3*^{76a} mutants, that eventually becomes the dorsal vessel, i.e. the major structural component of the circulatory system. Third, we observed a rare phenotype where mildly affected *pak*^{14}*pak3*^{76a} mutant embryos showed, in patches, Dlg restoration on one side of the dorsal midline but not the other (Figure 13C') (Bahri et al., 2010). We are certain that these opposing DME cells are in contact with each other as we co-stained such embryos with an anti-DE-Cad antibody that marks the adherens junctions (Figure 13C,C'') (Oda et al., 1994). Note, however, that DE-Cad is usually not restored in *pak*^{14}*pak3*^{76a} mutants (see the next section). One possible explanation for the cleft-like appearance in these *pak*^{14}*pak3*^{76a} mutant embryos is that the opposing leading edges come together in a zig zag pattern at the end of dorsal closure (Figure 13D). Thus, failure to restore Scrib complex proteins at the dorsal midline when viewed with immunofluorescence staining gives the impression of an open slit when in fact the epidermal flanks are directly in contact (Figure 13E).

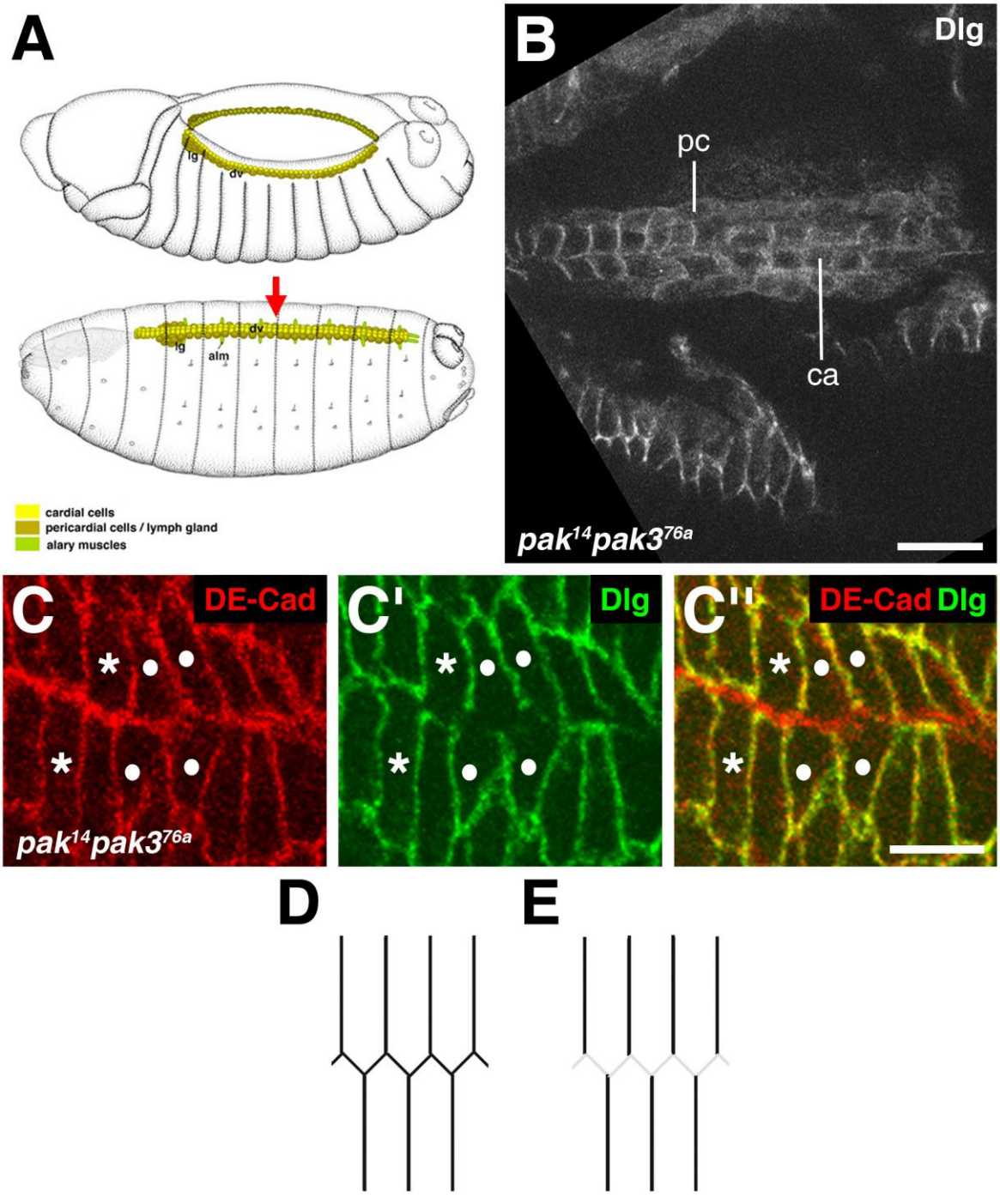
A
lg
dv
dv
lg
alm
cardial cells
pericardial cells / lymph gland
alary muscles
B
Dlg
pc
ca
pak14pak376a
C
DE-Cad
pak14pak376a
C'
Dlg
C''
DE-Cad Dlg
D
E

FIGURE 13 Evidence that *pak*^{14}*pak3*^{76a} mutant embryos complete dorsal closure.

(A) Schematic diagram of dorsal vessel formation. Two rows of cardioblast (yellow) and pericardial (brown) cells, which flank both sides of the dorsal hole, migrate with the overlying epidermis during dorsal closure. These cells meet and fuse at the dorsal midline upon dorsal closure completion, forming a four-row cellular structure that eventually becomes the dorsal vessel. Note that the images were modified from ''Atlas of Drosophila Development'' by Volker Hartenstein. **(B)** Dorsal view of a stage 15 *pak*^{14}*pak3*^{76a} mutant embryo, that lacks Dlg restoration at the dorsal midline, viewed just below the epidermis to visualize the dorsal vessel (see red arrow in panel A for orientation). In these particular embryos, the dorsal vessel forms normally indicating that dorsal closure has gone to completion. **(C-C'')** High magnification view of opposing DME cells at the dorsal midline co-stained with antibodies against Dlg and DE-Cad. In rare cases, mildly affected *pak*^{14}*pak3*^{76a} mutant embryos show Dlg restoration on one side of the midline but not the other (see cells with asterisks), as opposed to the more common observation where Dlg is missing on both sides (see cells with white dots). As demonstrated by DE-Cad staining in these embryos, the opposing DME cells are indeed in contact with each other. Note that DE-cad restoration in *pak*^{14}*pak3*^{76a} mutant embryos usually does not occur (see Figure 14). **(D-E)** Schematic diagram of Dlg immunoreactivity at the dorsal midline of stage 15 wild-type (D) and *pak*^{14}*pak3*^{76a} mutant (E) embryos. Opposing leading edges come together in a zig zag pattern at the end of dorsal closure. Thus, failure to restore Dlg at the dorsal midline when viewed by immunofluorescence staining gives the impression of an open slit when in fact the epidermal flanks are directly in contact with each other. Note that the illustrations were done by Dr. Harden. Scale bar in panel B represents 10µm (B), scale bar in panel C'' represents 5µm (C-C''). dv = dorsal vessel, lg = lymph gland, alm = alary muscles, ca = cardioblast cells, pc = pericardial cells.

To complement the results we observed in fixed embryos, we also tracked the Scrib complex near the end of dorsal closure by live imaging wild-type and *pak*^{14}*pak3*^{76a} mutant embryos expressing transgenic *UAS-dlgA-GFP* in the epidermis with the segmental *ptc-Gal4* driver. In wild-type embryos, DlgA-GFP was observed at the dorsal midline, first appearing shortly after opposing DME cells contact each other, usually several cells back from the canthi (see Figure 12G,H) (see Movie 3 in the attached CD-ROM) (Bahri et al., 2010). In *pak*^{14}*pak3*^{76a} mutant embryos, on the other hand, DlgA-GFP was not observed at the dorsal midline even though the dorsal hole had completely closed and the opposing epidermal flanks were clearly in contact with each other (see Figure 12I,J) (see Movie 4 in the attached CD-ROM) (Bahri et al., 2010).

1.4.5. Pak and Pak3 are also required for adherens junction formation at the leading edge membrane of DME cells upon dorsal closure completion

Although we are primarily interested in the regulation of polarity determinants and junctions along the basolateral membrane, we decided to examine the effects of Pak and Pak3 on adherens junction restoration along the apicolateral membrane of the leading edge of DME cells at the end of dorsal closure. We accomplished this by staining stage 15 embryos mutant for *pak*^{14}*pak3*^{76a} with an antibody against DE-Cad, a transmembrane protein that serves as a major component of the adherens junction complex (Oda et al., 1994). In *pak*^{14}*pak3*^{76a} mutant embryos, DE-Cad was usually not restored at the leading edge membrane of DME cells upon dorsal closure completion when compared to similarly staged wild-type embryos (Figure 14A,B) (Bahri et al., 2010). Given the requirement of the Group I Paks in adherens junction restoration at the end of dorsal closure, as well as the presence of Pak at the apical ends of embryonic epidermal cells (see Figure 7B'), we wondered if Pak and Pak3 exist in a complex with adherens junction proteins. For this particular experiment, we immunoprecipitated DE-Cad from wild-type whole adult fly extracts using the anti-DE-Cad antibody (Bahri et al., 2010). Under conditions in which Arm, a homologue to β-catenin which has been shown to bind to DE-Cad, was successfully pulled down with DE-Cad, neither Pak nor

Pak3 were pulled down (Figure 14C; data not shown) (Rimm et al., 1995; Bahri et al., 2010). We conclude that Pak and Pak3 are required for adherens junction restoration at the leading edge membrane of DME cells upon dorsal closure completion, but they do not specifically form a complex with adherens junction proteins.

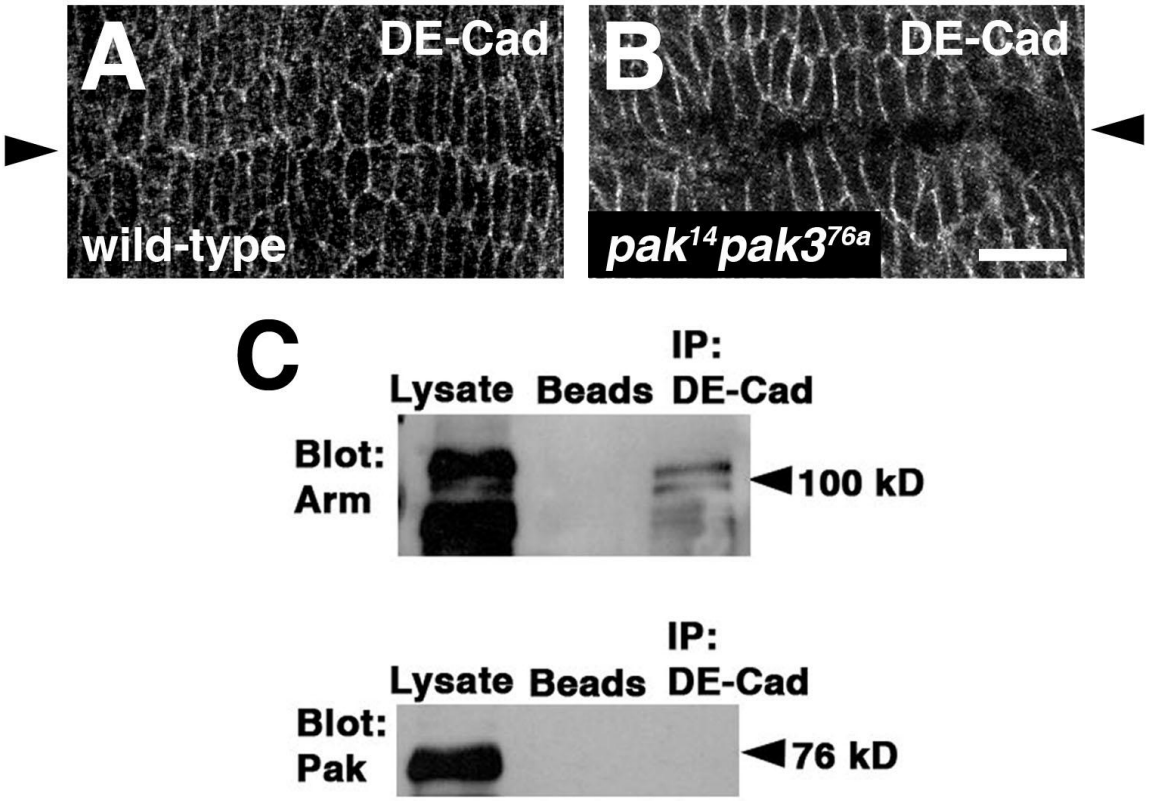
A
DE-Cad
wild-type
B
DE-Cad
pak14pak376a
C
IP:
Lysate Beads DE-Cad
Blot:
Arm
100 kD
IP:
Lysate Beads DE-Cad
Blot:
Pak
76 kD

FIGURE 14 Pak and Pak3 restore adherens junctions to the leading edge membrane of DME cells at the end of dorsal closure.

(A-B) Dorsal views of stage 15 wild-type (A) and $pak^{14}pak3^{76a}$ mutant (B) embryos stained with an anti-DE-Cad antibody. In $pak^{14}pak3^{76a}$ mutant embryos, DE-Cad is generally not restored to the leading edge membrane of DME cells at the end of dorsal closure when compared to similarly staged wild-type embryos. Dorsal midlines are denoted with black arrowheads. **(C)** Co-immunoprecipitation assays between Pak and DE-Cad. Endogenous DE-Cad was immunoprecipitated from wild-type whole adult fly extracts using the anti-DE-Cad antibody. Under conditions in which Arm (a 105-110kDa doublet) was successfully pulled down with DE-Cad, Pak was not pulled down. No proteins were pulled down in our negative control assays involving IgG (''Beads''). Scale bar in panel B represents 50μm (A-A'').

1.4.6. Pak distribution in the embryonic epidermis is integrin-dependent

Integrin-mediated recruitment of mammalian Paks to focal adhesion sites appears to be conserved in *Drosophila*, as Pak membrane localization in the follicular epithelium is dependent on integrins (reviewed in Bokoch, 2003; Conder et al., 2007). If Pak recruitment to the lateral membrane of embryonic epidermal cells is also integrin-dependent, we would expect to see appreciable levels of laterally localized integrins during embryonic development. Interestingly, it has been previously reported that there are high levels of integrins along the lateral membranes of amnioserosa cells and at the leading edge of DME cells during dorsal closure (see Figure 16A) (Narasimha and Brown, 2004). We determined whether the accumulation of Pak at the leading edge of DME cells during dorsal closure is integrin-dependent by examining Pak distribution in *mys* mutants. *mys* encodes for the main βPS-integrin found in *Drosophila* (reviewed in Takada et al., 2007). In mys^{G1} mutant embryos, Pak accumulation at the leading edge of DME cells was abolished, as was Pak localization along the lateral membrane throughout the epidermis when compared to wild-type (Figure 15A-D) (Jannuzi et al., 2002) (Bahri et al., 2010). Thus, Pak localization in the embryonic epidermis is integrin-dependent.

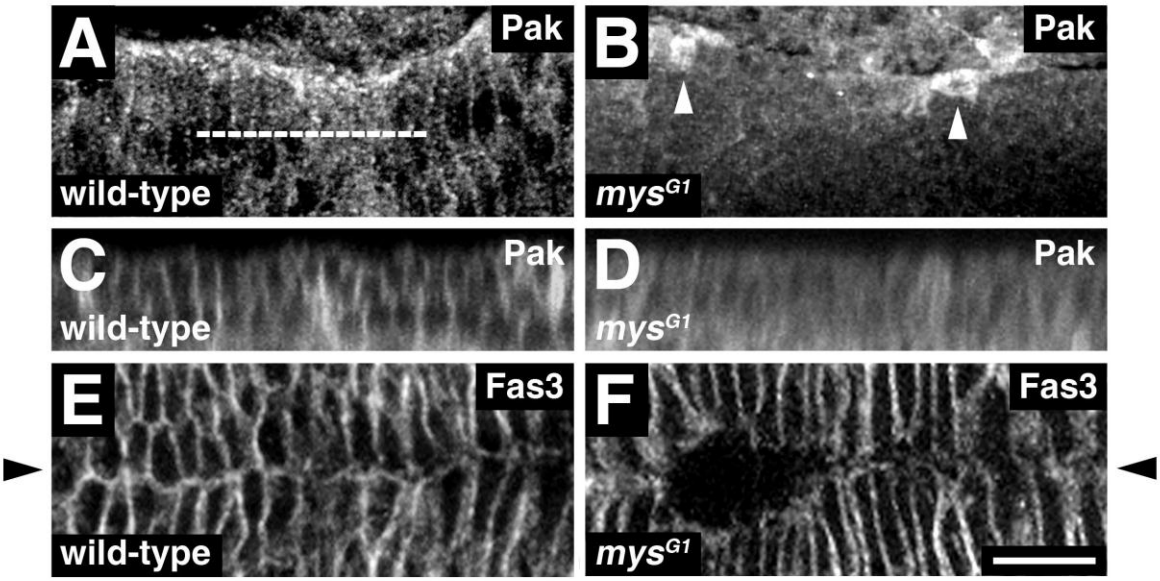
A
Pak
wild-type
B
Pak
mysG1
C
Pak
wild-type
D
Pak
mysG1
E
Fas3
wild-type
F
Fas3
mysG1

FIGURE 15 Pak distribution in embryonic epidermal cells during dorsal closure is dependent on integrins.

(A-B) Dorsolateral views of stage 14 wild-type (A) and *mys*^{G1} mutant (B) embryos stained with the anti-Pak antibody. In *mys*^{G1} mutant embryos, Pak accumulation along the leading edge of DME cells is disrupted, as is Pak cortical localization throughout the epidermis, in comparison to wild-type. However, Pak still concentrates around embryonic segment borders (see white arrowheads). **(C-D)** Cross-sectional view of a row of DME cells in wild-type (C) and *mys*^{G1} mutant (D) embryos stained with the anti-Pak antibody (see the dashed line in panel A as an example of where the z-sections were taken). Pak localization along the lateral membrane is disrupted in *mys*^{G1} mutants in comparison to wild-type. **(E-F)** Dorsal views of stage 15 wild-type (E) and *mys*^{G1} mutant (F) embryos stained with an antibody against the septate junction protein, Fas3. In *mys*^{G1} mutant embryos, septate junctions are not formed between opposing DME cells at the dorsal midline when compared to similarly staged wild-type embryos. Dorsal midlines are denoted with black arrowheads. Scale bar in panel F represents 10µm (A-B,E-F).

We postulated that the high levels of lateral integrins present at the leading edge membrane of DME cells during dorsal closure are responsible for the accumulation of Pak, which is in turn required for Scrib complex restoration and septate junction formation at the end of dorsal closure. If this is true, then integrins should also be involved in this process. To test our hypothesis, we assessed whether septate junctions were being formed at the end of dorsal closure in *mys* mutant embryos. This was challenging as *mys* mutant embryos tend to burst open at the end of dorsal closure (Bahri et al., 2010). However, we were able to find some mys^{XG43} mutant embryos where the epidermal flanks were still in contact at the end of dorsal closure, but the septate junction protein, Fas3, was not recruited to the leading edge membrane of DME cells (Figure 15E,F) (Bahri et al., 2010). Although we did not assess the status of the Scrib complex directly in these embryos, Dr. Vlachos has shown that the lateral localization of Dlg is disrupted in *mys* follicle cell clones (see the thesis entitled ''Characterization of the p21-activated kinase Pak during *Drosophila* oogenesis'' which was submitted to the SFU Library in 2012) (Bahri et al., 2010). These results collectively show that integrins are required for Scrib complex recruitment and septate junction formation in epithelial cells, presumably by regulating Pak localization.

During dorsal closure, the distribution of integrins along the lateral membrane of epithelial cells is strikingly complementary to the distribution of septate junction proteins (Figure 16A) (Bahri et al., 2010). Septate junction proteins, like Cora, are present throughout the epidermis with the exception of the leading edge membrane of DME cells. In addition, septate junction proteins are also absent in the amnioserosa. Lateral integrin levels, in contrast, are highest in the amnioserosa and at the leading edge of DME cells, but are present only at modest levels along the other membranes of the DME cells and throughout the rest of the epidermis where they are predominately found along the basal membrane. We hypothesized that the absence of septate junctions at the leading edge membrane of DME cells and amnioserosa cells removes a selective barrier, allowing for the accumulation of integrins up into the lateral

membrane. Interestingly, *pak*^{14}*pak3*^{76a} mutant embryos at the end of dorsal closure displayed persistently high levels of lateral integrins along the entire dorsal midline in comparison to wild-type embryos, which may be attributed to a lack of septate junction restoration (Figure 16B,C) (Bahri et al., 2010). We tested this hypothesis further by examining lateral integrin distribution in embryos mutant for septate junction components. In *cora*^{14} mutant embryos, we observed elevated levels of lateral integrins in DME cell membranes other than the leading edge (Figure 16D,E) (Lamb et al., 1998; Bahri et al., 2010). The idea that septate junctions restrict the lateral accumulation of integrins has further been supported by studies done in the egg chamber by Dr. Vlachos. She has reported that *scrib* mutant follicle cells, as well as *cora* mutant stalk cells, show ectopic integrin accumulation along the lateral membrane (see the thesis entitled ''Characterization of the p21-activated kinase Pak during *Drosophila* oogenesis'' which was submitted to the SFU Library in 2012) (Bahri et al., 2010). We propose that the absence of septate junctions along the leading edge membrane of DME cells results in the lateral accumulation of integrins necessary for Pak recruitment, which in turn is required for Scrib complex restoration and septate junction formation at the end of dorsal closure. In other words, the lack of septate junctions leads to a series of events which are necessary for its appearance later on.

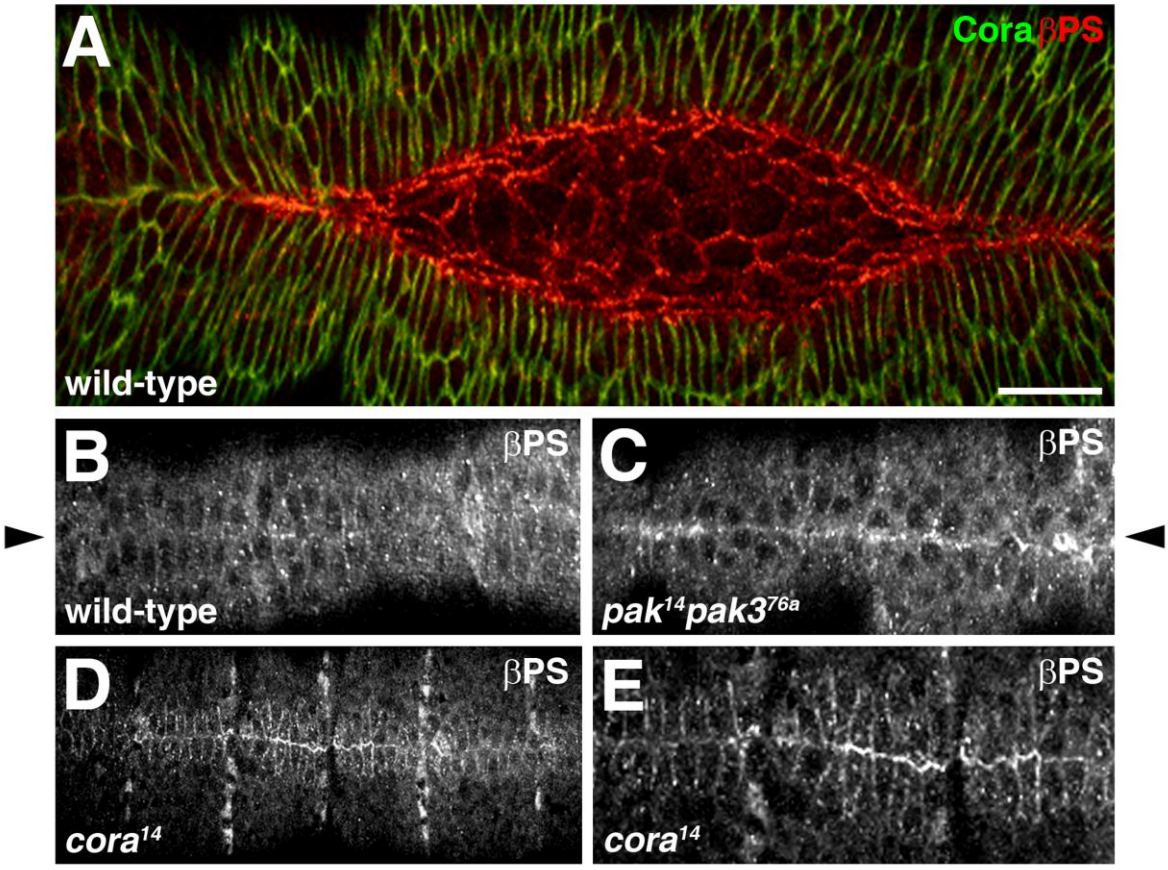
A
Cora βPS
wild-type
B
βPS
wild-type
C
βPS
pak14pak376a
D
βPS
cora14
E
βPS
cora14

FIGURE 16 The distribution patterns of septate junctions and integrins along the lateral membrane of epidermal cells are complementary.

(A) Dorsal view of a stage 15 wild-type embryo stained with antibodies against Cora and βPS-integrin. During dorsal closure, Cora is present throughout the epidermis with the exception of the leading edge membrane of DME cells. Additionally, Cora is absent in the amnioserosa. In contrast, lateral integrin levels are highest in the amnioserosa and at the leading edge of DME cells, but are present only at modest levels along the other membranes of the DME cells and throughout the rest of the epidermis. **(B-C)** Dorsal views of stage 15 wild-type (B) and $pak^{14}pak3^{76a}$ mutant (C) embryos stained with the anti-βPS-integrin antibody. $pak^{14}pak3^{76a}$ mutant embryos display persistently high levels of lateral integrins along the entire dorsal midline in comparison to similarly staged wild-type embryos. **(D-E)** Dorsal view of a stage 15 $cora^{14}$ mutant embryo stained with the anti-βPS-integrin antibody. In $cora^{14}$ mutant embryos, DME cell membranes other than the leading edge have elevated levels of lateral integrins when compared to wild-type. Scale bar in panel A represents 10µm (A-C,E).

1.5. Discussion

1.5.1. Pak and Pak3 are required for Scrib complex recruitment and septate junction formation at the leading edge membrane of DME cells upon dorsal closure completion

During dorsal closure, epithelial apicobasal polarity determinants and intercellular junctions are dynamically regulated at the leading edge membrane of DME cells, which we propose can serve as a model for EMTs and METs (Bahri et al., 2010). Such complexes, which include the Scrib complex and septate junctions, are missing at the leading edge as dorsal closure begins, but are then recruited to the leading edge as opposing DME cells meet at the dorsal midline upon dorsal closure completion. Our data reveal that Pak and Pak3 are components of the Scrib complex in the embryonic epidermis. We show that the Paks interact to promote Scrib complex recruitment and septate junction formation along the leading edge membrane of DME cells at the end of dorsal closure (Figure 17). We provide evidence that the absence of the Scrib complex and septate junction proteins at the leading edge membrane during dorsal closure, allows for the accumulation of lateral integrins. Lateral integrins are used to anchor Pak, which in turn recruits the Scrib complex and septate junction proteins back to the leading edge membrane at the end of dorsal closure. Thus, the absence of septate junctions allows the recruitment of proteins needed for the assembly of septate junctions later on. Our results indicate that the Paks only regulate apicobasal polarity at the leading edge membrane of the DME cells, and not the other membranes of the DME cells or the rest of the embryonic epidermis. We propose that the Paks restore apicobasal polarity only in membranes undergoing MET, or MET-like events. This is supported by previous work done in our lab which shows that Pak can regulate apicobasal polarity in the follicular epithelium, a tissue derived from an MET (Conder et al., 2007; Bahri et al, 2010).

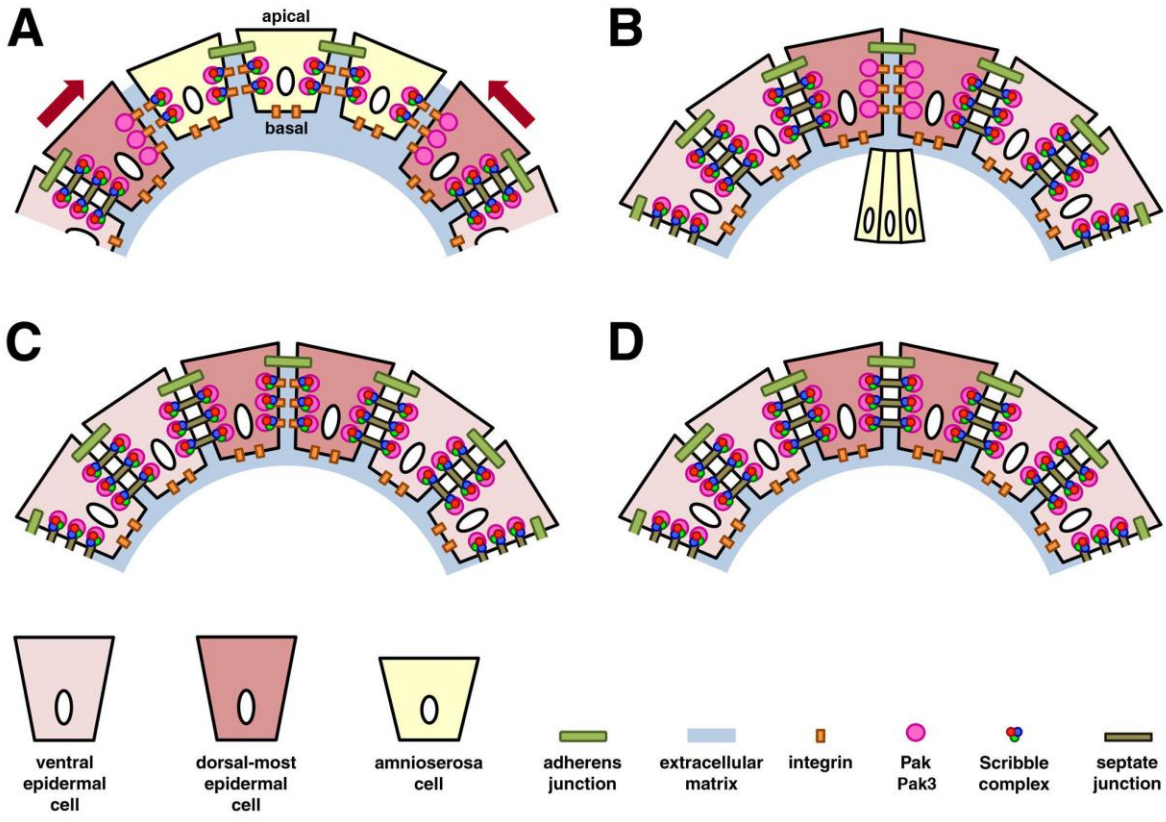
A
apical
basal
B
C
D
ventral epidermal cell
dorsal-most epidermal cell
amnioserosa cell
adherens junction
extracellular matrix
integrin
Pak Pak3
Scribble complex
septate junction

FIGURE 17 Model for Pak-mediated Scrib complex recruitment and septate junction formation at the leading edge membrane of DME cells upon dorsal closure completion.

(A-D) Schematic of an embryo viewed in cross-section during different stages of dorsal closure. (A) During dorsal closure, the Scrib complex and septate junction proteins are missing at the leading edge membrane of DME cells. Due to the absence of septate junctions, high levels of integrins amass laterally along the apicobasal axis leading to the progressive accumulation of Pak, and possibly Pak3. (B) Upon dorsal closure completion, DME cells on opposing epidermal flanks meet at the dorsal midline as the amnioserosa is internalized. (C) Pak and Pak3 interact to recruit the Scrib complex back to the leading edge membrane. (D) As septate junctions form between opposing DME cells, the lateral integrins are displaced and become once again restricted predominately to the basal membrane.

Previous mammalian cell studies have shown that Scrib recruits the Paks to the leading edge during cell migration (Nola et al., 2008). Activated by Cdc42/Rac signalling, the Paks promote actin polymerization and contributes to cytoskeleton reorganization. In this thesis, we show that the relationship between the Paks and the Scrib complex can act in the opposite direction at the end of cell migration. We propose that Scrib at the newly formed leading edge initially sets up the recruitment of the Rac/Cdc42 signalling complex which includes Pak, allowing for the acquisition of mesenchymal characteristics and polarized cell migration. At the end of cell migration, events can be reversed with Pak recruiting Scrib back to the leading edge, thereby contributing to the restoration of apicobasal polarity and cell adhesion. Thus, we view the Scrib-Pak interaction as a ''toggle switch'', enabling the epithelial membrane to shift back and forth between a migratory state characterized by actin-based extensions and an apicobasal polarized state characterized by cell-cell adhesion.

1.5.2. Pak distribution in the embryonic epidermis is integrin-dependent

We show that the localization of Pak along the lateral membrane of embryonic epidermal cells, as well as its accumulation at the leading edge of DME cells during dorsal closure, is integrin-dependent. Similar observations were made by Dr. Vlachos, as she has shown that Pak localization in the follicular epithelium is also dependent on integrins (see the thesis entitled ''Characterization of the p21-activated kinase Pak during *Drosophila* oogenesis'' which was submitted to the SFU Library in 2012) (Bahri et al., 2010). We propose that during dorsal closure, lateral integrins along the leading edge membrane are required to recruit Pak, which in turn restores the Scrib complex at the end of dorsal closure. Our hypothesis thus implicates integrins in apicobasal polarity. In this thesis, we show that *mys* mutant embryos, which are deficient in the main βPS-integrin found in *Drosophila*, fail to recruit the septate junction protein, Fas3, to the leading membrane of DME cells upon dorsal closure completion. Additionally, our lab has previously implicated integrins in regulating apicobasal polarity in follicular

epithelial cells during oogenesis (Conder et al., 2007; Bahri et al., 2010). Our work has been supported by several studies done in the midgut, organ culture of embryonic kidney mesenchyme and MDCK cells, which are all derived from METs. These results all show that integrins are required for apicobasal polarity in epithelial cells that are derived from METs. Our work indicates the existence of a transitory link between the Scrib complex and integrins, which is mediated by Pak, in epithelial cells. Interestingly, a previous study has shown that Dlg and βPS-integrin co-immunoprecipitate in fly head extracts, thus demonstrating that these proteins exist in a complex in neuronal and/or epithelial tissue (Beumer et al., 2002).

1.5.3. The distribution patterns of septate junctions and integrins along the lateral membrane of epithelial cells are complementary.

During dorsal closure, the distribution of integrins along the lateral membrane of epithelial cells is strikingly complementary to the distribution of septate junction proteins (Narasimha and Brown, 2004). We provide evidence that the absence of septate junction proteins at the leading edge membrane of DME cells removes a diffusion barrier which allows integrins to accumulate along the lateral membrane. At the end of dorsal closure, septate junctions are normally restored at the leading edge membrane between opposing DME cells, which is accompanied by a downregulation of lateral integrins along the dorsal midline. However, in $pak^{14}pak3^{76a}$ mutant embryos, which are deficient in septate junction formation at the leading edge membrane, lateral integrins along the dorsal midline persists. Furthermore, embryos mutant for the septate junction protein, Cora, have elevated levels of lateral integrins in DME cell membranes other than the leading edge.

Our hypothesis that septate junctions can prevent the accumulation of integrins along the lateral membrane is supported by a study done on the transcription factor, **Grainy head** (**Grh**). Grh is implicated in the development and repair of the epidermis as mice deficient in the Grh-related gene, GRHL3, show defects in the outer layer of the

skin (Ting et al., 2005). In *Drosophila*, Grh has been shown to promote the expression of multiple septate junction proteins including Fas3, Cora and Nrx-IV (Narasimha et al., 2008). When Grh is expressed in the amnioserosa, a tissue normally devoid of septate junctions, the localization of βPS-integrin at the lateral membrane is disrupted, instead appearing diffuse across the apical surface.

1.5.4. Pak and Pak3 are required for adherens junction formation at the leading edge membrane of DME cells upon dorsal closure completion

We provide evidence that Pak and Pak3 are also required for restoring adherens junctions to the leading edge membrane of DME cells at the end of dorsal closure. We suspect that the Paks are acting through different routes when regulating the adherens junctions versus the Scrib complex and the septate junctions at the leading edge membrane for a couple of reasons. In moderately affected $pak^{14}pak3^{76a}$ mutant embryos, there were some DME cells that had restored DE-Cad at the leading edge membrane but not Dlg. Furthermore, Pak and Pak3 can form a complex with select Scrib complex members, but we could not co-immunoprecipitate either Pak or Pak3 with DE-Cad in similar assays. The apicobasal polarity determinants, Crb and Baz/PAR-3 complexes, are important for the formation of adherens junction (reviewed in Tepass et al., 2001). Interestingly, Dr. Harden has shown that $pak^{14}pak3^{76a}$ mutant embryos fail to recruit Crb to the leading edge membrane of DME cells at the end of dorsal closure (Bahri et al., 2010). However, we are not certain about the status of the Baz/PAR-3 complex in $pak^{14}pak3^{76a}$ mutant. Future work will further investigate Pak and Pak3 regulation of the Crb and Baz/PAR-3 complexes, as well as the adherens junctions.

1.5.5. Determining whether Pak and Pak3 regulation of apicobasal polarity is kinase-dependent or kinase-independent

In this thesis, we provide genetic evidence that Pak and Pak3 are involved in restoring the Scrib complex back to the leading edge membrane of DME cells upon dorsal closure completion. Future studies will involve molecularly characterizing this

mode of regulation by determining whether it requires Pak and/or Pak3 kinase activity. Previous studies have shown that phosphorylation of Scrib complex proteins can regulate the complex's localization to the membrane in *Drosophila*. In neuroblasts, Lgl can be phosphorylated at three conserved serine residues by aPKC, a serine/threonine kinase that is a core member of the Baz/PAR-3 complex, thus releasing Lgl from the membrane (Betschinger et al., 2005). Furthermore, Dlg localization at the postsynaptic membrane of third instar larval NMJs is disrupted through phosphorylation of the second PDZ domain by CaMKII or the GUK domain by PAR-1 (discussed in more detail in the next chapter) (Koh et al., 1999; Zhang et al., 2007). Although these cases demonstrate that phosphorylation disrupts the localization of the Scrib complex at the membrane, there may be unidentified sites present in Scrib, Dlg and/or Lgl that can promote their recruitment to the membrane.

With the use of *UAS-pak-AID* and *UAS-pak3-AID* transgenes, we will determine whether regulation of apicobasal polarity by the Paks is kinase-dependent. The transgenes encode for the AID domain, which binds to and blocks the catalytic domain of Pak and Pak3, thus inhibiting their kinase activity (reviewed in Bokoch, 2003). We will express these transgenes during dorsal closure to determine whether blocking Pak or Pak3 kinase activity can disrupt Scrib complex recruitment to the leading edge membrane of DME cells upon dorsal closure completion. Another way to determine whether the Paks require their kinase activity to regulate apicobasal polarity is to create Pak and Pak3 kinase dead transgenes. We show that overexpression of wild-type Pak can rescue the late dorsal closure defects observed in $pak^{14}pak3^{76a}$ mutants. If expression of the kinase dead transgenes fail to rescue the same defects, this may suggest that Pak and Pak3 regulation of apicobasal polarity is kinase-dependent. In addition to these genetic approaches, we will also perform *in vitro* kinase assays between the Paks and the Scrib complex proteins. We have already subcloned Scrib, Lgl and Dlg into the pGEX vector which will allows us to express and purify them as GST fusion proteins. We are currently performing *pak* and *pak3* subcloning. Although there

is a possibility that Pak and Pak3 may not directly phosphorylate the Scrib complex, we are just testing these proteins as a first pass.

2. Characterizing the roles of Hu-li tai shao during larval neuromuscular junction development

2.1. Introduction

2.1.1. Amyotrophic lateral sclerosis

Amyotrophic lateral sclerosis (**ALS**), also known as Lou Gehrig's disease in North America, is a rapidly progressive and fatal neurodegenerative disease (reviewed in Eisen, 2009). The disease is characterized by the degeneration of both upper and lower motor neurons which results in the loss of voluntary muscle movement. ALS can strike anyone: male or female, any ethnic group, and at any age although the usual onset occurs between the ages of 40 and 70. Approximately 2500-3000 Canadians currently suffer from the disease, with an estimated incidence rate of 2 out of 100,000 people per year (according to the ALS Society of Canada). At present, there is no cure for ALS, nor is there an effective treatment that significantly prolongs life. Today, renowned physicist Dr. Stephen Hawking is the best-known person with ALS though his is an unusual case as he has lived with the disease for over 50 years.

ALS is a debilitating disease that affects voluntary muscle control (reviewed in Eisen, 2009). Early symptoms of ALS typically include weakness, twitches, cramps or stiffness of the affected muscles. The parts of the body that are first affected can vary but patients may initially experience some of the following: awkwardness when walking or running; stumbling over a ''dropped foot'' that drags along the ground; difficulty with tasks that require manual dexterity such as writing or buttoning a shirt; and problems with speaking or swallowing. As the disease progresses, motor neuron degeneration eventually spreads throughout the body leading to total paralysis, although control of

the bladder and bowel sphincters, as well as the muscles responsible for eye movement, is usually left intact. Most patients die within three to five years of diagnosis due to respiratory failure, however, some patients can survive for longer periods, i.e. in excess of ten years. Since ALS specifically targets motor neurons, cognition is generally, but not always, spared. Additionally, the autonomic nervous system and the senses are usually not affected.

Three forms of ALS have been described: sporadic, familial and guamanian (reviewed in Eisen, 2009). Sporadic ALS is the most common form, occurring in 90-95% of all cases. Sporadic ALS occurs without any known family history and, therefore, is not considered hereditary. Currently, there is no universally accepted model as to its causes. Familial ALS, which is hereditary, occurs in only 5-10% of all cases. Familial ALS is identified as occurring more than once in a family lineage, and most cases are inherited in an autosomal dominant pattern. Guamanian ALS is the rarest form where a high incidence of the disease, i.e. 400 out of 100,000 people each year, was detected in the Chamorro natives of Guam from the 1940's to the 1960's. Today, the incidence rate in the region has dropped considerably leading some to claim that the disease was caused by the diet at the time, thus suggesting that certain environmental factors may be a contributing factor of the disease.

To better understand the molecular nature of ALS, Dr. Charles Krieger (Department of Biomedical Physiology and Kinesiology, Simon Fraser University) evaluated the levels of several neuronal kinases, phosphatases and phosphoproteins in ALS patients (Hu et al., 2003). Abberations in the expression and activity of protein and lipid kinases have been previously reported in ALS (reviewed in Wagey and Krieger, 1998; reviewed in Hu and Krieger, 2002). The expression levels of 78 kinases and 24 phosphatases, as well as the phosphorylation states of 31 proteins, in thoracic spinal cord tissue taken from control subjects and ALS patients were compared. ALS patients show elevated levels of a number of kinases and phosphatases including **Protein kinase**

C (**PKC**). Moreover, the phosphorylation levels of adducin, a known PKC substrate, is increased in ALS patients (Matsuoka et al., 1998). Similar results were also observed in mice overexpressing a mutant form of human **superoxide dismustase 1** (**SOD1**), a commonly used animal model for ALS (Shan et al., 2005). However, it remains unclear whether PKC-mediated hyperphosphorylation of adducin is a causative factor of ALS.

2.1.2. Mammalian adducins

The mammalian adducins are a family of cytoskeletal proteins that regulate actin filaments and are encoded by three closely related genes: α-adducin, β-adducin and γ-adducin (reviewed in Matsuoka et al., 2000). The α and γ isoforms are found ubiquitously whereas the β isoform is found predominately in the brain and erythrocytes. All three adducin proteins contain an N-terminal globular head domain, a neck domain and at the C-terminus, a protease-sensitive tail region which harbors a **myristoylated alanine-rich C kinase substrate** (**MARCKS**) domain that has homology to the MARCKS protein (see Figure 18 for a schematic of the domain organization in the conserved *Drosophila* orthologue). The adducins, which function as α/γ or α/β tetramers, regulate actin by bundling and capping actin filaments, as well as cross-linking actin with spectrin. The head and neck domains are required for oligomerization, whereas the MARCKS domain is required for its interaction with spectrin and actin.

Few studies have examined the distribution of adducin in the nervous system. In the rat brain, α-adducin localizes to areas with high synapse densities such as the hippocampus, corpus striatum, cerebral cortex and cerebellum (Seidel et al., 1995). Specifically, α-adducin can be found in a subset of dendrites and dendritic spines of neurons in the CA1 and CA3 regions of the hippocampus, at the terminal ends of parallel fibers in the cerebellum, and in the processes of astroglia in both the hippocampus and cerebellum. In addition, phosphorylation of adducin at the PKC target sites in the MARCKS homology domain is detected in the dendritic spines of hippocampal neurons

in rats, as well as in motor neurons and astroglia in the spinal cords of mice (Matsuoka et al., 1998; Shan et al., 2003).

Adducin-dependent regulation of actin is inhibited through PKC phosphorylation of the MARCKS homology domain, occurring in multiple cell types including neurons (Matsuoka et al., 1998; Gilligan et al., 2002; Barkalow et al., 2003). PKC phosphorylation leads to the translocation of adducin from the membrane cytoskeleton to the cytosol. As mentioned previously, ALS patients show elevated levels of phospho-adducin in their spinal cord tissue, caused potentially by aberrant PKC activity (Hu et al., 2003). This observation may suggest that certain forms of neurodegeneration are possibly linked to a loss of adducin function. Interestingly, β-adducin knockout mice display defects in motor coordination (Porro et al., 2010). Furthermore, adducin has been implicated in processes associated with memory, behaviour and learning in mice, nematodes and sea slugs (Gruenbaum et al., 2003; Rabenstein et al., 2005; Porro et al., 2010; Bednarek and Caroni, 2011; Vukojevic et al., 2012). However, the mechanisms underlying adducin's role in these functions are poorly characterized.

2.1.3. Hu-li tai shao, the Drosophila *adducin*

The orthologue of the mammalian adducins in *Drosophila* is encoded by the single gene, ***hu-li tai shao*** (***hts***), which means ''too little nursing'' in Chinese (Yue and Spradling, 1992). Prior to the start of our studies, Hts was only described with regard to its effects on oogenesis, although it is present throughout development including in the embryonic central nervous system (Zaccai and Lipshitz, 1996b). Two studies, however, have recently been published concerning Hts function in the *Drosophila* nervous system and will be discussed later in this chapter (Ohler et al., 2011; Pielage et al., 2011). *hts* was first characterized during oogenesis where mutant females are sterile, producing egg chambers that contain fewer than the normal 15 nurse cells and often no oocyte – hence its name (Yue and Spradling, 1992). The phenotype is attributed, in part, to the abnormal formation of ring canals, actin-rich intercellular bridges that are required for

the transport of essential proteins and RNA from the nurse cells to the oocyte (Yue and Spradling, 1992; Robinson et al., 1994; Petrella et al., 2007).

Alternative splicing results in four distinct Hts proteins during oogenesis: ShAdd, Ovhts, Add1 and Add2 (Figure 18) (Whittaker et al., 1999; Petrella et al., 2007). Each isoform shares common N-terminal head and neck domains that are conserved in mammals, but carry unique C-terminal domains. At the C-terminus, ShAdd lacks a protease-sensitive tail domain found in other isoforms, instead containing a short stretch of 23 amino acids not homologous with any known protein. Ovhts, on the other hand, contains a truncated tail domain followed by a large **Ring Canal** (**RC**) domain that is novel to *Drosophila* adducins. The Add1 and Add2 isoforms are most similar to the mammalian adducins as both contain the tail domain as well as the MARCKS homology domain. In developing egg chambers, Shadd and OvHts are expressed in the germ line nurse cells whereas Add1 and Add2 are expressed in the somatic follicle cells. A fifth Hts isoform called HtsPD, which contains most of the tail domain but lacks the MARCKS domain, is predicted by FlyBase. HtsPD has yet to be detected *in vivo*, but it has been implicated in photoreceptor guidance during eye development as a transgene can rescue defects caused by *hts* mutations (Ohler et al., 2011).

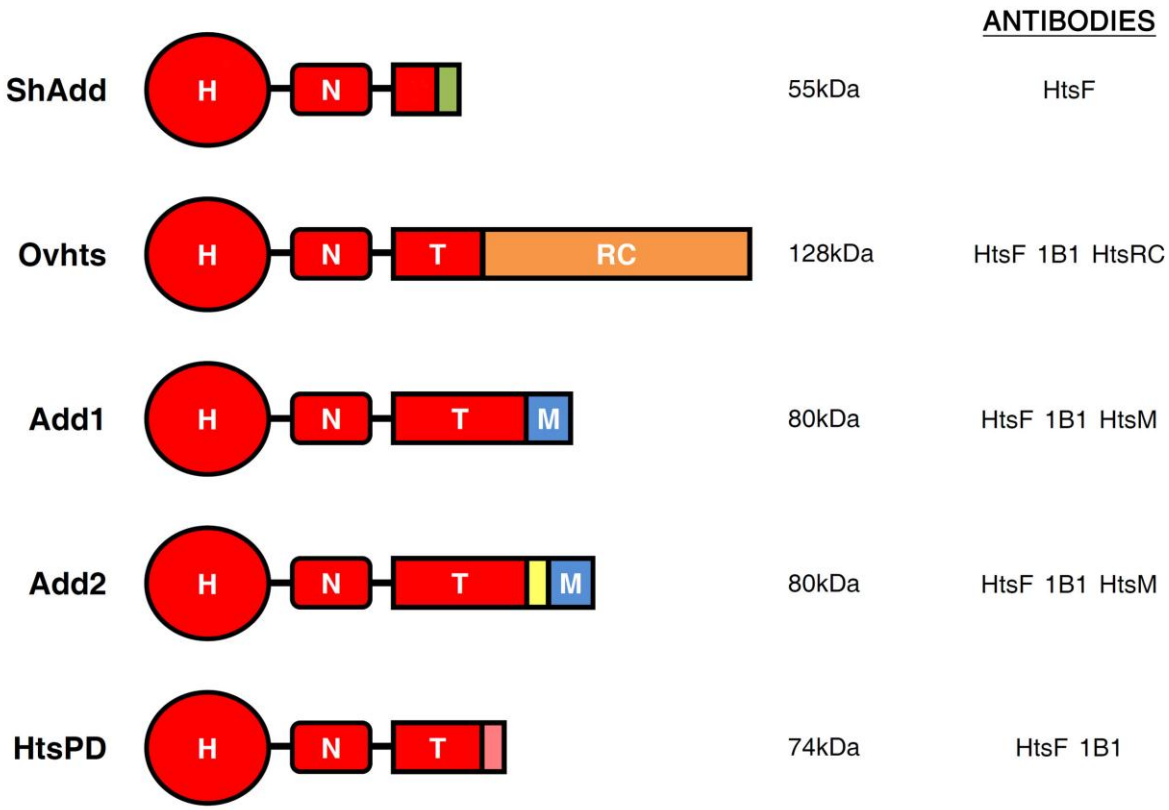
ANTIBODIES
ShAdd
H
N
55kDa
HtsF
Ovhts
H
N
T
RC
128kDa
HtsF 1B1 HtsRC
Add1
H
N
T
M
80kDa
HtsF 1B1 HtsM
Add2
H
N
T
M
80kDa
HtsF 1B1 HtsM
HtsPD
H
N
T
74kDa
HtsF 1B1

FIGURE 18 Hts protein isoforms.

Schematic diagram of the different Hts protein isoforms produced by alternative splicing (not to scale). Each isoform shares common N-terminal head and neck domains that are conserved in mammals, but carry unique C-terminal domains. At the C-terminus, ShAdd lacks the tail domain found in the other isoforms and instead contains a short stretch of 23 amino acids (green) not homologous with any known protein. Ovhts contains a truncated tail domain followed by a large RC domain (orange) that is novel to *Drosophila* adducins. The Add1 and Add2 isoforms are most similar to the mammalian adducins as both contain the tail domain as well as the MARCKS homology domain (blue). Add2 contains an additional 23 amino acids (yellow) (according to Petrella et al., 2007). HtsPD, which is predicted by FlyBase, contains part of the tail domain as well as a novel domain (pink) not present in the other isoforms. Also shown are the Hts antibodies used in this study and the isoforms they detect. Note that the illustration was modelled after Petrella et al., 2007 and Ohler et al., 2011. H = head, N = neck, T = tail, RC = Ring Canal, M = MARCKS.

2.1.4. The larval neuromuscular junction: a model for synaptic plasticity

The third instar larval **neuromuscular junction** (**NMJ**) which innervates the muscles of the body wall has become a heavily used system for the study of many key neurobiological questions (reviewed in Beckett and Baylies). The NMJ represents the synapse between the motor neuron and its muscle target. The features that make the larval NMJ an ideal model are its easy accessibility, relative simplicity and the presence of large, identifiable muscles with well-defined synapses, in addition to the wide array of tools available to Drosophilists.

A larval body wall preparation can be dissected in as little as five minutes (described in Ramachandran and Budnik, 2010a). With the use of a dissecting microscope and micro-dissecting scissors, the anterior- and posterior-most segments of crawling third instar larvae are cut off, followed by an incision along the entire length of the dorsal midline between the two tracheal tracts. The larvae are then unfurled open and pinned down at the corners with minutien pins. Finally, viscera and fat bodies are removed with forceps while taking care to leave the muscles that are attached to the body wall intact.

The larval body wall preparation consists of eight abdominal segments, with each segment divided into two hemisegments by the ventral midline (Figure 19) (reviewed in Beckett and Baylies). Each hemisegment contains an identical pattern of 30 uniquely identifiable muscle cells. Since individual muscles within a hemisegment can be identified based on their position, it is possible to observe the same muscle in the same abdominal hemisegment from animal to animal. Typically, each muscle is polyinnervated by at least two motor neurons which branch over the cell in a characteristic pattern forming boutons, i.e. bulbous structures that contain active zones for neurotransmitter release. Boutons form along the NMJ branch and their appearance has been likened to ''beads on a string''. The most abundant class of motor neuron are type I neurons which release glutamate, the main excitatory transmitter at the larval

NMJ. The other classes, type II and type III, are modulatory synapses that release octopamine and neuropeptides.

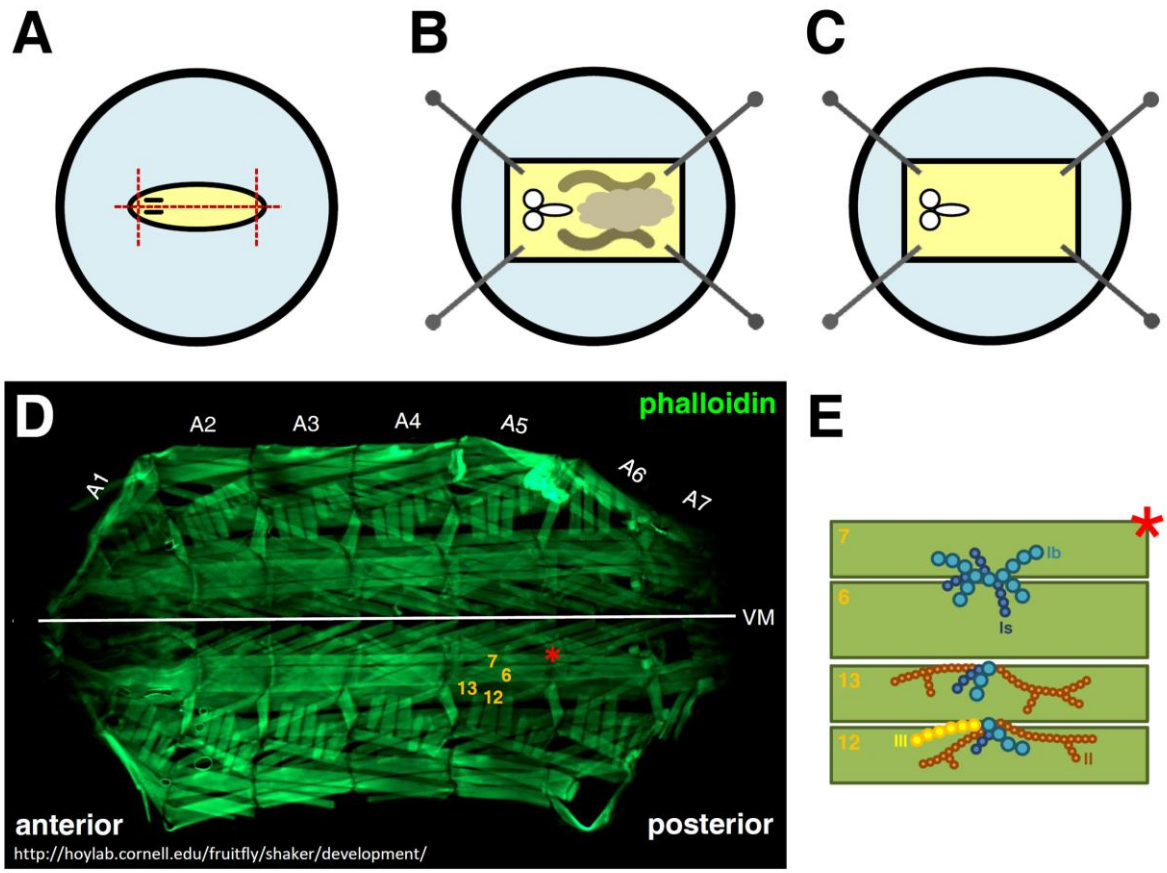
A
B
C
D
phalloidin
A1
A2
A3
A4
A5
A6
A7
VM
7
6
13
12
anterior
posterior
http://hoylab.cornell.edu/fruitfly/shaker/development/
E
7
Ib
6
Is
13
12
III
II

FIGURE 19 The larval body wall.

(A-C) Schematic diagram showing the preparation of a third instar larval body wall. (A) With the use of micro-dissecting scissors, the anterior- and posterior-most segments of the crawling third instar larva are cut off, followed by an incision made along the entire length of the dorsal midline between the two tracheal tracts (see dotted lines for incisions). (B) The larva is then unfurled open and pinned down at the corners with minutien pins. (C) Finally, viscera and fat bodies are removed with forceps while taking care to leave the muscles that are attached to the body wall intact. Note that the figure was modeled after Ramachandran and Budnik, 2010. **(D)** Body wall preparation of a third instar larva stained with phalloidin to detect F-actin. A body wall consists of eight abdominal segments, seven of which are shown, with each segment divided into two hemisegments by the ventral midline (denoted by the white dotted line). Muscles 6/7 and 12/13 in abdominal segments 3 to 5 are commonly used in this thesis. Note that the body wall was dissected and prepared by the Hoy lab (Cornell University, New York) (http://hoylab.cornell.edu/fruitfly/shaker/development). **(E)** Schematic diagram showing the three types of *Drosophila* motor neuron in muscles 6/7 and 12/13 (see red astericks in panel D for positioning). Note that the figure was modeled after Guan et al., 1996. VM = ventral midline.

Similar to epithelial cells, neuronal cells can also alter their shape and interactions with other cells in a process known as synaptic plasticity (reviewed in Griffith and Budnik, 2006). Neurons can undergo changes to both their structural and functional properties, which consequently modifies the strength of their synaptic signal. Synaptic plasticity is believed to play critical roles in the processes of learning and memory. Interestingly, the larval NMJ also experiences synaptic plasticity. From the time of hatching to the time of pupation, which is roughly four days, larvae grow by a factor of more than 100-fold. To allow the larva to maintain control of its constantly growing musculature, the NMJ must also rapidly and constantly grow in order to properly innervate the muscle. While the NMJ is clearly not a synapse central to learning, the molecular mechanisms behind synaptic plasticity in the muscle and the brain are believed to be conserved.

2.2. Objective

As mentioned before, Dr. Krieger has previously shown that the levels of phosphorylated adducin in the spinal cord tissue of ALS patients are elevated (Hu et al., 2003). However, it remains unknown whether aberrant adducin phosphorylation is a contributing factor in the degeneration of motor neurons observed during ALS progression. Interestingly, mice mutant for β-adducin display defects in motor coordination (Porro et al., 2010). In collaboration with Dr. Krieger, our lab decided to further investigate the role of adducin in motor neurons by studying the *Drosophila* orthologue, Hts, at the well-characterized third instar larval NMJ in body wall muscles.

2.3. Materials and Methods

Recipes for reagents shown in bold can be found in Appendix B – Recipes.

2.3.1. Fly Stocks

Flies were maintained under standard conditions at 25°C unless otherwise stated (Ashburner and Roote, 2007). w^{1118} was used as a wild-type control unless otherwise stated. The following lines were ordered from the Bloomington Stock Center (Indiana University, Indiana): w^{1118} (3605), hts^{01103} (10989) (Spradling et al., 1999), hts^{k06121} (10607) (Spradling et al., 1999), *Df(2R)BSC26* (24335) (Parks et al., 2004), dlg^{G0342} (11976) (Peter et al., 2002), dlg^{G0456} (12301) (Peter et al., 2002), *mef2-Gal4* (27390), *prd-Gal4* (1947), *In(2LR)Gla/CyO, twi-Gal4, UAS-GFP* (6662). The following lines were ordered from the Vienna *Drosophila* RNAi Center (Campus Vienna Biocenter, Austria): *UAS-hts-RNAi* (29102) (Dietzl et al., 2007). The following lines were ordered from the *Drosophila* Genetic Resource Center (Kyoto Institute of Technology, Japan): *GS10063* (202293) (Toba et al., 1999), *GS13376* (no longer available) (Toba et al., 1999) and *GS13858* (204998) (Toba et al., 1999).

The following lines were made by our collaborators: $UAS\text{-}hts^{S705S}$ and $UAS\text{-}hts^{S705A}$ were made by Vincent Chui (see the thesis entitled ''The regulation and function of Hu-li tai shao (Hts) at the *Drosophila* neuromuscular junction'' which was submitted to the SFU Library in 2011) (unpublished) and $UAS\text{-}hts^{S705D}$ was made by Tomas Kuca (undocumented and unpublished).

2.3.2. Cuticle Preparation

Cuticle preparations were performed as previously described but with some modifications (Stern and Sucina, 2011). Cages and plates were incubated at 25°C unless otherwise stated. Experiments and their controls were always done at the same time under identical conditions.

Flies placed in cages, made from 100mL tricornered plastic beakers with small holes poked in them, were allowed to lay eggs on **grape juice agar plates** with **yeast paste** for 24 hours. The flies were then removed and the plates were aged for an

additional 48 hours. Progeny ranging in age from 48 to 72 hours after egg laying were collected in baskets (see Stern and Sucina, 2011) and dechorionated in **50% bleach** for three minutes. The progeny were then washed in 0.01% Triton X-100 (diluted from Sigma-Aldrich – T8787) three times for a minimum of 30 seconds each and mounted onto slides with **Hoyer's medium**. Weights were added to flatten the samples and the slides were incubated at 65°C for three days, or until all soft tissue was digested leaving behind only cleared cuticle. Embryonic phenotypes were scored on a Nikon TMS inverted phase contrast microscope with a minimum sample size of 250 progeny. Representative phenotypes were imaged on a Zeiss Axioplan 2 microscope with Openlab software, and the images were processed using Adobe Photoshop CS5.

2.3.3. Embryo Fixation

Embryo fixations were performed as previously described but with some modifications (Rothwell and Sullivan, 2007a; Rothwell and Sullivan, 2007b; Rothwell and Sullivan, 2007c). Cages were incubated at 25°C unless otherwise stated. Experiments and their controls were always done at the same time under identical conditions.

Flies placed in cages, made from 100mL tricornered plastic beakers with small holes poked in them, were allowed to lay eggs on **grape juice agar plates** with **yeast paste** for 16 hours. Embryos ranging in age from 0 to 16 hours after egg laying were collected in baskets (see Stern and Sucina, 2011) and dechorionated in **50% bleach** for three minutes. The embryos were then washed in 0.01% Triton X-100 (diluted from Sigma-Aldrich – T8787) three times for a minimum of 30 seconds each. To remove the vitelline membrane, the embryos were transferred to 20mL glass scintillation vials containing a devitellinization mixture composed of two phases: a bottom aqueous layer consisting of 5mL of **4% paraformaldehyde** and a top organic layer consisting of 5mL of heptane (Caledon Laboratories – 5400-1). The embryos were then shaken vigorously for 25 minutes. After shaking, the bottom paraformaldehyde layer was removed and replaced with 5mL of methanol (Caledon Laboratories – 6700-1). The embryos were

then shaken for an additional minute causing properly devitellinized, and thus fixed, embryos to sink to the bottom methanol layer. The top heptane layer, along with improperly devitellinized embryos, were discarded. Fixed embryos were stored in methanol at -20°C until ready for staining. Note that embryos were typically stained within one month of fixation.

2.3.4. Larval Body Wall Dissection

Larval body wall dissections were performed as previously described but with some modifications (Ramachandran and Budnik, 2010a; Brent et al., 2009). Stocks and crosses were raised at 25°C unless otherwise stated. Experiments and their controls were always done at the same time under identical conditions.

Crawling third instar larvae were collected from either vials or bottles using forceps and rinsed with **PBS**. Mutant stocks were re-balanced over GFP-tagged balancers allowing for homozygotes to be selected based on the absence of GFP signal when viewed under an epifluorescent microscope. For transgenic analysis, homozygous *UAS*-transgene-bearing males were crossed to homozygous *Gal4*-bearing virgin females ensuring that all progeny carried one copy of each. Each larva was dissected in PBS on a SYLGARD disc under a dissecting microscope. Using micro-dissecting scissors, the anterior- and posterior-most segments of the larva were cut off, followed by an incision made along the entire length of the dorsal midline between the two tracheal tracts. The dissected larva was then unfurled open, gently stretched along the anterior-posterior axis, and pinned down at the corners with minutien pins (Fine Science Tools – 26002-10). Viscera and fat bodies were removed with fine forceps (Almedic – A10-704) while taking care to leave the muscles that are attached to the body wall intact. The body walls were then incubated in either **4% paraformaldehyde** or Bouin's solution for 30 minutes at room temperature. After fixation, the body walls were rinsed with **PBT** and then unpinned. The body walls were stored in PBT at 4°C until ready for staining. Note that body walls were always stained within five days of dissection.

2.3.5. Immunohistochemistry

Immunostaining of embryos and larval body walls was performed as previously described with some modifications (Ramachandran and Budnik, 2010b; Swedlow, 2011). Experiments and their controls were always done at the same time under identical conditions. All steps were performed at room temperature unless otherwise stated.

Fixed embryos and larval body walls were immunostained using the same protocol. Samples were first washed with **PBT** three times for ten minutes each, and then blocked with **1% BSA** for one hour. The samples were next incubated with primary antibodies overnight at 4°C (see a list of the primary antibodies in the next paragraph). Following three washes with PBT for ten minutes each, the samples were incubated with fluorescently-conjugated secondary antibodies for two hours (see a list of the secondary antibodies in the next paragraph). As the fluorophores are light sensitive, the samples were protected from light for the remainder of the protocol. After incubation with the secondary antibodies, the samples were then washed with PBT three times for ten minutes each, and subsequently equilibrated with VECTASHIELD Mounting Medium (Vector Laboratories – H-1000) overnight at 4°C. The samples were mounted onto platform slides, consisting of 22×22mm cover slips adhered onto microscope slides with clear nail polish, and stored at -20°C until ready for imaging. Samples were imaged on either a Zeiss LSM 410 laser scanning confocal microscope or a Nikon A1R laser scanning confocal microscope. All images were processed with Adobe Photoshop CS5.

The following primary antibodies were used: 1:500 rat anti-HtsF from Dr. Budnik (Lin et al., 1994; Robinson et al., 1994), 1:5 mouse anti-Hts (Developmental Studies Hybridoma Bank – 1B1) (Zaccai and Lipshitz, 1996b), 1:200 rabbit anti-HtsM from Dr. Vivian Budnik (University of Massachusetts, Massachusetts) (Petrella et al., 2007), 1:10 mouse anti-HtsRC (Developmental Studies Hybridoma Bank – hts RC) (Robinson et al., 1994), 1:500 rabbit anti-Hrp, 1:10 mouse anti-Dlg (Developmental Studies Hybridoma Bank – 4F3) (Parnas et al., 2001), 1:250 mouse anti-CSP (Developmental Studies

Hybridoma Bank – CSP2) (Zinsmaier et al., 1994), 1:200 rabbit anti-p-Dlg from Dr. Bingwei Lu (Stanford University, California) (Zhang et al., 2007), 1:200 rabbit anti-PAR-1 from Dr. Anne Ephrussi (European Molecular Biology Laboratory, Germany) (Tomancak et al., 2000) and 1:1000 rabbit anti-CaMKII from Dr. Leslie Griffith (Brandeis University, Massachusetts) (Koh et al., 1999). The following secondary antibodies were used: Fluorescein-labeled horse anti-mouse (Vector Laboratories – FI-2000), Texas Red-labeled horse anti-mouse (Vector Laboratories – TI-2000), Fluorescein-labeled goat anti-rabbit (Vector Laboratories – FI-1000), Texas Red-labeled goat anti-rabbit (Vector Laboratories – TI-1000), Fluorescein-labeled anti-rat, Texas Red-labeled anti-rat, Fluorescein-labeled anti-guinea pig and Texas Red-labeled anti-guinea pig. Both primary and secondary antibodies were diluted in 1% BSA. All secondary antibodies were used at a 1:200 dilution.

2.3.6. Quantification

Quantifications were performed with Adobe Photoshop CS5 unless otherwise stated. Images were first converted to grayscale (Image > Mode > Grayscale), and their resolutions were standardized to 300 pixels/inch (Image > Image Size).

2.3.6.1. Dlg immunofluorescence intensity at the NMJ

Dlg postsynaptic localization at third instar larval NMJs was quantified by measuring Dlg immunofluorescence intensity normalized against Hrp immunofluorescence intensity, which was used as a control stain. Dlg immunofluorescence signal at the NMJ was selected with the Color Range tool (Select > Color Range). The selection was further refined using the Smooth feature under the Modify tool (Select > Modify > Smooth). Dlg immunofluorescence intensity was then measured as mean gray value (Analysis > Record Measurements). Hrp immunofluorescence signal at the NMJ was selected and measured using the same procedure. Note that the parameters used to quantify either Dlg or Hrp immunofluorescence intensity were kept constant within data sets.

Measurements were performed on NMJs innervating muscles 6/7 at abdominal segments 3, 4 and 5. A minimum sample size of 24 NMJs from 12 larval body walls, i.e. two NMJs per body wall, was analyzed for each genotype. Data were expressed as relative values to the control and presented as ''mean±sem''. Student's t-tests were performed for all statistical comparisons using GraphPad (http://www.graphpad.com/quickcalcs).

2.3.6.2. p-Dlg puncta levels in the muscle

p-Dlg postsynaptic levels during third instar larval NMJ development were quantified by measuring extrasynaptic p-Dlg immunoreactive puncta using ImageJ. Images were first converted to grayscale (Image > Type > 8-bit) and inverted (Edit > Invert). The threshold was then adjusted to create a black and white image (Image > Adjust > Threshold), with black representing p-Dlg immunofluorescence signal and white representing the background. p-Dlg immunoreactive puncta throughout the muscle was measured as the number of black pixels (Analyze > Histogram) found within a fixed selection size in areas of the muscle that did not contain signal from the NMJ. Note that the parameters used to quantify p-Dlg immunoreactive puncta were kept constant within data sets.

Measurements were performed on both muscles 6 and 7 at abdominal segments 3, 4 and 5. A sample size of 12 muscle pairs from 24 larval body walls, i.e. two muscle pairs per body wall, was analyzed for each genotype. Data were expressed as relative values, and presented as ''mean±sem''. Student's t-tests were performed for all statistical comparisons using GraphPad (http://www.graphpad.com/quickcalcs).

2.3.7. Western Blot

Western blotting was performed as previously described but with some modifications (Wang et al., 2011). Experiments and their controls were always done at

the same time under identical conditions. All steps were performed at room temperature unless otherwise stated.

Stocks and crosses were raised at 25°C unless otherwise stated. Crawling third instar larvae were collected from either vials or bottles using forceps and rinsed with **PBS**. Mutant stocks were re-balanced over GFP-tagged balancers allowing for homozygotes to be selected based on the absence of GFP signal when viewed under an epifluorescent microscope. For transgenic analysis, homozygous *UAS*-transgene-bearing males were crossed to homozygous *Gal4*-bearing virgin females ensuring that all progeny carried one copy of each. For each genotype, body walls dissected from 25 third instar larvae were homogenized by hand with a pestle in 150µL of **Lysis Buffer I** on ice. The lysate was then centrifuged at 13000rpm for ten minutes at 4°C. The pellet was discarded and the extract was analyzed by Bradford assay using the Bio-Rad Protein Assay (Bio-Rad – 500-0006). The total protein concentration for each sample, which was determined with a standard curve created from known concentrations of BSA, was standardized to 1µg/µL. Loading dye (Thermo Fisher Scientific – 39000) was subsequently added and the samples were stored at -20°C until ready for SDS-PAGE.

After boiling the samples for ten minutes, 20µg of total protein for each sample was loaded onto an 8% discontinuous SDS-PAGE gel (see Simpson, 2006) along with a prestained ladder (Bio-Rad – 161-0318). The samples were run at 100V in **Running Buffer** until the dye front migrated to the end of the gel, and then were transferred onto a nitrocellulose membrane (Bio-Rad – 162-0115) at 15V with **Transfer Buffer** for one hour using a semi-dry transfer apparatus. The membranes were stored in **TBS** at 4°C until ready for immunoblotting.

The membranes were first washed with **TBST** three times for ten minutes each, and then blocked with **5% BSA** for one hour. The membranes were next incubated with a primary antibody overnight at 4°C (see a list of the primary antibodies in the next paragraph). Following two washes with TBST and two blocks with **2.5% BSA** for ten

minutes each, the membranes were incubated with an HRP-conjugated secondary antibody for two hours (see a list of the secondary antibodies in the next paragraph). The membranes were then washed with TBST four times for 15 minutes each. Detection was accomplished with the BM Chemiluminescence Western Blotting Peroxidase Substrate (Roche Applied Science – 11500694001). Maximum sensitivity film (Cedarlane – CLMS810) was exposed from anywhere between 5 seconds to one hour, depending on the strength of the signal, and developed. If multiple blottings of a single membrane were required, the membrane was stripped with **Stripping Solution** two times for 30 minutes each at 50°C. Comparative analyses of band size and intensity were performed as outlined by Dr. Luke Miller (Stanford University, California) (http://www.lukemiller.org/journal/2007/08/quantifying-western-blots-without.html).

The following primary antibodies were used: 1:7500 rat anti-HtsF from Dr. Lynn Cooley (Yale University, Connecticut) (Lin et al., 1994; Robinson et al., 1997), 1:1500 mouse anti-Hts (Developmental Studies Hybridoma Bank – 1B1) (Zaccai and Lipshitz, 1996b), 1:5000 rabbit anti-HtsM from Dr. Cooley (Petrella et al., 2007), 1:10 mouse anti-HtsRC (Developmental Studies Hybridoma Bank – hts RC) (Robinson et al., 1994), 1:1000 mouse anti-Dlg (Developmental Studies Hybridoma Bank – 4F3) (Parnas et al., 2001) and 1:1000 mouse anti-Actin (Developmental Studies Hybridoma Bank – JLA20) (Lin, 1981). The following secondary antibodies, which were diluted to 1:2000, were used: Peroxidase-labeled horse anti-mouse (Vector Laboratories – PI-2000), Peroxidase-labeled goat anti-rabbit (Vector Laboratories – PI-1000) and Peroxidase-labeled anti-rat. Both primary and secondary antibodies were diluted in 2.5% BSA.

2.3.8. Immunoprecipitation

Immunoprecipitations were performed as previously described but with some modifications (Wang et al., 2011). Experiments and their controls were always done at the same time under identical conditions. All steps were performed at room temperature unless otherwise stated.

Stocks and crosses were raised at 25°C unless otherwise stated. Crawling third instar larvae were collected from either vials or bottles using forceps and rinsed with **PBS**. Mutant stocks were re-balanced over GFP-tagged balancers allowing for homozygotes to be selected based on the absence of GFP signal when viewed under an epifluorescent microscope. For transgenic analysis, homozygous *UAS*-transgene-bearing males were crossed to homozygous *Gal4*-bearing virgin females ensuring that all progeny carried one copy of each. For each genotype, body walls dissected from 25 to 50 third instar larvae were homogenized by hand with a pestle in 150µL of **Lysis Buffer I** on ice. The lysate was then centrifuged at 13000rpm for ten minutes at 4°C. The pellet was discarded and the extract was analyzed by Bradford assay using the Bio-Rad Protein Assay (Bio-Rad – 500-0006). The total protein concentration for each extract, which was determined with a standard curve created from known concentrations of BSA, was standardized to the concentration of the least concentrated sample. The extracts were then stored at -80°C until ready for immunoprecipitation.

All steps regarding protein immunoprecipitation were performed at 4°C. For each sample, 25µL of 50% Protein G Agarose slurry (Santa Cruz Biotechnology – sc-2002) was centrifuged at 13000rpm for five minutes, after which the supernatant was discarded. The beads were subsequently washed with PBS for five minutes, and then centrifuged at 13000rpm for five minutes. The supernatant was discarded and two more PBS washes were performed. After the final wash was removed, the beads were incubated with 5µL of antibody in 150µL of Lysis Buffer I overnight (see a list of the antibodies in the last paragraph of this section). The beads were next centrifuged at 13000rpm for five minutes, after which the supernatant was discarded. The beads were subsequently washed with Lysis Buffer I for ten minutes, and then centrifuged at 13000rpm for five minutes. The supernatant was discarded and two more Lysis Buffer I washes were performed. After the final wash was removed, equal volumes of each larval body wall extract were incubated with the beads for two hours. The beads were next centrifuged at 13000rpm for five minutes, after which the supernatant was

discarded. The beads were subsequently washed with **Lysis Buffer II** for ten minutes, and then centrifuged at 13000rpm for five minutes. The supernatant was discarded and two more Lysis Buffer II washes were performed. After the final wash was removed, loading dye (Thermo Fisher Scientific – 39000) was added and the samples were stored at -20°C until ready for SDS-PAGE.

After boiling the samples for ten minutes, each sample was loaded onto an 8% discontinuous SDS-PAGE gel (see Simpson, 2006) along with a prestained ladder (Bio-Rad – 161-0318). The samples were run at 100V in **Running Buffer** until the dye front migrated to the end of the gel, and then were transferred onto a nitrocellulose membrane (Bio-Rad – 162-0115) at 15V with **Transfer Buffer** for one hour using a semi-dry transfer apparatus. The membranes were stored in **TBS** at 4°C until ready for immunoblotting.

The membranes were first washed with **TBST** three times for ten minutes each, and then blocked with **5% BSA** for one hour. The membranes were next incubated with a primary antibody overnight at 4°C (see a list of the primary antibodies in the next paragraph). Following two washes with TBST and two blocks with **2.5% BSA** for ten minutes each, the membranes were incubated with an HRP-conjugated secondary antibody for two hours (see a list of the secondary antibodies in the next paragraph). The membranes were then washed with TBST four times for 15 minutes each. Detection was accomplished with the BM Chemiluminescence Western Blotting Peroxidase Substrate (Roche Applied Science – 11500694001). Maximum sensitivity film (Cedarlane – CLMS810) was exposed from anywhere between 5 seconds to one hour, depending on the strength of the signal, and developed. If multiple blottings of a single membrane were required, the membrane was stripped with **Stripping Solution** two times for 30 minutes each at 50°C. Comparative analyses of band size and intensity were performed as outlined by Dr. Luke Miller (Stanford University, California) (http://www.lukemiller.org/journal/2007/08/quantifying-western-blots-without.html).

The following antibodies were used for immunoprecipitation: mouse anti-Dlg (Developmental Studies Hybridoma Bank – 4F3) (Parnas et al., 2001). The following primary antibodies were used for immunoblotting: 1:1500 rabbit anti-p-Dlg from Dr. Bingwei Lu (Stanford University, California) (Zhang et al., 2007) and 1:1000 mouse anti-Dlg (Developmental Studies Hybridoma Bank – 4F3) (Parnas et al., 2001). The following secondary antibodies, which were all diluted to 1:2000, were used for immunoblotting: Peroxidase-labeled goat anti-rabbit (Vector Laboratories – PI-1000) and Peroxidase-labeled horse anti-mouse (Vector Laboratories – PI-2000). Both the primary and secondary antibodies used for immunoblotting were diluted in 2.5% BSA.

2.4. Results

Some of the work from this section was published in ''*Drosophila* adducin regulates Dlg phosphorylation and targeting of Dlg to the synapse and epithelial membrane'' by Simon Wang, Jing Yang, Amy Tsai, Tomas Kuca, Justina Sanny, Jeehwa Lee, Kevin Dong, Nicholas Harden and Charles Krieger (Developmental Biology 2011; 357:392-403). Jing Yang and I contributed equally to this publication. Note that work done by others is credited throughout the text. A special thanks goes to Amy Tsai, a former research technician under Dr. Charles Krieger, for her countless hours of dissecting body walls – I hope your neck is feeling better.

2.4.1. Hts is present at the postsynaptic membrane of larval NMJs

We first determined whether Hts is present in *Drosophila* motor neurons by staining the muscles attached to the body walls of wild-type third instar larvae with antibodies against Hts and the neuronal marker, **Horseradish peroxidase** (**Hrp**). The anti-Hts antibody used predominantly in our studies, called 1B1, detects every Hts isoform except ShAdd (see Figure 18) (Zaccai and Lipshitz, 1996b; Petrella et al., 2007). The anti-Hrp antibody, on the other hand, cross-reacts with glycoproteins present in

insect neuronal membranes (reviewed in Paschinger et al., 2009). In muscles 12/13 which are innervated by all three types of motor neurons, Hts localized to type Ib and Is, but not type II and type III, motor neurons (Gorczyca and Budnik, 2006) (Figure 20A-A''). Further analysis of muscles 6/7 which are innervated only by type I motor neurons confirmed that Hts localized to both type Ib and Is motor neurons particularly at the synaptic boutons, but was also present throughout the muscle (Figure 20B-B'') (Gorczyca and Budnik, 2006; Wang et al., 2011). Higher magnifications of the synaptic boutons revealed that Hts mostly accumulated circumferentially to the neuronal membrane indicating a postsynaptic distribution at the NMJ. However, Hts is also present presynaptically. This was determined through the expression of transgenic *hts* RNAi in the muscle via *mef2-Gal4* since Hts immunoreactivity in the neuron is observed after Hts muscle-specific knockdown, as well as by another independent research group (Figure 20C-C'') (Pielage et al., 2011). Our results show that Hts is present predominately at the postsynaptic membrane of type Ib and Is boutons during larval NMJ development, although Hts is also present throughout the muscle and in the presynaptic motor neuron.

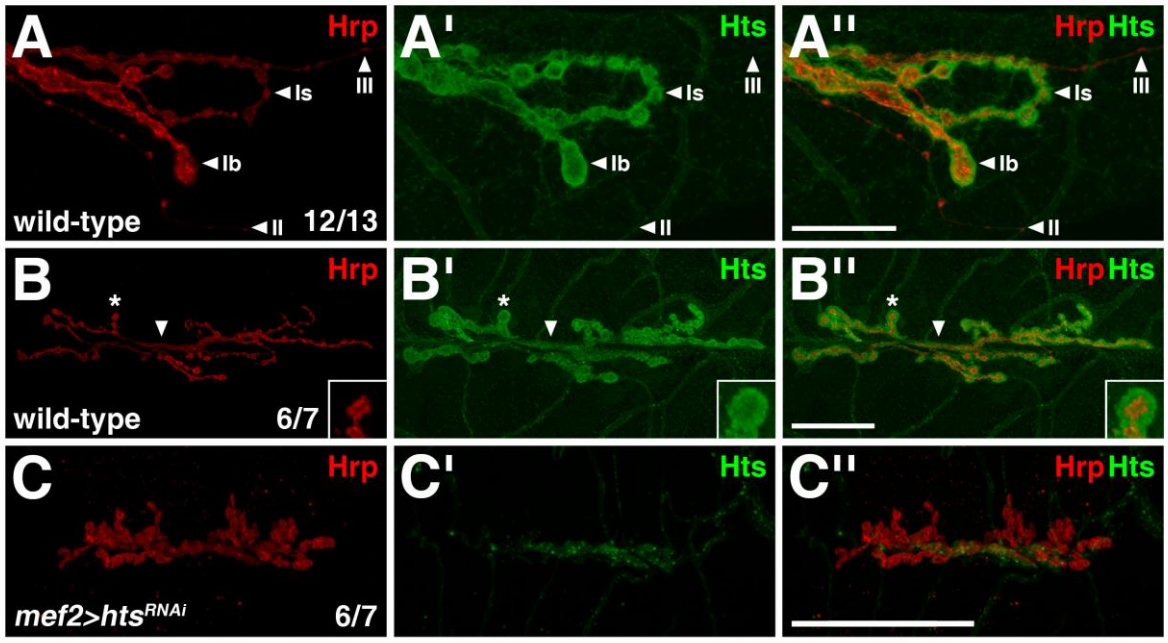
A
Hrp
Is
III
Ib
wild-type
II
12/13
A'
Hts
Is
III
Ib
II
A''
Hrp Hts
Is
III
Ib
II
B
Hrp
*
wild-type
6/7
B'
Hts
*
B''
Hrp Hts
*
C
Hrp
mef2>hts^RNAi
6/7
C'
Hts
C''
Hrp Hts

FIGURE 20 Hts localizes predominately at the postsynaptic membrane of type I boutons duringlarval NMJ development.

(A-B'') Wild-type third instar larval NMJs stained with antibodies against Hts, using the 1B1 antibody, and Hrp. (A) NMJ innervating muscles 12/13. Hts localizes to type Ib and Is, but not type II and type III, motor neurons. (B) NMJ innervating muscles 6/7. Hts localizes to type Ib and Is synaptic boutons, but Is also present throughout the muscle and in the neuron (see white arrowheads). Insets denote higher magnifications of a single synaptic bouton (see asterisks) showing that Hts is predominately found at the postsynaptic side of the NMJ. **(C)** *mef2>hts*^{RNAi} third instar larval NMJ at muscles 6/7 stained with antibodies against Hts, using the 1B1 antibody, and Hrp. Expression of transgenic *hts* RNAi in the muscle with *mef2-Gal4* confirms that Hts is also present at the presynaptic side of the NMJ as Hts immunoreactivity in the neuron is observed after Hts muscle-specific knockdown. Note that the body wall preparation is not properly stretched, thus morphological comparisons cannot be made between this NMJ and the wild-type control shown in panel B. Scale bar in panel A'' represents 20µm (A-A''), scale bar in panel B'' represents 50µm (B-B''), scale bar in panel C'' represents 50µm (C-C'').

We next sought to identify which Hts isoforms are present at the larval NMJ through the use of isoform-specific antibodies. Comparable immunoreactivity patterns were observed between the 1B1 antibody and an anti-Hts antibody called HtsF that detects all Hts isoforms (data not shown; see Figure 18) (Lin et al., 1994; Robinson et al., 1994; Petrella et al., 2007). We also obtained similar results with an anti-Hts antibody called HtsM that only detects the MARCKS domain of the Add1 and Add2 isoforms (see Figure 20B'; see Figure 24A'; see Figure 18) (Petrella et al., 2007). This suggests that the adducin isoforms of Hts are the main isoforms at the NMJ. In support of this argument, no detectable immunoreactivity was observed at the NMJ with an anti-Hts antibody called HtsRC that only detects the RC domain of the Ovhts isoform (data not shown; see Figure 18) (Robinson et al., 1994; Petrella et al., 2007). This particular result was not surprising as Ovhts is not expressed in males, indicating that it is restricted to the female germ line (Telonis-Scott et al., 2009). Western blot analysis of wild-type third instar larval body wall lysates revealed two bands when blotting with the 1B1 antibody (Figure 21). The larger band at approximately 80kDa is consistent with the sizes of Add1 and/or Add2, and was confirmed with the HtsM antibody (Figure 21). The smaller band at around 74kDa is consistent with the size of Hts-PD. To determine whether ShAdd is present during larval NMJ development, we also used the HtsF antibody to check for additional bands not detected with the 1B1 antibody. Indeed, the blot contained an extra, faint band at approximately 55kDa which may represent ShAdd (Figure 21). On a side note, ShAdd is detected in late third instar larval brains (Ohler et al., 2011). Based on these results, we conclude that Add1 and/or Add2, the *Drosophila* proteins most similar to the mammalian adducins, are present at the postsynaptic region of type I boutons during larval NMJ development, though other Hts isoforms are also present.

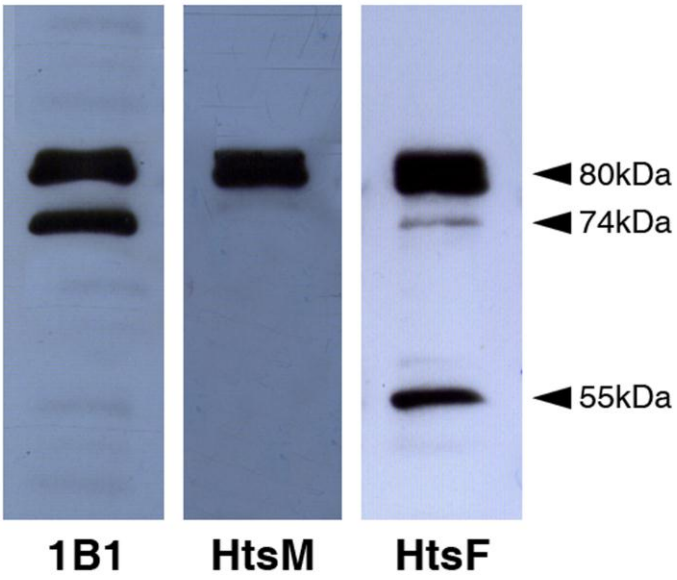
80kDa
74kDa
55kDa
1B1
HtsM
HtsF

FIGURE 21 Add1 and/or Add2 are present during larval NMJ development.

Comparative Western blot analysis of wild-type third instar larval body wall lysates blotted with various Hts antibodies. Blotting with the 1B1 antibody reveals two bands. The larger band at approximately 80kDa is consistent with the sizes of Add1 and/or Add2 which was confirmed with the HtsM antibody. The smaller band at around 74kDa is consistent with the size of Hts-PD. To determine whether ShAdd is present during larval NMJ development, we also used the HtsF antibody to check for additional bands not detected with the 1B1 antibody. Indeed, the blot contains an extra, faint band at approximately 55kDa which may represent ShAdd.

2.4.2. Postsynaptic Hts regulates larval NMJ morphogenesis

To investigate the role of Hts at the NMJ, we examined third instar larvae that were homozygous mutant for *hts*^{01103}, an allele that contains a P-element insertion upstream of the ATG start site (Figure 22A) (Spradling et al., 1999). *hts*^{01103} most likely represents a null mutation as mutants lacked Hts immunoreactivity at the NMJ (Figure 22C) (Wang et al., 2011). In addition, Western blot analysis of third instar larval body wall lysates did not reveal any detectable bands in comparison to wild-type (Figure 22E) (Wang et al., 2011). In *hts*^{01103} mutants, NMJs innervating muscles 6/7 were clearly underdeveloped in terms of synaptic branching when compared to wild-type, thus implicating Hts in NMJ morphogenesis (see Figure 25A,B) (Wang et al., 2011). We chose not to analyze *hts*^{01103} transheterozygotes over *Df(2R)BSC26*, the only available deficiency that removes the *hts* gene, as the deficiency also removes *cora*, a member of the spectrin-actin cytoskeleton that likewise participates in NMJ development (Parks et al., 2004; Chen et al., 2005; Bogdanik et al., 2008). However, to ensure that the NMJ defects observed in *hts*^{01103} mutants were not due to a second site mutation, we examined another *hts* allele, *hts*^{k06121}, which also contains a P-element insertion upstream of the *hts* gene (Figure 22A) (Spradling et al., 1999). Similar to *hts*^{01103} mutants, *hts*^{k06121} mutants had clearly underdeveloped NMJs at muscles 6/7 (data not shown). In addition, Mannan Wang, an M.Sc. student under Dr. Wade Parkhouse (Department of Biomedical Physiology and Kinesiology, Simon Fraser University), has shown that expression of transgenic *hts* RNAi in developing somatic muscles with the *mef2-Gal4* driver can also result in underdeveloped NMJs (see the thesis entitled ''Muscle-associated *Drosophila* adducin regulates larval neuromuscular junction development and the location of Draper to the synapse'' which will be submitted to the SFU Library in 2013). These results indicate that Hts, more specifically postsynaptic Hts, promotes NMJ growth.

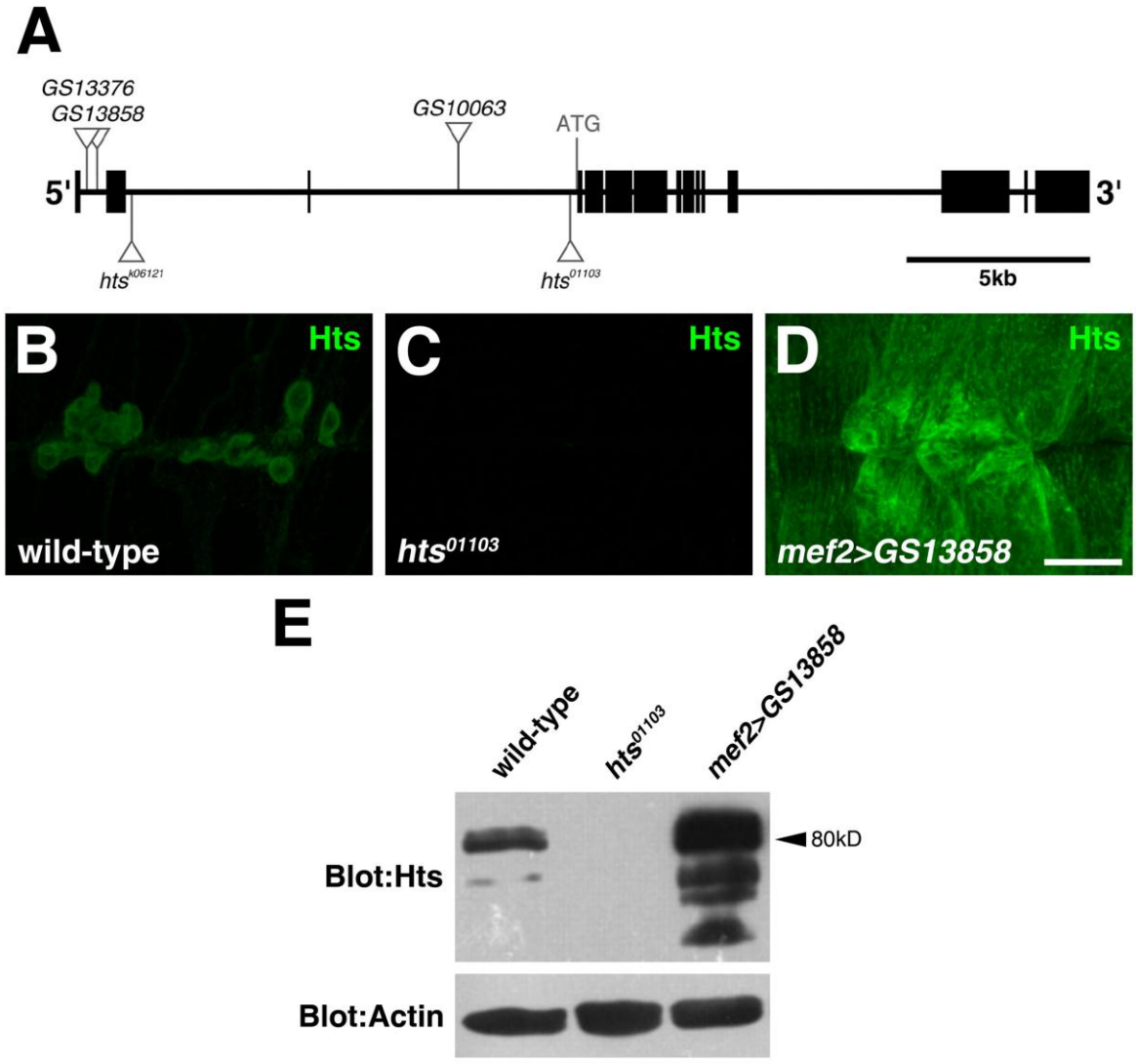
A
GS13376
GS13858
GS10063
ATG
5'
3'
hts k06121
hts 01103
5kb
B
Hts
wild-type
C
Hts
hts 01103
D
Hts
mef2>GS13858
E
wild-type
hts 01103
mef2>GS13858
80kD
Blot:Hts
Blot:Actin

FIGURE 22 P-element insertions used to study Hts function.

(A) Schematic diagram of the *hts* gene (in true scale). Exons are denoted with vertical bars whereas introns are denoted with horizontal bars. P-element insertions are indicated with white triangles. hts^{01103} and hts^{k06121} contain transposon insertions upstream of the ATG start site. *GS10063*, *GS13376* and *GS13858* contain inserted UAS sequences. **(B-D)** Comparative analysis of third instar larval NMJs at muscles 6/7 stained for Hts using the 1B1 antibody. (B) A typical wild-type NMJ. (C) hts^{01103} mutants lack Hts immunoreactivity at the NMJ. (D) *GS13858* driven in the muscle with *mef2-Gal4* elevates Hts immunoreactivity throughout the muscle, with higher concentrations around the NMJ. **(E)** Western blot analysis of third instar larval body wall lysates blotted for Hts using the 1B1 antibody. hts^{01103} mutants display no detectable bands in comparison to wild-type, whereas *GS13858* expressed with *mef2-Gal4* results in elevated levels of multiple bands. Actin was used as a loading control. Scale bar in panel D represents 20µm (B-D).

We wondered if the NMJ defects observed in *hts*^{01103} mutant third instar larvae resulted in any noticeable effects on motor function. During the *Drosophila* life cycle, first instar larvae burrow into the food medium shortly after hatching from eggs. In the food, the first instar larvae molt into second instar larvae, which then molt into third instar larvae. Eventually, mature third instar larvae crawl out of the food to pupate. Although *hts*^{01103} mutant third instar larvae have underdeveloped NMJs, they were still able to crawl out of the food to pupate. While we did not evaluate if the larvae had any locomotory defects, we did notice that the homozygous mutants were generally delayed by a few days when crawling out of the food in comparison to their heterozygous siblings. Interestingly, *hts*^{01103} mutants died as pharate adults, i.e. the adult flies completed metamorphosis but failed to eclose from their pupal cases. Newly formed *hts*^{01103} mutant pharate adults that were dissected out of their pupal cases were still alive but moved feebly when compared to wild-type, indicating that they were too weak to emerge from their pupal cases on their own. This result was also observed when expressing transgenic *hts* RNAi in developing and adult somatic muscles with *mef2-Gal4* (see Movies 5 and 6 in the attached CD-ROM). Our results suggest that postsynaptic Hts is important for maintaining motor function, however, more extensive functional studies need to be performed. In particular, we are currently in collaboration with Dr. Bryan Stewart (Department of Cell & Systems Biology, University of Toronto) who will be performing electrophysiology studies. During a meeting with Dr. David Baillie (Department of Molecular Biology and Biochemistry, Simon Fraser University), he quipped that the loss of motor function observed only at later stages of the *Drosophila* life cycle may have interesting parallels to the late onset nature of ALS.

To further investigate the role of Hts at the NMJ, we also performed overexpression studies using the Gal4-UAS system (reviewed in Duffy, 2002). *hts* was overexpressed in the muscle by crossing a **Gene Search** (**GS**) line, *GS13858*, which bears UAS sequences upstream of the endogenous *hts* gene, to *mef2-Gal4* (Figure 22A) (Toba et al., 1999). *GS13858* driven with *mef2-Gal4* elevated Hts immunoreactivity

throughout the muscle, with higher concentrations found around the NMJ (Figure 22D) (Wang et al., 2011). Western blot analysis of third instar larval body wall lysates revealed increased levels of multiple Hts isoforms including Add1 and/or Add2 (Figure 22E) (Wang et al., 2011). In contrast to *hts*^{01103} mutants, *GS13858* expressed in the muscle with *mef2-Gal4* resulted in clearly overdeveloped NMJs in terms of synaptic branching at muscles 6/7 when compared to wild-type (see Figure 25A,C) (Wang et al., 2011). This result was confirmed using two other GS lines, *GS10063* and *GS13376*, as well as a *hts* transgene that encodes for the Add1 isoform (Figure 22A; data not shown). We conclude that postsynaptic Hts, more specifically the Add1 isoform, participates in regulating NMJ morphogenesis during larval development. As for the roles of presynaptic Hts during larval NMJ development, we chose not pursue this as we became aware that this was being studied by another research group (Pielage et al., 2011).

We performed a quantitative assessment of the Hts-associated NMJ morphological defects by measuring bouton number, branch number and branch length. This was done by staining the body walls of third instar larvae with an antibody against the synaptic vesicle protein, **Cysteine string protein** (**CSP**), which allowed us to visualize the boutons (see Figure 23A-C for representative images) (Zinsmaier et al., 1994). *hts*^{01103} mutant NMJs innervating muscles 6/7 had fewer and shorter branches but no significant difference in bouton number in comparison to wild-type (Figure 23D) (Wang et al., 2011). In contrast, *GS13858* driven in the muscle with *mef2-Gal4* resulted in NMJs at muscles 6/7 with significant increases in bouton number as well as branch number and length when compared to wild-type, the *mef2-Gal4* driver alone and *hts*^{01103} mutants (Figure 23D) (Wang et al., 2011). Note that the counts were performed by Jing Yang, a former M.Sc. student under Dr. Krieger (see the thesis entitled ''Regulation of neuromuscular synapse development by Hts in *Drosophila*'' which was submitted to the SFU Library in 2008) (Wang et al., 2011).

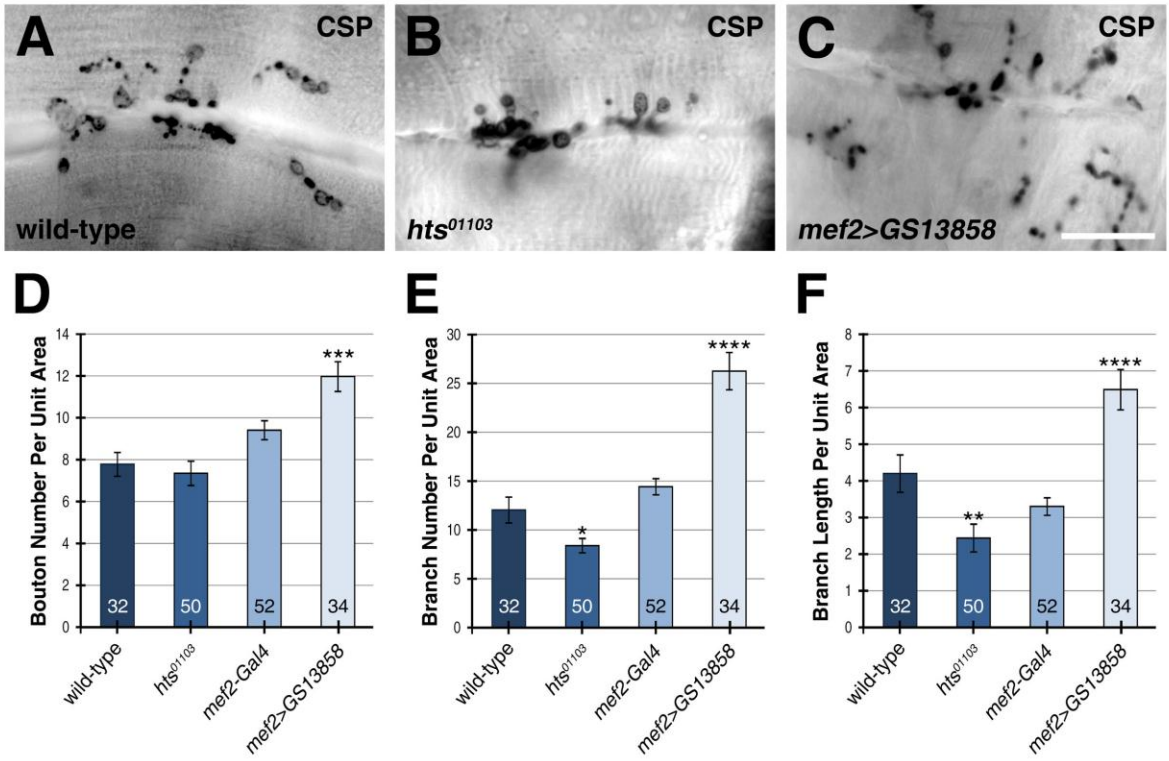
A
CSP
wild-type
B
CSP
hts01103
C
CSP
mef2>GS13858
D
Bouton Number Per Unit Area
14
12
10
8
6
4
2
0
***
32
50
52
34
wild-type
hts01103
mef2-Gal4
mef2>GS13858
E
Branch Number Per Unit Area
30
25
20
15
10
5
0
*
****
32
50
52
34
wild-type
hts01103
mef2-Gal4
mef2>GS13858
F
Branch Length Per Unit Area
8
7
6
5
4
3
2
1
0
**
****
32
50
52
34
wild-type
hts01103
mef2-Gal4
mef2>GS13858

FIGURE 23 Postsynaptic Hts regulates bouton number, branch number and branch length during larval NMJ development.

(A-C) Representative images of third instar larval NMJs stained with an anti-CSP antibody that was used for quantification. Immunoreactive signal was detected with a DAB colour reaction. Typical examples of wild-type (A), *hts*^{01103} (B) and *mef2>GS13858* (C) NMJs are shown. **(D-E)** Quantification of bouton number (D), branch number (E) and branch length (F) per unit surface area of muscle. *hts*^{01103} mutant NMJs have fewer and shorter branches but no significant difference in bouton number in comparison to wild-type. Conversely, *GS13858* expressed in the muscle with *mef2-Gal4* results in NMJs with significant increases in bouton number, branch number and branch length when compared to *mef2-Gal4* alone. Measurements were made on NMJs innervating muscles 6/7 in abdominal segment 4. Numbers in the bars of the graphs represent the total number of NMJs evaluated. As we measured NMJs from both hemisegments in each body wall, the number of third instar larvae that were examined is half. * $p<0.05$, ** $p<0.01$, *** $p<0.005$, **** $p<0.001$. Scale bar in Panel C represents 30µm (A-C).

2.4.3. Hts regulates Dlg postsynaptic targeting to the larval NMJ

As mentioned in the previous chapter, Dlg is a member of the MAGUK family of scaffolding proteins that plays critical roles in epithelial apicobasal polarity as a member of the Scrib complex (reviewed in Humbert et al., 2003; reviewed in Yamanaka and Ohno, 2008; reviewed in Roberts et al., 2012). At the larval NMJ, Dlg functions as a major scaffolding protein that orchestrates the assembly of large protein complexes that regulate both synaptic structure and function (reviewed in Ataman et al., 2006). We wondered if Hts interacts with Dlg during larval NMJ development as both are involved in regulating NMJ morphology (Lahey et al., 1994; Budnik et al., 1996; Mendoza et al., 2003; Mendoza-Topaz et al., 2008). In addition, the distribution of Hts at the postsynaptic region of the NMJ is similar to Dlg (Lahey et al., 1994). Interestingly, mammalian Dlg1/hDlg has been shown to bind to the homologue of Cora, Protein 4.1, which is a spectrin-actin cytoskeletal protein (Lue et al., 1994; reviewed in Baines, 2010). As adducin is a critical regulator of the spectrin-actin cytoskeleton, we hypothesized that Hts and Dlg interact to control synaptic plasticity during larval NMJ development (reviewed in Matsuoka et al., 2000).

We addressed whether Hts and Dlg interact during larval NMJ development by first determining if they co-localize at the postsynaptic membrane of type I boutons. This was done by co-staining wild-type third instar larval body walls with antibodies against Hts and Dlg. The Dlg antibody, which was also used in our Pak and Pak3 studies, is specific for the second PDZ domain at the N-terminus (Parnas et al., 2001). We chose to use the HtsM antibody for this particular experiment as the 1B1 antibody was made in the same species as the Dlg antibody. In NMJs innervating muscles 6/7, the localizations of the adducin isoforms of Hts and Dlg overlapped around the periphery of type I boutons (Figure 24A-A'') (Wang et al., 2011). However, their distribution patterns were not identical as Dlg immunoreactivity is more pronounced at type Ib than Is boutons, whereas Hts immunoreactivity appeared equal at both type I boutons (Lahey et al., 1994; Wang et al., 2011). We next determined whether Hts and Dlg can form a

complex through co-immunoprecipitation assays which were performed primarily by Jing Yang (see the thesis entitled ''Regulation of neuromuscular synapse development by Hts in *Drosophila*'' which was submitted to the SFU library in 2008). In whole wild-type third instar larval lysates, Hts immunoprecipitates blotted for Dlg revealed two bands at approximately 97kDa and 116kDa (Figure 24B) (Wang et al., 2011). The sizes are consistent for DlgA and DlgS97, an isoform of Dlg found at the NMJ (Lahey et al., 1994; Mendoza et al., 2003; Mendoza-Topaz et al., 2008). In reciprocal assays, Dlg immunoprecipitates blotted for Hts using the 1B1 antibody revealed a doublet at approximately 80kDa which is consistent for the sizes of Add1 and Add2, though the doublet may also represent posttranslational modifications of one of the isoforms (Figure 24B) (Wang et al., 2011). Our results show that the Add1 and/or Add2 isoforms of Hts overlap with Dlg at the postsynaptic membrane of larval NMJs, where they most likely form a complex with each other.

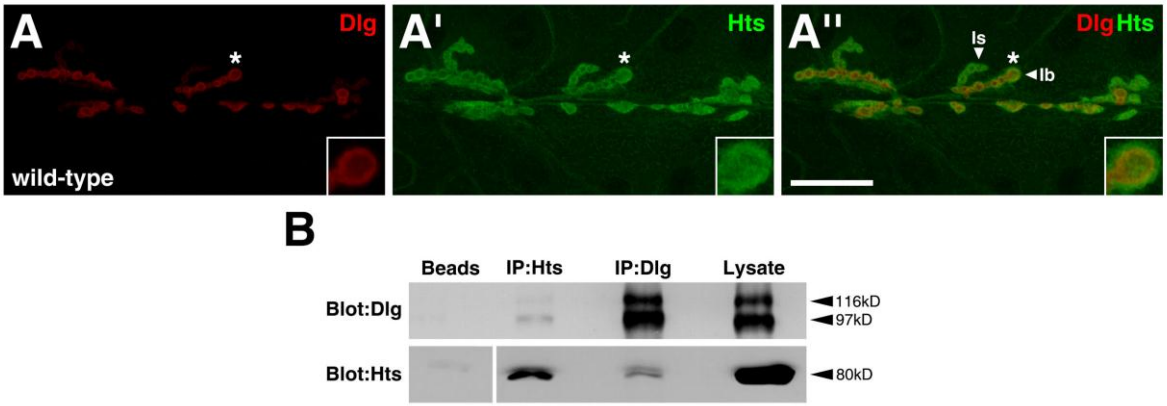
A
Dlg
wild-type
A'
Hts
A''
Dlg Hts
Is
Ib
B
Beads
IP:Hts
IP:Dlg
Lysate
Blot:Dlg
116kD
97kD
Blot:Hts
80kD

FIGURE 24 Hts and Dlg have similar distribution patterns at the postsynaptic membrane of larval NMJs, and exist in a complex.

(A-A'') Wild-type third instar larval NMJ at muscles 6/7 stained with antibodies against Hts, using the HtsM antibody, and Dlg. The localizations of the adducin isoforms of Hts and Dlg overlap at the postsynaptic membrane of type I boutons. However, their distribution patterns are not identical as Dlg is more pronounced at type Ib than Is boutons, whereas Hts appears equal at both type I boutons. Insets are higher magnifications of a single synaptic bouton (see asterisks). **(B)** Co-immunoprecipitation assays between Hts and Dlg. In whole wild-type third instar larval lysates, Hts immunoprecipitates blotted for Dlg reveal two bands at approximately 97kDa and 116kDa which are consistent for the DlgA and DlgS97 isoforms. In reciprocal assays, Dlg immunoprecipitates blotted for Hts using the 1B1 antibody reveals a doublet at approximately 80kDa which is consistent for the Add1 and/or Add2 isoforms. Hts and Dlg were not immunoprecipitated in our control assays involving naked beads. Scale bar in panel A'' represents 50μm (A-A'').

We next aimed to characterize the interaction between Hts and Dlg during larval NMJ development by determining whether Hts regulates Dlg localization. This was accomplished by examining Dlg postsynaptic targeting in hts^{01103} mutant NMJs. As mentioned previously, Dlg localizes to the postsynaptic membrane of type I boutons in wild-type third instar larvae (Figure 25A-A'') (Lahey et al., 1994). In hts^{01103} mutants, Dlg appeared to still localize tightly to the postsynaptic membrane giving us the initial impression that Hts does not affect Dlg localization (Figure 25B-B'') (Wang et al., 2011). However, upon closer analysis through measuring the ratio between the fluorescence intensities of Dlg immunoreactivity at the NMJ versus Hrp immunoreactivity, where Hrp was used as a control stain, it was revealed that Dlg levels were actually reduced when compared to wild-type (Figure 25E) (Wang et al., 2011). In Western blot analysis of third instar larval body wall lysates, hts^{01103} mutants had similar overall levels of Dlg in comparison to wild-type indicating that Hts regulates Dlg localization and not Dlg protein levels (Figure 25D) (Wang et al., 2011).

To confirm that Hts regulates Dlg postsynaptic targeting at the larval NMJ, we also performed overexpression studies. When *GS13858* was expressed in the muscle with *mef2-Gal4*, Dlg no longer localized tightly to the postsynaptic membrane, instead appearing diffuse and extending away from the NMJ into the surrounding muscle (Figure 25C-C'') (Wang et al., 2011). This result was confirmed using a *hts* transgene that encodes for the Add1 isoform (see Figure 33B-B''). Measurement of the ratio between Dlg and Hrp fluorescence intensities revealed that Dlg levels at the NMJ were severely reduced when compared to both wild-type and hts^{01103} mutants (Figure 25E) (Wang et al., 2011). Western blot analysis of third instar larval body wall lysates showed that *GS13858* driven with *mef2-Gal4* had no effect on the overall levels of Dlg in comparison to wild-type, further indicating that Hts does not regulate Dlg protein levels (Figure 25D) (Wang et al., 2011). To ensure that the disruption of Dlg postsynaptic targeting is specific and not due to general defects in muscle development, Mannan Wang examined the distribution patterns of other postsynaptic proteins. Although

there were mild decreases in the levels of Pak and Glutamate receptor IIB when *GS13858* was expressed in the muscle with *mef2-Gal4*, both proteins were not delocalized indicating that both proteins were still preferentially targeted to the postsynaptic region of the NMJ (see the thesis entitled ''Muscle-associated *Drosophila* adducin regulates larval neuromuscular junction development and the location of Draper to the synapse'' which will be submitted to the SFU Library in 2013).

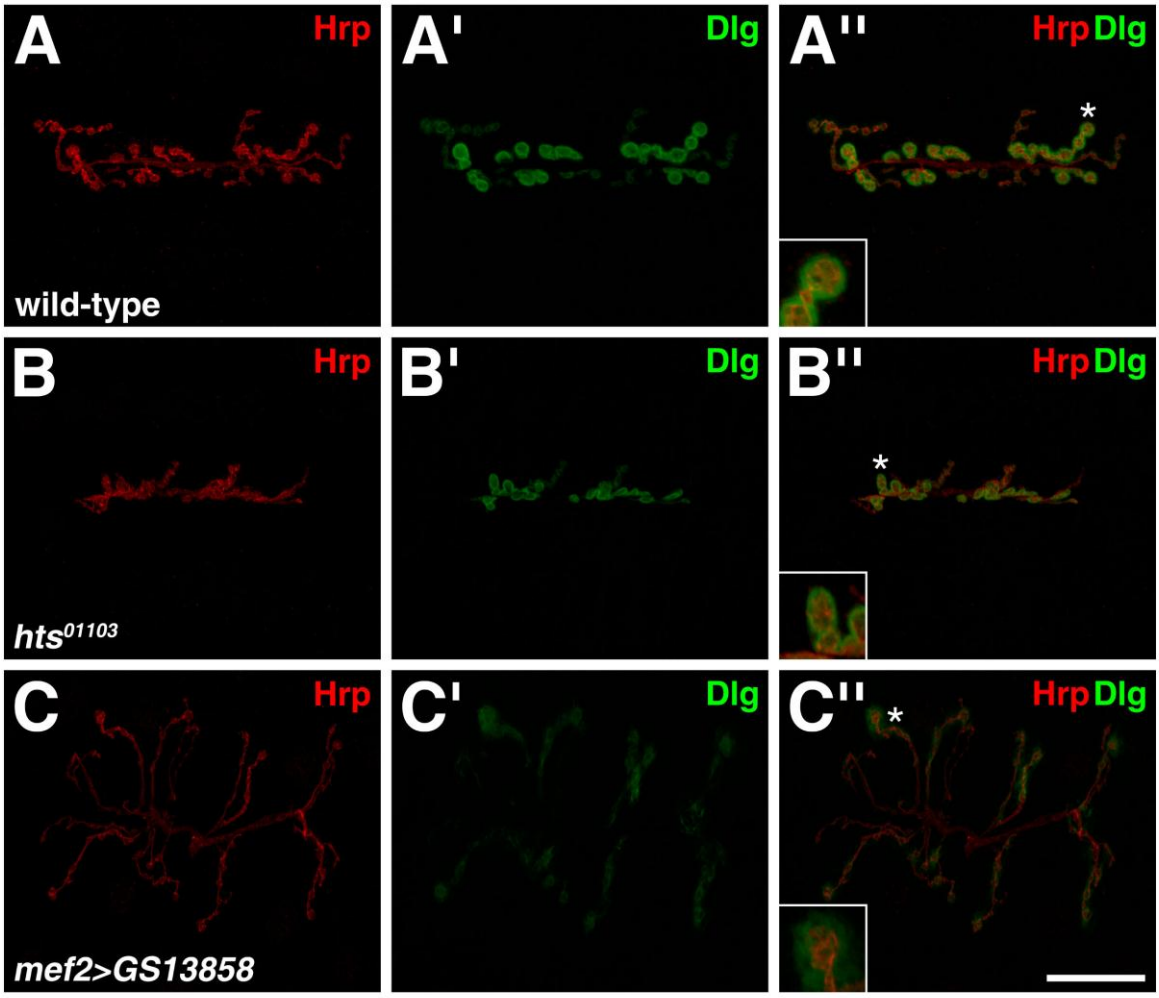
A
Hrp
A'
Dlg
A''
Hrp Dlg
wild-type
B
Hrp
B'
Dlg
B''
Hrp Dlg
hts01103
C
Hrp
C'
Dlg
C''
Hrp Dlg
mef2>GS13858

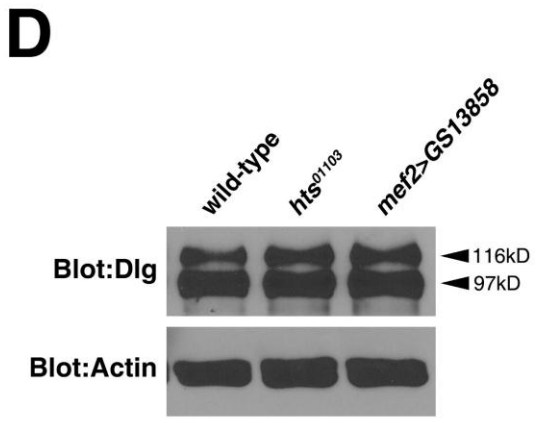
D
wild-type
hts01103
mef2>GS13858
Blot:Dlg
116kD
97kD
Blot:Actin

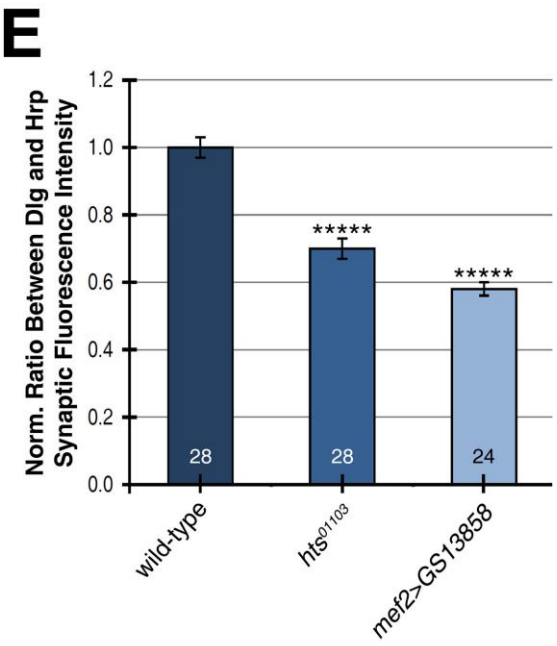
E
Norm. Ratio Between Dlg and Hrp Synaptic Fluorescence Intensity
1.2
1.0
0.8
0.6
0.4
0.2
0.0
*****
*****
28
28
24
wild-type
hts01103
mef2>GS13858

FIGURE 25 Hts disrupts Dlg localization at the postsynaptic membrane during larval NMJ development.

(A-C'') Comparative analysis of third instar larval NMJs at muscles 6/7 stained with antibodies against Hrp and Dlg. (A) A typical wild-type NMJ. (B) In hts^{01103} mutants, Dlg appears to still localize to the postsynaptic membrane. (C) When *GS13858* is driven in the muscle with *mef2-Gal4*, Dlg no longer localizes tightly to the postsynaptic membrane, instead appearing diffuse and extending away from the NMJ into the surrounding muscle. Insets are higher magnifications of a single synaptic bouton (see asterisks). **(D)** Western blot analysis of third instar larval body wall lysates blotted for Dlg. Overall Dlg protein levels remain unaffected in both hts^{01103} mutants and when *GS13858* is expressed with *mef2-Gal4* in comparison to wild-type. Actin was used as a loading control. **(E)** Quantification of the ratio between the fluorescence intensities of Dlg immunoreactivity versus Hrp immunoreactivity at the NMJ. hts^{01103} mutants and *GS13858* expression in the muscle result in significantly reduced levels of Dlg at the NMJ when compared to wild-type. Measurements were made on NMJs at muscles 6/7 in abdominal segments 3 to 5, and normalized against wild-type. Numerical values in the bars of the graph represent the total number of NMJs evaluated. As we examined NMJs from two hemisegments in each body wall, the number of third instar larvae that were evaluated is half. ***** $p<0.0001$. Scale bar in panel C'' represents 30µm (A-C'').

Based on our overexpression studies, it appears that Hts disrupts Dlg postsynaptic targeting to the larval NMJ. According to this hypothesis, we would expect to see higher levels of Dlg at the NMJs of *hts*^{01103} mutants. It has been previously reported, however, that the *hts*^{01103} mutation also causes defects in the structure of the **subsynaptic reticulum** (**SSR**), an elaborate organization of muscle membrane folds that surround type I boutons and is required for Dlg localization (Lahey et al., 1994; Pielage et al., 2011). This makes examining the effects of *hts* loss-of-function mutations directly on Dlg localization at the NMJ difficult to interpret as there are also synaptic structural defects. In recent work done in collaboration with Mannan Wang, we decided to reduce *hts* transcript levels with the use of a transgenic RNAi line (Dietzl et al., 2007). We hoped that a knockdown of Hts function would result in a weaker effect on SSR development, thus allowing us to study Dlg localization directly. Indeed, preliminary data have indicated that the expression of transgenic *hts* RNAi in the muscle with *mef2-Gal4* leads to higher levels of Dlg at the NMJ (data not shown) (see the thesis entitled ''Muscle-associated *Drosophila* adducin regulates larval neuromuscular junction development and the location of Draper to the synapse'' which will be submitted to the SFU Library in 2013). From the evidence that is presented in this section, we conclude that Hts negatively regulates the localization of Dlg at the postsynaptic membrane during larval NMJ development.

2.4.4. Hts and Dlg genetically interact during embryonic development

Due to our interests in epithelial apicobasal polarity, we were curious to see if Hts also plays a role in the process as we have shown that Hts regulates Dlg localization during larval NMJ development. As detailed in the previous chapter, there is a dynamic regulation of Dlg localization at the leading edge membrane of DME cells during dorsal closure. Previous studies have shown that Hts is restricted to the anterior pole of the early embryo (Zaccai and Lipshitz, 1996a; Zaccai and Lipshitz, 1996b). Stage 14 and 15 wild-type embryos stained with the 1B1 antibody revealed that Hts localized

predominately to the membranes of both the epidermal and amnioserosa cells (data not shown; see comparable results with the HtsM antibody in Figure 26A',B'). Surprisingly, Hts was missing along the leading edge membrane of DME cells during dorsal closure, but subsequently restored as opposing DME cells met at the dorsal midline, similar to the Scrib complex proteins such as Dlg (Wang et al., 2011). In order to make a more detailed comparative analysis between Hts and the Scrib complex proteins, we co-stained stage 14 and 15 wild-type embryos with antibodies against Hts, using the HtsM antibody, and Dlg. Similar to our observations made at the larval NMJ, Hts and Dlg immunoreactive signals overlapped but were not identical in the embryonic epidermis (Figure 26A-B''). In DME cells, for instance, Hts did not extend as far dorsally towards the leading edge membrane when compared to Dlg (Figure 26A-A'') (Wang et al., 2011). In addition, Hts extended more basally along the apicobasal axis than Dlg (Figure 26C-C'') (Wang et al., 2011).

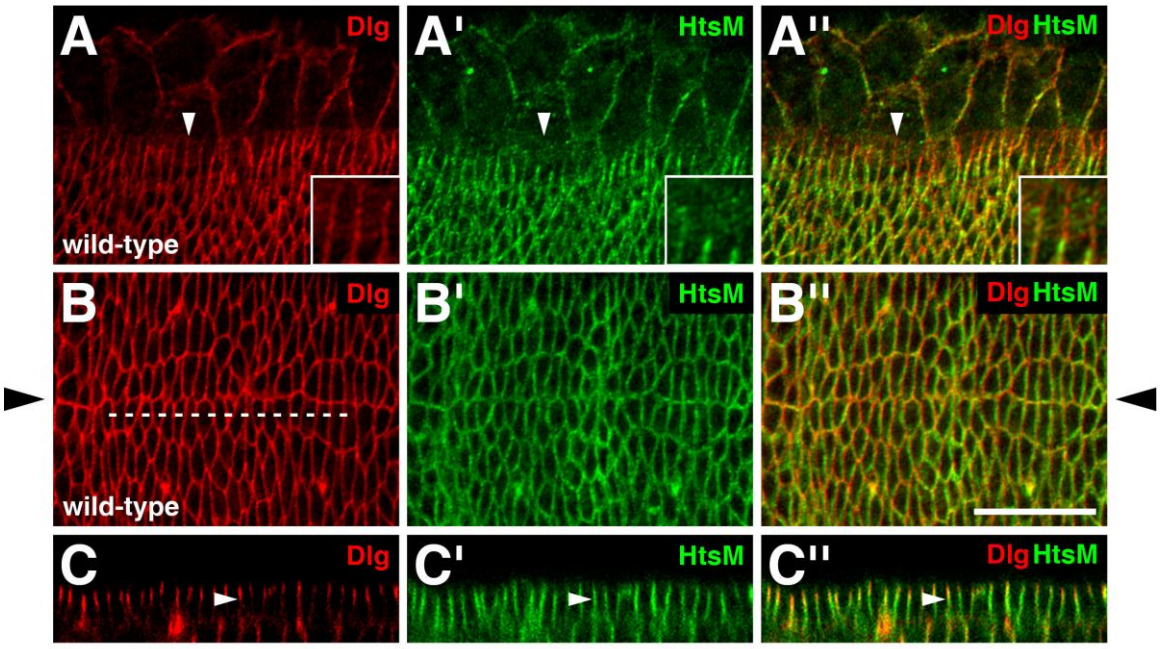
A
Dlg
A'
HtsM
A''
Dlg HtsM
wild-type
B
Dlg
B'
HtsM
B''
Dlg HtsM
wild-type
C
Dlg
C'
HtsM
C''
Dlg HtsM

FIGURE 26 Hts and Dlg have similar distribution patterns during dorsal closure.

(A-C'') Wild-type embryos stained with antibodies against Hts, using the HtsM antibody, and Dlg. (A-A'') Dorsolateral view of a stage 14 embryo. The distribution patterns of Hts and Dlg overlap at the cell membranes of the epidermis and amnioserosa. Similar to the Scrib complex proteins, Hts is missing along the leading edge membrane of DME cells during dorsal closure. However, Hts does not extend as dorsally towards the leading edge when compared to Dlg (see white arrowheads). Insets are higher magnifications of a few DME cells. (B-B'') Dorsal view of a stage 15 embryo. Hts, like the Scrib complex proteins, is restored at the leading edge membrane of DME cells when the opposing epidermal flanks meet at the dorsal midline (denoted by black arrowheads) upon dorsal closure completion. (C-C'') Cross-sectional view of a row of DME cells (the dashed line in panel B is where the z-section was taken). Dlg and Hts overlap along the apicobasal axis, but Hts extends more basally than Dlg (see white arrowheads). Scale bar in panel B'' represents 30μm (A-B'').

Owing to its distribution during late embryonic development, we decided to investigate whether Hts is required for dorsal closure. This was done by examining *hts*^{01103} mutant embryos via cuticle preparation. During dorsal closure, Hts immunoreactivity was not detected at the epidermal and amnioserosa cell membranes in *hts*^{01103} mutant embryos (see Figure 28A). In cuticle preparations, the *hts*^{01103} mutant stock, i.e. *hts*^{01103}*/CyO* males crossed to *hts*^{01103}*/CyO* females, showed only a low frequency of embryonic defects when compared to a wild-type control (Figure 27D) (Wang et al., 2011). The most prevalent defects were embryos with head holes, indicating problems with head involution, and embryos that had secreted only a small amount of cuticle, indicating problems with epithelial integrity (see Figure 27A-C for representative images). We observed similar embryonic defects at more appreciable levels when the *hts*^{01103} mutant stock was outcrossed to wild-type, i.e. *hts*^{01103}*/+* males crossed to *hts*^{01103}*/+* virgin females, thus demonstrating that the *hts* mutation itself, and not the balancer, is responsible for the defects observed in embryonic development (Figure 27D) (Wang et al., 2011). We were also able to reproduce these results when the *hts*^{01103} mutant stock was crossed to a deficiency that removes the *hts* gene, i.e. *hts*^{01103}*/CyO* males crossed to *Df(2R)BSC26/CyO* virgin females, as well as in a different *hts* mutant stock, *hts*^{k06121}*/CyO*, thereby ruling out the possibility of interfering second site mutations (Figure 27D) (Wang et al., 2011). One potential reason as to why we observe a low penetrance of embryonic defects could be due to a maternal effect, as Hts is present during early embryogenesis (Ding et al., 1993; Zaccai and Lipshitz, 1996a; Zaccai and Lipshitz, 1996b). Unfortunately, we could not induce germline clones as Hts is also required for oogenesis (Yue and Spradling, 1992; Lin et al., 1994; Zaccai and Lipshitz, 1996a; Deng and Lin, 1997; Petrella et al., 2007). Although we did not observe any appreciable defects in dorsal closure, the *hts* mutant embryos that displayed defects in epithelial integrity may indicate a possible role for Hts in establishing apicobasal polarity. Interestingly, a previous study has implicated mammalian adducins in intercellular junction remodelling where α- and γ-adducin promote the assembly and

antagonize the stimuli-induced disassembly of both the adherens and tight junctions in human epithelial cells (Naydenov and Ivanov, 2010).

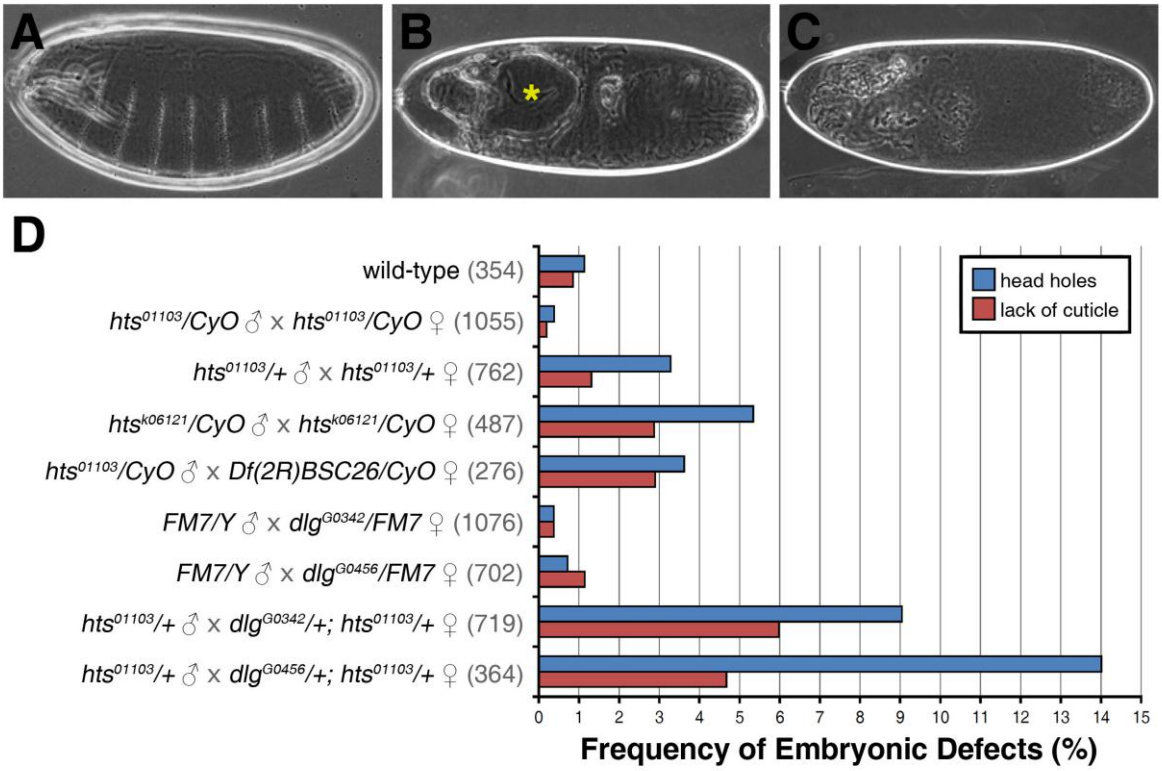
A
B
C
D
wild-type (354)
hts01103/CyO ♂ x hts01103/CyO ♀ (1055)
hts01103/+ ♂ x hts01103/+ ♀ (762)
htsk06121/CyO ♂ x htsk06121/CyO ♀ (487)
hts01103/CyO ♂ x Df(2R)BSC26/CyO ♀ (276)
FM7/Y ♂ x dlgG0342/FM7 ♀ (1076)
FM7/Y ♂ x dlgG0456/FM7 ♀ (702)
hts01103/+ ♂ x dlgG0342/+; hts01103/+ ♀ (719)
hts01103/+ ♂ x dlgG0456/+; hts01103/+ ♀ (364)
head holes
lack of cuticle
0 1 2 3 4 5 6 7 8 9 10 11 12 13 14 15
Frequency of Embryonic Defects (%)

FIGURE 27 Hts and Dlg genetically interact during embryonic development.

(A-C) Representative images of embryonic cuticle phenotypes resulting from *hts* and *dlg* mutations. (A) A typical wild-type cuticle. (B-C) The most prevalent defects observed in *hts* and *dlg* mutants are head holes (see yellow asterisk) (B) and embryos that secrete only a small amount of cuticle (C). **(D)** Quantification of embryos that either had a head hole or failed to secrete a cuticle. Progeny were examined from stocks and crosses bearing various *hts* and *dlg* alleles, and are listed to the left of each bar of the graph. Numerical values in brackets denote the total number of progeny counted. Note that the highest percentage of defects is observed in embryos that were homozygous mutant for *hts* and heterozygous mutant for *dlg* in comparison to *hts* and *dlg* mutants alone. This suggests that the two genes genetically interact during embryonic development.

We next wanted to assess whether Hts and Dlg interact during embryonic development, owing to their similar distributions during dorsal closure and Hts' potential role in apicobasal polarity. This was accomplished by examining embryos that were both homozygous mutant for *hts* and heterozygous mutant for *dlg* through cuticle preparations. In this experiment, we utilized two P-element insertion alleles of *dlg* that are post-embryonic lethal: dlg^{G0342} and dlg^{G0456} (Peter et al., 2002). When crossing hts^{01103}/+ males to either dlg^{G0342}/+; hts^{01103}/+ or dlg^{G0456}/+; hts^{01103}/+ virgin females, the resulting progeny exhibited embryonic defects at a frequency that was substantially higher than what was observed in the *hts* and *dlg* mutant stocks alone (Figure 27D) (Wang et al., 2011). Again, the most predominant defects were embryos that either had a head hole or failed to secrete a cuticle. These results strongly implicate the existence of a genetic interaction between Hts and Dlg during embryonic development.

We postulated that Hts regulates Dlg localization along the apicobasal axis of epithelial cell membranes during embryogenesis based on our studies at the larval NMJ. In hts^{01103} mutant embryos, Dlg cortical localization in the epidermis and amnioserosa appeared unaffected (Figure 28B,C). Furthermore, the distribution of Dlg at the leading edge membrane of DME cells throughout dorsal closure was normal. That is, Dlg was still missing along the leading edge during dorsal closure, and was still subsequently restored upon dorsal closure completion. When we expressed *GS13858* in embryonic segmental stripes with the *prd-Gal4* driver, however, Dlg cortical localization was disrupted in the amnioserosa but not in the epidermis (Figure 28D-D'') (Wang et al., 2011). Our results show that Hts can also negatively regulate the membrane localization of Dlg in a subset of embryonic epithelia, indicating that Hts-mediated regulation of Dlg is conserved in non-neuronal tissue.

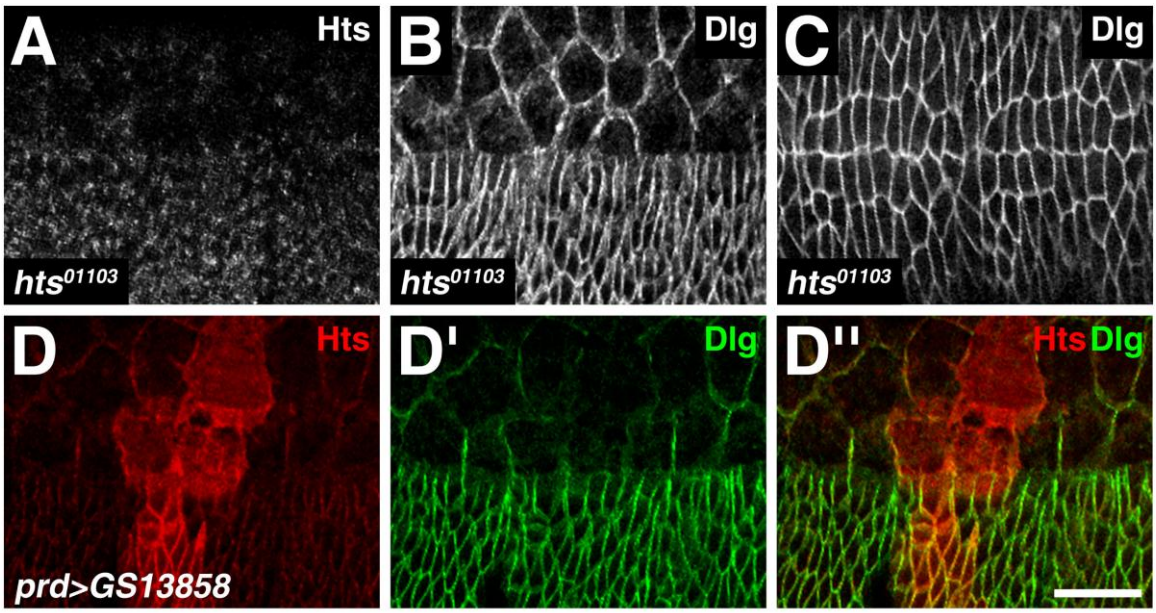
A
Hts
hts01103
B
Dlg
hts01103
C
Dlg
hts01103
D
Hts
prd>GS13858
D'
Dlg
D''
Hts Dlg

FIGURE 28 Hts disrupts Dlg localization in the amnioserosa during dorsal closure.

(A) Dorsolateral view of a stage 14 *hts*^{01103} mutant embryo stained for Hts using the 1B1 antibody. Hts immunoreactivity is not detected at the epidermal and amnioserosa cell membranes. **(B-C)** *hts*^{01103} mutant embryos stained with the anti-Dlg antibody. (B) Dorsolateral view of a stage 14 mutant embryo. Dlg cortical localization in the epidermis and amnioserosa is unaffected. Furthermore, Dlg is still missing along the leading edge during dorsal closure. (C) Dorsal view of a stage 15 mutant embryo. Dlg is still restored at the leading edge upon dorsal closure completion. **(D-D'')** Dorsolateral view of a stage 14 *prd>GS13858* embryo stained with antibodies against Hts, using the 1B1 antibody, and Dlg. When expressing *GS13858* in epidermal stripes with the segmental *prd-Gal4* driver, Dlg cortical localization is disrupted in the amnioserosa but not in the epidermis. Scale bar in panel D'' represents 30µm (A-D'').

2.4.5. Hts regulates Dlg phosphorylation through PAR-1 and CaMKII in both muscle and epithelial cells

Previous studies have reported that the overexpression of two protein kinases during larval NMJ development in *Drosophila* can disrupt the localization of Dlg at the postsynaptic membrane through phosphorylation (Koh et al., 1999; Zhang et al., 2007). These studies strongly resemble our result when Hts levels are elevated in the muscle. The two kinases are **Partitioning-defective 1** (**PAR-1**) and **Calcium/calmodulin-dependent protein kinase** (**CaMKII**). We wondered if Hts acts through PAR-1 or CaMKII mediated phosphorylation to regulate Dlg postsynaptic targeting at the larval NMJ.

PAR-1 is a conserved serine/threonine kinase that regulates polarity in oocytes, neurons and epithelia (reviewed in Goldstein and Macara, 2007). In mammals, the PAR-1 homologues, the **microtubule affinity regulating kinases** (**MARKs**), can phosphorylate the microtubule associated protein tau (Drewes et al., 1997). Abnormal tau phosphorylation is observed in neurodegenerative disorders such as Alzheimer's disease and aberrant activation of PAR-1 can lead to neurodegeneration in *Drosophila* (Augustinack et al., 2002; Nishimura et al., 2004). PAR-1 negatively regulates the localization of Dlg at the postsynaptic membrane of *Drosophila* larval NMJs by phosphorylating a conserved serine 797 residue in the GUK domain (Zhang et al., 2007).

CaMKII is a ubiquitously expressed, broad-specificity serine/threonine kinase that is regulated by intracellular calcium levels, and is highly enriched in the CNS (reviewed in Cammarota et al., 2002; reviewed in Ataman et al., 2006). CaMKII undergoes autophosphorylation at threonine 286 when stimulated by Ca^{2+}/calmodulin, resulting in CaMKII activity that is no longer dependent on the initial Ca^{2+} signal (reviewed in Griffith, 2004b). Due to its ability to transform transient Ca^{2+} concentrations into more persistent states of kinase activity, CaMKII has been implicated in learning and memory processing (reviewed in Griffith, 2004a). At the *Drosophila* larval NMJ, CaMKII also negatively regulates the localization of Dlg at the

postsynaptic membrane, but by phosphorylating a conserved serine 48 residue in the second PDZ domain (Koh et al., 1999).

We tested whether Hts can promote Dlg phosphorylation by first using an antibody that detects PAR-1-dependent phosphorylation of Dlg at serine 797 in the GUK domain (Zhang et al., 2007). Low levels of **phosphorylated Dlg** (**p-Dlg**) are present at the NMJ and throughout the muscle in wild-type body walls (Figure 29A) (Zhang et al., 2007). Though not originally reported, we show that p-Dlg also localized to punctate structures in the muscle (Wang et al., 2011). In hts^{01103} mutants, p-Dlg puncta levels in the muscle were significantly reduced when compared to wild-type (Figure 29B,D) (Wang et al., 2011). p-Dlg levels specifically at the NMJ also appeared reduced, though we did not quantify this attribute. We were able to confirm these results through Western blot analysis of third instar larval body wall lysates, as hts^{01103} mutants had lower overall levels of p-Dlg in comparison to wild-type (Figure 29E) (Wang et al., 2011). In overexpression experiments, *GS13858* driven with *mef2-Gal4* resulted in significant elevations of p-Dlg puncta levels throughout the muscle (Figure 29C,D) (Wang et al., 2011). This result was also confirmed through Western blot analysis, as muscle-specific *GS13858* expression lead to higher overall levels of p-Dlg (Figure 29E) (Wang et al., 2011). We were initially surprised that we did not see elevated levels concentrated around the NMJ. However, postsynaptic overexpression of PAR-1 also causes an increase in p-Dlg levels not specifically at the NMJ, but broadly distributed throughout the muscle (Zhang et al., 2007). One possible explanation for this observation is that as Dlg postsynaptic targeting is disrupted, p-Dlg at the NMJ is spread out over a larger area and is more difficult to detect. As we have shown that Hts can disrupt Dlg membrane localization in the amnioserosa, we also assessed whether Hts can promote Dlg phosphorylation during dorsal closure. Indeed, overexpression of *GS13858* in epidermal stripes with the segmental *prd-Gal4* driver caused elevated p-Dlg levels in the epidermis and amnioserosa (Figure 29F-F'') (Wang et al., 2011). Unfortunately, we could not perform parallel experiments to test whether Hts can promote CaMKII-dependent

phosphorylation of Dlg at serine 48 in the second PDZ domain, as there was no available phospho-specific antibody against the site at the time. From these results, we conclude that Hts promotes Dlg phosphorylation, at least at the PAR-1 target site at serine 797 in the GUK domain, in both neuronal and epithelial cells.

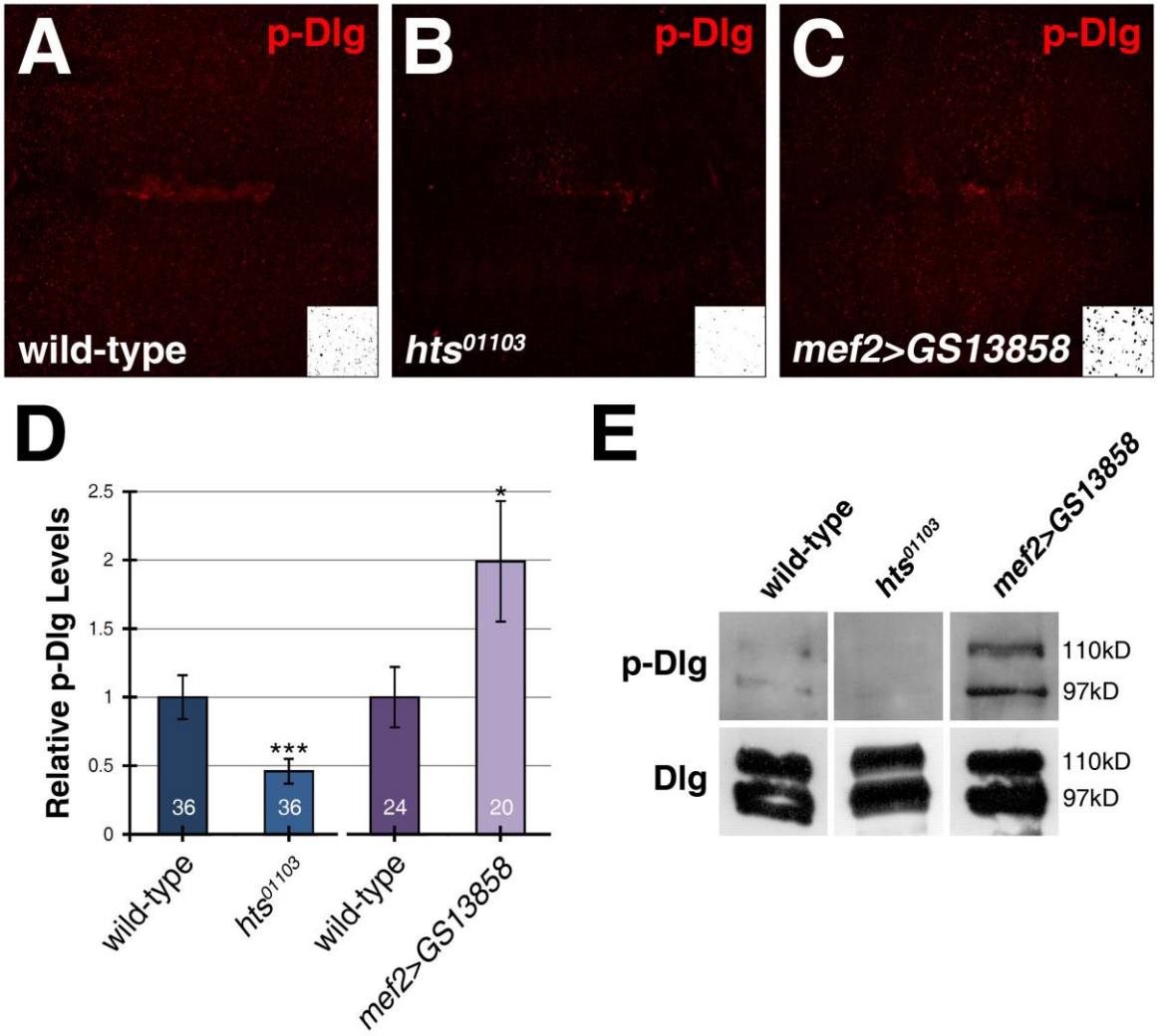
A
p-Dlg
wild-type
B
p-Dlg
hts01103
C
p-Dlg
mef2>GS13858
D
Relative p-Dlg Levels
2.5
2
1.5
1
0.5
0
*
***
36
36
24
20
wild-type
hts01103
wild-type
mef2>GS13858
E
wild-type
hts01103
mef2>GS13858
p-Dlg
110kD
97kD
Dlg
110kD
97kD

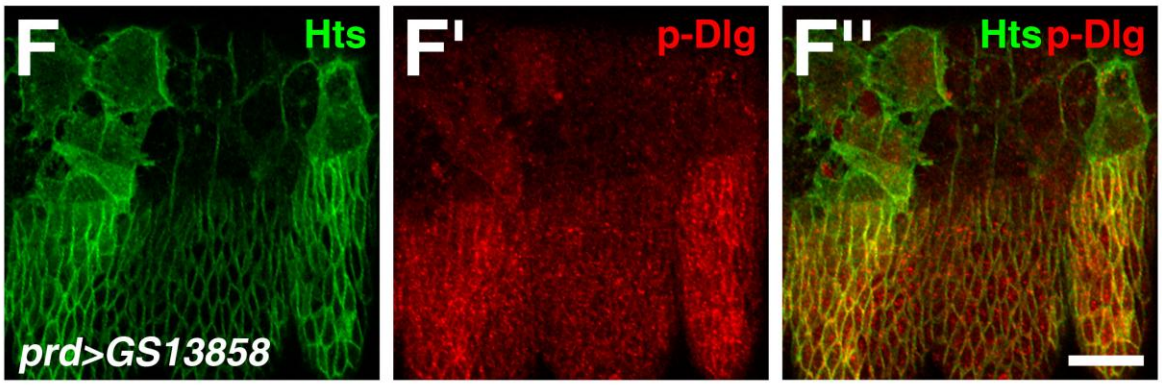
F
Hts
prd>GS13858
F'
p-Dlg
F''
Hts p-Dlg

FIGURE 29 Hts promotes Dlg phosphorylation in muscle and epithelial cells.

(A-C) Comparative analysis of third instar larval NMJs at muscles 6/7 stained with an anti-p-Dlg antibody that detects phosphorylation at serine 797 in the GUK domain, i.e. the PAR-1 target site. (A) A typical wild-type NMJ with p-Dlg immunoreactive puncta throughout the muscle. (B) In hts^{01103} mutants, p-Dlg puncta levels are reduced. (C) When *GS13858* is driven in the muscle with *mef2-Gal4*, p-Dlg puncta levels are elevated. Insets are black and white, inverted images of a section of muscle to allow for easier visualization of the p-Dlg puncta. **(D)** Quantification of p-Dlg puncta levels in the muscle. Measurements were performed by converting the images to black and white, inverted images (see insets in panels A-C for examples) and measuring the number of black pixels. When compared to wild-type, hts^{01103} mutants have significantly reduced p-Dlg levels whereas *GS13858* expression in the muscle results in significantly elevated p-Dlg levels. Measurements were made on muscles 6 and 7 in abdominal segments 3 to 5, and normalized against wild-type. Numerical values in the bars of the graph represent the total number of muscle 6/7 pairs evaluated. As we examined muscles from two hemisegments in each body wall, the number of third instar larvae that were evaluated is half. * $p<0.05$, *** $p<0.005$. **(E)** Western blot analysis of third instar larval body wall lysates blotted for p-Dlg. Overall p-Dlg levels in hts^{01103} mutants are reduced when compared to wild-type. In contrast, *GS13858* expression with *mef2-Gal4* results in elevated overall levels of p-Dlg. Total Dlg protein levels were used as a control. **(F-F'')** Dorsolateral view of a stage 14 *prd>GS13858* embryo stained for Hts, using the 1B1 antibody, and p-Dlg. When expressing *GS13858* in epidermal stripes with the segmental *prd-Gal4* driver, p-Dlg levels are elevated in both the epidermis and amnioserosa. Scale bar in panel F'' represents 20µm (F-F'').

We next tested whether Hts regulates Dlg phosphorylation at the kinase level through the use of antibodies against PAR-1 and CaMKII (Koh et al., 1999; Zhang et al., 2007). PAR-1 and CaMKII concentrate at the postsynaptic membrane of type I boutons in wild-type NMJs, with lower levels found uniformly throughout the muscle (Figure 30A,D) (Koh et al., 1999; Zhang et al., 2007). In hts^{01103} mutants, PAR-1 and CaMKII levels appeared reduced (Figure 30B,E) (Wang et al., 2011). That is, the distribution of PAR-1 and CaMKII was altered as both kinases were no longer uniform throughout the muscle but appeared concentrated around muscle nuclei. This may suggest that Hts is required for proper PAR-1 and CaMKII processing and/or trafficking. When *GS13858* was expressed in the muscle with *mef2-Gal4*, PAR-1 and CaMKII protein levels were both dramatically elevated throughout the muscle (Figure 30C,D) (Wang et al., 2011). The effects of Hts on PAR-1 localization at the postsynaptic membrane could not be determined as our PAR-1 immunostainings showed only weak NMJ localization in contrast to what was originally reported (Zhang et al., 2007). This is probably due to the fact that we could not obtain the PAR-1 antibody used in that study and had to rely on a different antibody used primarily to study PAR-1 during oogenesis (Tomancak et al., 2000). We did not determine the effects of Hts on CaMKII localization at the postsynaptic membrane as well, since we could not distinguish between presynaptic and postsynaptic CaMKII. We were able to confirm Hts' ability to regulate PAR-1 and CaMKII protein levels by overexpressing *GS13858* in epidermal stripes with the segmental *prd-Gal4* driver during dorsal closure (Figure 30G-H'') (Wang et al., 2011). PAR-1 levels were elevated in both the epidermis and amnioserosa, but CaMKII was only elevated in the amnioserosa though recent results from our lab indicate that CaMKII levels are also elevated in the epidermis. Thus, these results show that Hts can promote PAR-1 and CaMKII protein levels in both neuronal and epithelial cells.

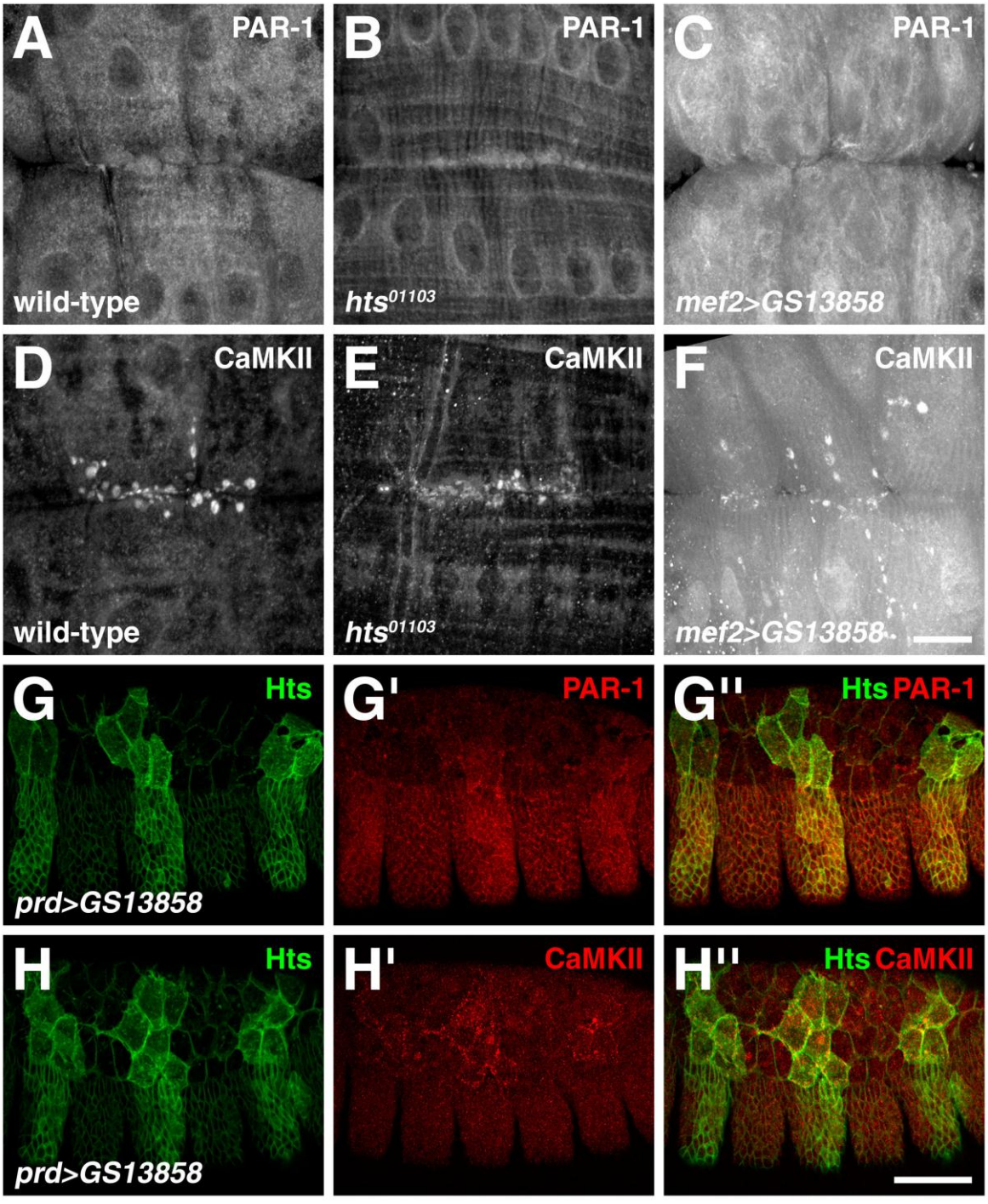
A
PAR-1
wild-type
B
PAR-1
hts01103
C
PAR-1
mef2>GS13858
D
CaMKII
wild-type
E
CaMKII
hts01103
F
CaMKII
mef2>GS13858
G
Hts
prd>GS13858
G'
PAR-1
G''
Hts PAR-1
H
Hts
prd>GS13858
H'
CaMKII
H''
Hts CaMKII

FIGURE 30 Hts elevates PAR-1 and CaMKII levels in muscle and epithelial cells.

(A-F) Comparative analysis of third instar larval NMJs at muscles 6/7 stained with PAR-1 (A-C) and CaMKII (D-F) antibodies. (A,D) PAR-1 (A) and CaMKII (D) localize to the postsynaptic membrane of wild-type NMJs, with lower levels found uniformly throughout the muscle. (B,E) In hts^{01103} mutants, PAR-1 (B) and CaMKII (E) levels are reduced. That is, the distribution of PAR-1 and CaMKII appears altered as both kinases are no longer uniform throughout the muscle. (C,F) When *GS13858* is driven in the muscle with *mef2-Gal4*, PAR-1 (C) and CaMKII (F) levels are both dramatically elevated throughout the muscle. **(G-H'')** Dorsolateral view of stage 14 *prd>GS13858* embryos stained for Hts, using the 1B1 antibody, and either PAR-1 (G-G'') or CaMKII (H-H''). When expressing *GS13858* in epidermal stripes with the segmental *prd-Gal4* driver, PAR-1 levels are elevated in both the epidermis and amnioserosa (G-G''), however, CaMKII elevations were only observed in the amnioserosa (H-H'') though we do observe elevations in the epidermis in some cases. Scale bar in panel F represents 20µm (A-F), scale bar in panel H'' represents 40µm (G-H'').

2.4.6. Hts phosphorylation at the MARCKS domain partially suppresses Hts' ability to regulate Dlg postsynaptic targeting to the larval NMJ

To study the *in vivo* effects of Hts phosphorylation at the MARCKS domain during NMJ development, we created non-phosphorylatable and phospho-mimetic *hts* transgenes. Single amino acid substitutions were made to the putative PKC target site in Hts by altering the codon sequence in cDNA encoding the Add1 isoform through site-directed mutagenesis (reviewed in Matsuoka et al., 2000). The non-phosphorylatable *hts* transgene, *UAS-hts*^{S705A}, contains a substitution of the serine at position 705 to an alanine, a non-phosphorylatable amino acid. In contrast, the phospho-mimetic *hts* transgene, *UAS-hts*^{S705D}, contains a substitution of the serine to an aspartic acid, a negatively charged amino acid that mimics a phosphorylative state. A wild-type *hts* transgene, i.e. *UAS-hts*^{S705S}, was also made to serve as a control. All three transgenes were created by Vincent Chui and Tomas Kuca, former students under Dr. Krieger (see the thesis entitled ''The regulation of Hu-li tai shao (Hts) at the *Drosophila* neuromuscular junction'' which was submitted to the SFU Library in 2011).

Before we could perform a comparative analysis between the different *hts* transgenes, the expression levels of each transgene first had to be evaluated. P element transposition, and not the more recently developed ϕC31 integrase system which allows for transgene insertion into predetermined sites in the *Drosophila* genome, was used to make the transgenic flies (Bateman et al., 2006). Since P element transposition into the *Drosophila* genome is random, differences in the location of each transgene may lead to different expression levels thus making direct comparisons between the transgenes difficult. We expressed the wild-type, non-phosphorylatable and phospho-mimetic *hts* transgenes throughout the muscle with the *mef2-Gal4* driver. We then measured total Hts protein levels in third instar larval body wall lysates through Western blot analysis using the 1B1 antibody. All three transgenes showed comparable elevations in Hts protein levels over the wild-type control (Figure 31). Thus, we can make direct comparisons between the different *hts* transgenes due to their similar expression levels.

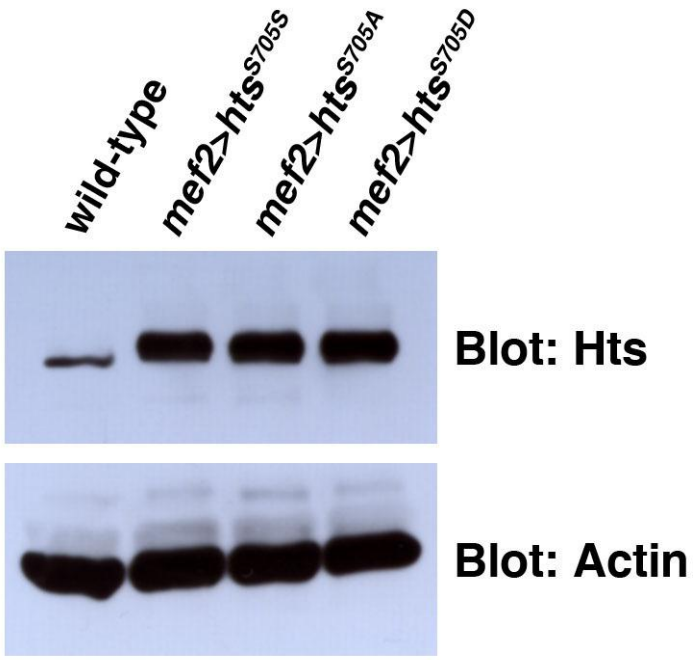
wild-type
mef2>hts^{S705S}
mef2>hts^{S705A}
mef2>hts^{S705D}
Blot: Hts
Blot: Actin

FIGURE 31 Expression levels of the wild-type, non-phosphorylatable and phospho-mimetic *hts* transgenes.

Western blot analysis of third instar larval body wall lysates blotted for Hts using the 1B1 antibody. The wild-type (*UAS-hts*^{S705S}), non-phosphorylatable (*UAS-hts*^{S705A}) and phospho-mimetic *hts* (*UAS-hts*^{S705D}) transgenes were expressed in the muscle with *mef2-Gal4*. All three *hts* transgenes show comparable elevations in Hts protein levels over the wild-type control. Actin was used as a loading control.

We first determined whether phosphorylation of Hts at the MARCKS domain regulates its localization to the postsynaptic membrane of larval NMJs. PKC phosphorylation of adducin leads to the translocation of adducin from the membrane cytoskeleton to the cytosol (reviewed in Matsuoka et al., 2000). We examined the localization of wild-type, non-phosphorylatable and phospho-mimetic Hts during larval NMJ development when expressing the transgenes in the muscle with *mef2-Gal4*. Both wild-type and non-phosphorylatable Hts still localized to the postsynaptic membrane of NMJs with no apparent difference between the two (Figure 32B-C''). However, phospho-mimetic Hts levels were drastically reduced at the NMJ (Figure 32D-D''). These results show that phosphorylation at the putative PKC target site of the MARCKS domain negatively regulates Hts localization at the postsynaptic membrane of larval NMJs.

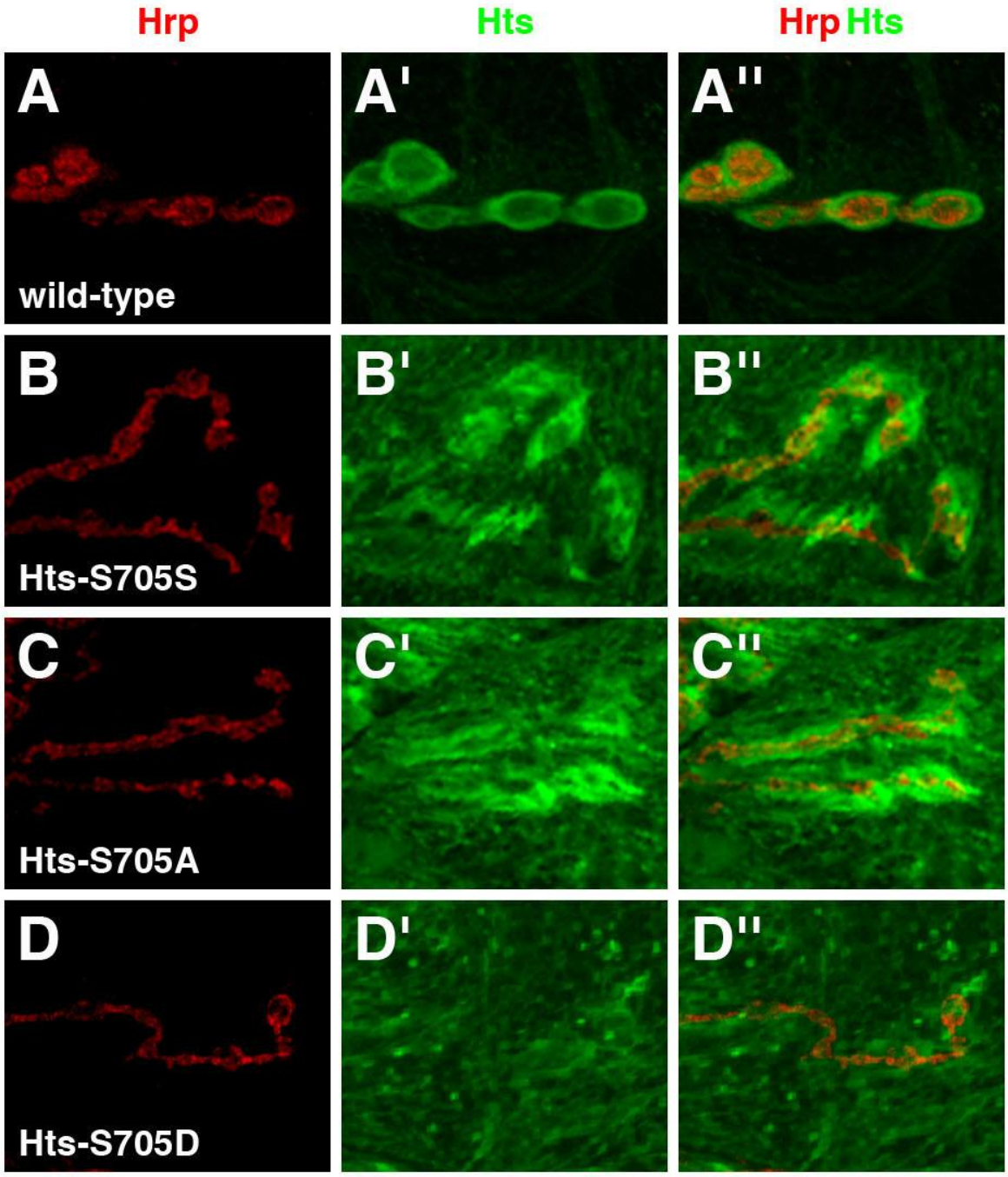
Hrp
Hts
Hrp Hts
A
A'
A''
wild-type
B
B'
B''
Hts-S705S
C
C'
C''
Hts-S705A
D
D'
D''
Hts-S705D

FIGURE 32 Hts phosphorylation at the MARCKS domain regulates Hts' localization at the postsynaptic membrane of larval NMJs.

(A-D'') Comparative analysis of third instar larval NMJs at muscles 6/7 stained with antibodies against Hts, using the 1B1 antibody, and Hrp. (A-A'') High magnification of a few boutons from a typical wild-type NMJ. (B-C'') Both wild-type and non-phosphorylatable Hts, when expressed in the muscle with *mef2-Gal4*, still localize at the NMJ. (D-D'') In contrast, phospho-mimetic Hts levels at the NMJ are drastically reduced.

Previous studies have shown that the actin-capping and spectrin-recruiting activities of mammalian adducin are inhibited by PKC phosphorylation (Matsuoka et al., 1998). Together with our result that phospho-mimetic Hts does not concentrate at the postsynaptic membrane of NMJs, we hypothesized that phosphorylation of the MARCKS domain suppresses Hts-dependent regulation of NMJ morphogenesis. We have previously shown that postsynaptic overexpression of *hts* using the Gene Search line, *GS13858*, promotes NMJ growth (Wang et al., 2011). Similarly, expression of the wild-type *hts* transgene also promoted NMJ growth when compared to wild-type (data not shown). Surprisingly, expression of either the non-phosphorylatable or phospho-mimetic *hts* transgene can also elevate NMJ growth to similar levels as the wild-type *hts* transgene (data not shown). A recent study has shown that presynaptic expression of a phospho-mimetic *hts* transgene, one similar to the one our group has made, can partially rescue the neuromuscular junction defects observed in *hts* mutants (Pielage et al., 2011). One possible reason as to why phospho-mimetic Hts still retains some activity is that there are other phosphorylation sites outside of the MARCKS domain, as seen in mammalian adducin (reviewed in Matsuoka et al., 2000). Some of these sites may be required to be phosphorylated to completely block Hts function.

Although there were no apparent differences between the effects of the three *hts* transgenes on NMJ size, we were still curious to see if Hts-mediated regulation of Dlg localization at the NMJ is controlled through phosphorylation of the MARCKS domain. We evaluated the localization of Dlg at the postsynaptic membrane when expressing the wild-type, non-phosphorylatable and phospho-mimetic *hts* transgenes with *mef2-Gal4*. As mentioned previously, we have shown that Hts negatively regulates Dlg localization through the use of the GS line, *GS13858* (Wang et al., 2011). We were able to confirm this result by overexpressing wild-type Hts in the muscle, which also resulted in the disruption of Dlg postsynaptic targeting when compared to the wild-type control (Figure 33B-B''). Interestingly, non-phosphorylatable Hts expression in the muscle appeared to disrupt Dlg postsynaptic targeting more severely when compared to

wild-type Hts expression, as Dlg localization around the NMJ appeared more diffuse and Dlg levels in the surrounding muscle were much higher (Figure 33C-C''). Phospho-mimetic Hts expression in the muscle also disrupted Dlg postsynaptic targeting, but Dlg localization appeared less diffuse when compared to wild-type and non-phosphorylatable Hts expression (Figure 33D-D''). Our results indicate that phosphorylation of Hts in the MARCKS domain partially suppresses its ability to negatively regulate Dlg localization at the postsynaptic membrane during larval NMJ development.

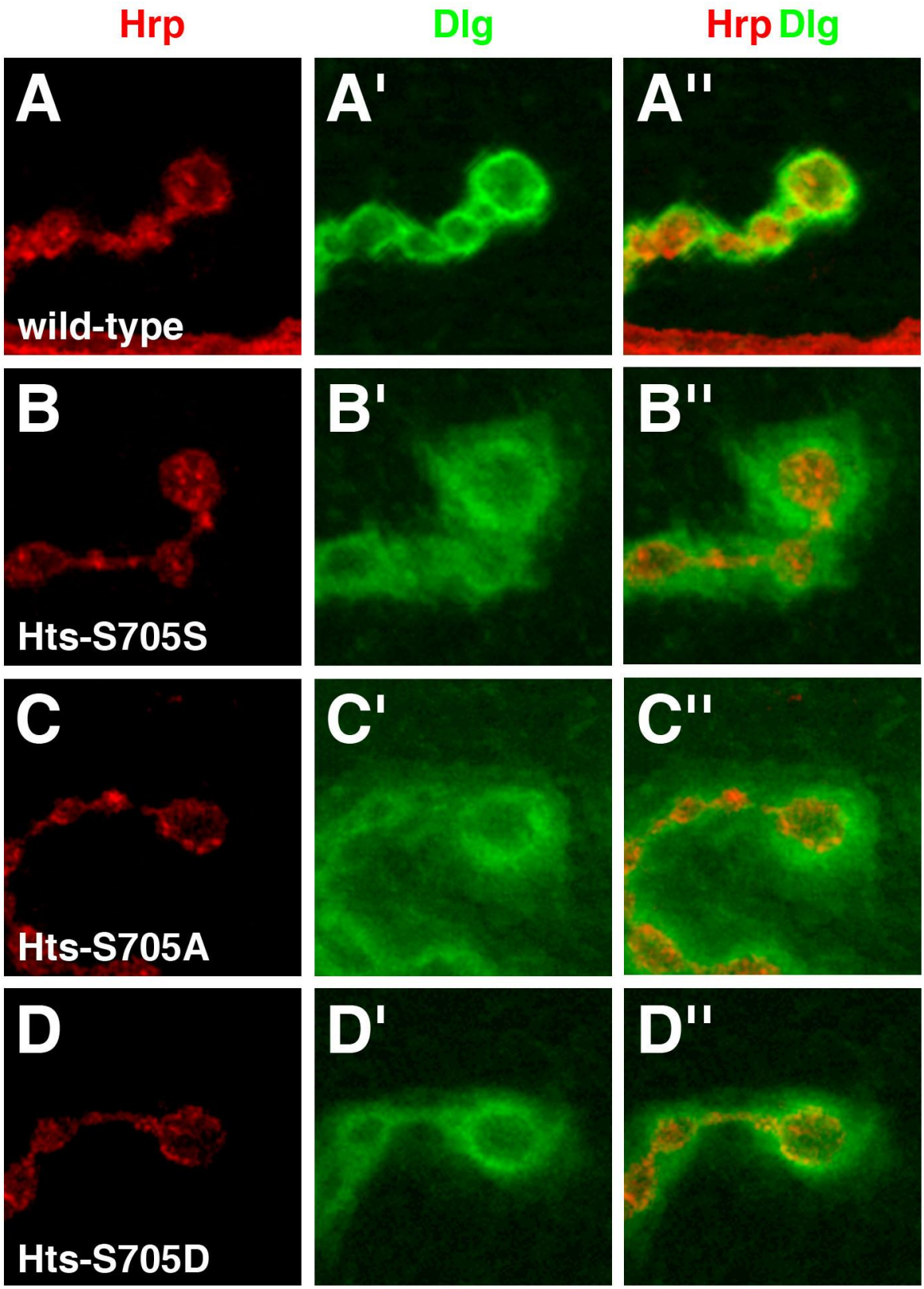
Hrp
Dlg
Hrp Dlg
A
A'
A''
wild-type
B
B'
B''
Hts-S705S
C
C'
C''
Hts-S705A
D
D'
D''
Hts-S705D

FIGURE 33 Hts phosphorylation at the MARCKS domain partially suppresses Hts' ability to regulate Dlg postsynaptic targeting to the larval NMJ.

(A-D'') Comparative analysis of third instar larval NMJs at muscles 6/7 stained with antibodies against Hrp and Dlg. (A-A'') High magnification of a few boutons from a typical wild-type NMJ. (B-B'') Wild-type Hts expression in the muscle with *mef2-Gal4* disrupts Dlg localization to the postsynaptic membrane. (C-C'') Non-phosphorylatable Hts disrupts Dlg postsynaptic targeting more severely when compared to wild-type Hts expression, as Dlg localization around the NMJ appears more diffuse and Dlg levels in the surrounding muscle are much higher. (D-D'') Phospho-mimetic Hts also disrupts Dlg postsynaptic targeting, but Dlg localization appears less diffuse when compared to wild-type and non-phosphorylatable Hts expression.

2.5. Discussion

2.5.1. Hts controls NMJ growth through regulation of Dlg postsynaptic targeting during larval development

Previous studies by Dr. Krieger have shown that adducin is hyperphosphorylated in the spinal cord tissue of ALS patients, though it remains unknown whether this is a causative factor of the disease (Hu et al., 2003). To further explore the roles of adducin in the nervous system, we decided to study *Drosophila* adducin, which is encoded by the *hts* locus, at the well-characterized NMJs of third instar larval body wall muscles. In this thesis, we show that the adducin isoforms of Hts localize predominantly to the postsynaptic membrane where they form a complex with Dlg, a MAGUK scaffolding protein that is essential for synaptic plasticity (Figure 34A) (reviewed in Ataman et al., 2006; reviewed in Thomas et al., 2010; reviewed in Oliva et al., 2011). This interaction may be mediated by the spectrin-actin cytoskeletal protein Cora, as the mammalian homologue, Protein 4.1, can bind to hDlg (Lue et al., 1994). We provide evidence that postsynaptic Hts promotes NMJ growth, in part, through the disruption of Dlg postsynaptic targeting (Figure 34B). Other studies have shown that Dlg localization to the postsynaptic membrane is negatively regulated via phosphorylation by the PAR-1 and CaMKII kinases (Koh et al., 1999; Zhang et al., 2007). Here, we show that Hts can elevate PAR-1 and CaMKII protein levels through an as yet unidentified mechanism, thereby promoting Dlg phosphorylation. Through transgenic analysis, we also show that Hts' ability to regulate Dlg localization is partially suppressed when the putative target site for PKC in the MARCKS domain is mutated (Figure 34C). We conclude that Hts is a signalling-responsive component of the actin-spectrin cytoskeleton that contributes to structural synaptic plasticity during larval NMJ development. This is accomplished through the negative regulation of Dlg postsynaptic targeting via PAR-1, and possibly CaMKII, dependent phosphorylation.

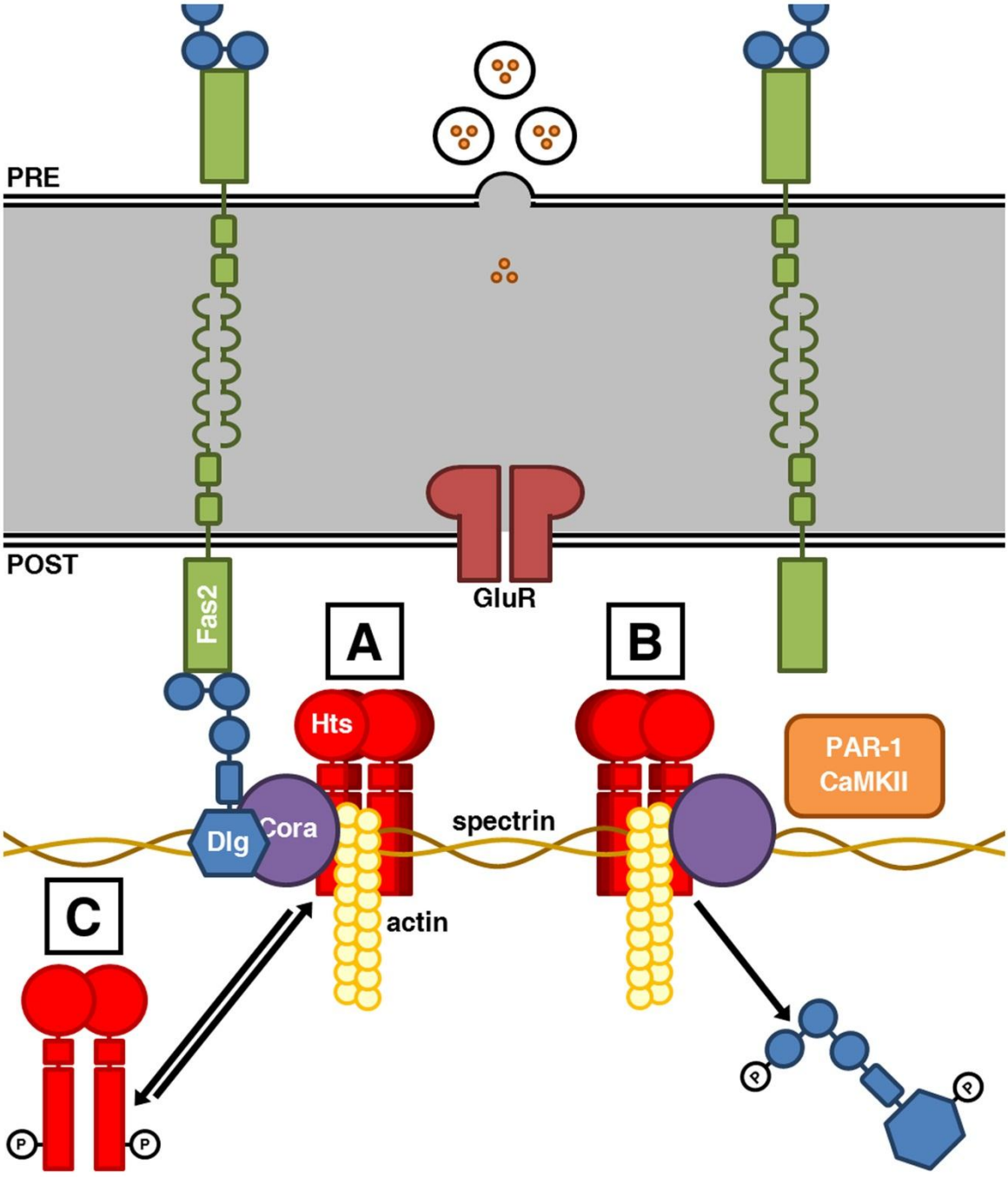
PRE
POST
GluR
Fas2
A
B
Hts
Dlg
Cora
spectrin
actin
PAR-1
CaMKII
C
P
P
P
P

FIGURE 34 Model for Hts-mediated NMJ growth through regulation of Dlg localization at the postsynaptic membrane via indirect phosphorylation.

Schematic of a larval NMJ viewed in cross-section, with the presynaptic side shown at the top and the postsynaptic side shown at the bottom. **(A)** At the postsynaptic membrane, Dlg localizes to spectrin-actin complexes in association with the septate junction protein, Cora (Lue et al., 1994). Homophilic adhesion between Fas2 transmembrane molecules links the presynaptic and postsynaptic sides, with the intracellular carboxyl-terminal domains anchored to the first and second PDZ domains of Dlg (Thomas et al., 1997). Hts also forms a complex with Dlg at the postsynaptic membrane. **(B)** Hts negatively regulates Dlg localization at the postsynaptic membrane by elevating PAR-1 and CaMKII kinase levels in the muscle. PAR-1 and CaMKII phosphorylate Dlg at serine 797 in the GUK domain and serine 48 in one the PDZ domains respectively (Koh et al., 1999; Zhang et al., 2007). Phosphorylation at either one of these sites disrupts Dlg postsynaptic targeting. **(C)** PKC-dependent phosphorylation of serine 705 in the MARCKS domain translocates Hts from the postsynaptic membrane into the cytoplasm, thus suppressing the ability of Hts to regulate Dlg (Matsuoka et al., 1998).

As previously mentioned, there were no publications regarding Hts function in the *Drosophila* nervous system when we began our work. However, three studies were published in 2011. The first study that was published implicates Hts in the axonal guidance of photoreceptors during eye development (Ohler et al., 2011). The second study to be published, which was independent to – but overlapped with – our work, also characterizes Hts at the larval NMJ (Pielage et al., 2011). However, this study focuses on Hts function at the presynaptic, and not the postsynaptic, side of the NMJ. The third paper that was published was from our group (Wang et al., 2011).

Some of the work that was done by Dr. Jan Pielage (Friedrich Miescher Institute, Switzerland) and Dr. Graeme Davis (University of California, San Francisco, California) overlapped with our group's work. Fortunately, most of their results complimented our results, thereby validating our data. However, they report that various *hts* mutations, including trans-allelic combinations involving the hts^{01103} allele, can actually result in an expansion of the NMJ in terms of increased bouton numbers and neuronal protrusions (Pielage et al., 2011). This result was reproduced through expression of transgenic *hts* RNAi in the neuron. They provide evidence that their phenotype is due to the disruption of Hts' actin-capping activities, a function that is shared by the mammalian adducins, thus relieving a constraint on actin polymerization and consequently neuronal extension. We, on the other hand, observe that hts^{01103} homozygous mutants possess underdeveloped NMJs in terms of reduced synaptic branching. We stand by this result as Mannan Wang can reproduce it through the expression of transgenic *hts* RNAi in the muscle (see the thesis entitled ''Muscle-associated *Drosophila* adducin regulates larval neuromuscular junction development and the location of Draper to the synapse'' which will be submitted to the SFU Library in 2013). We attribute our phenotype to the disruption of Hts' ability to negatively regulate Dlg postsynaptic targeting, as muscle-specific overexpression of Hts delocalizes Dlg at the NMJ. Based on these conflicting data, it appears that Hts may have two roles at the larval NMJ: 1.) Hts restricts synaptic growth through its actin-capping activites at the presynaptic side of the NMJ and 2.) Hts

promotes synaptic growth through negative regulation of Dlg localization at the postsynaptic side of the NMJ. It is quite possible that the contradictory phenotypes observed by our two groups may be due to which regulatory role prevails under given conditions. The outcome may be influenced by multiple factors such as genetic background (e.g. they looked at trans-allelic combinations of multiple *hts* alleles whereas we looked at hts^{01103} homozygotes), the muscle or abdominal segment that is observed (e.g. they looked at muscle 4 whereas we looked at muscles 6/7 in abdominal segments 3, 4 and 5) and the conditions in which the flies were raised in. In support of the idea that Hts plays dual opposing roles at the larval NMJ, the Pielage-Davis group also report that a subset of synapses within *hts* mutant NMJs can undergo retraction and elimination, which more resembles our data, though the overgrowth phenotype is predominant (Pielage et al., 2011). Furthermore, Jing Yang originally observed an overgrowth phenotype at muscles 6/7 in hts^{01103} mutant NMJs, in terms of increased synaptic branching, but only in abdominal segment 2 (see the thesis entitled ''Regulation of neuromuscular synapse development by Hts in *Drosophila*'' which was submitted to the SFU Library in 2008).

How does Hts regulate larval NMJ growth through Dlg? The answer may lie in one of Dlg's multiple interacting proteins during NMJ development. Among these is **Fasciclin 2** (**Fas2**), a homophilic transmembrane cell adhesion molecule that belongs to the **neural cell adhesion molecule** (**NCAM**) family of the immunoglobulin superfamily (reviewed in Ataman et al., 2006). At the NMJ, Fas2 is present at both the presynaptic and postsynaptic membranes where the intracellular carboxyl terminus binds to the first and second PDZ domains of Dlg (Schuster et al., 1996a; Schuster et al., 1996b; Thomas et al., 1997). Fas2 levels are reduced in *dlg* mutant NMJs indicating that Fas2 acts as a downstream effector of Dlg (Thomas et al., 1997; Zito et al., 1997). Several studies have shown that variations in Fas2 levels can modulate NMJ growth (reviewed in Ataman et al., 2006). In severe *fas2* mutations that reduce Fas2 levels to 10%, the NMJs are underdeveloped due to a lack of adhesion between the neuron and the muscle

(Schuster et al., 1996a; Schuster et al., 1996b). However, moderate *fas2* mutants that only reduce Fas2 levels to 50% result in overdeveloped NMJs. This is because the neuron can still adhere to the muscle, but a constraint due to Fas2 homophilic adhesion is partially released allowing the neuron to grow out more. We hypothesize that Hts disruption of Dlg postsynaptic targeting results in a partial loss of Fas2, thereby causing NMJ growth. Future studies will determine whether Hts-mediated NMJ growth is through Fas2.

2.5.2. Hts promotes Dlg phosphorylation

We are confident that Hts promotes Dlg phosphorylation at the GUK domain via PAR-1 due to results with an anti-pDlg antibody that specifically detects phosphorylation at serine 797 (Zhang et al., 2007). However, the same cannot be said about whether Hts can also promote Dlg phosphorylation at the first PDZ domain via CaMKII, as there was no equivalent anti-pDlg antibody available at the time that detects phosphorylation at serine 48. Although we provide evidence that Hts can elevate CaMKII protein levels in the muscle, a previous study has shown that overexpression of only constitutively active CaMKII, but not wild-type CaMKII, disrupts Dlg postsynaptic targeting at the NMJ (Koh et al., 1999). In mammalian studies, activated CaMKII can be detected with anti-pCaMKII antibodies against phosphorylation at threonine 286, and such antibodies have been successfully used in *Drosophila* tissues. Additionally, David Cheng, a current M.Sc. student under Dr. Harden, has recently made an anti-pDlg antibody specific against phosphorylation at serine 48. Future studies will involve examining whether Hts can promote CaMKII activation, as well as Dlg phosphorylation at the first PDZ domain, with the use of these antibodies.

We hope to further establish our model that Hts promotes larval NMJ growth by regulating Dlg phosphorylation, and thus localization, with the use of *dlg* non-phosphorylatable transgenes. Other research groups have created *UAS-dlg-S48A* and *UAS-dlg-797A* transgenes where the serines at positions 48 in the first PDZ domain and

797 in the GUK domain are altered to alanines (Koh et al., 1999; Zhang et al., 2007). CaMKII and PAR-1 are not able to disrupt Dlg-S48A and Dlg-S797A postsynaptic targeting, respectively, as their corresponding target sites in Dlg are mutated. Future studies will involve co-expressing Hts with either Dlg-S48A or Dlg-S797A in a *dlg* mutant background in order to determine whether blocking phosphorylation at these sites can inhibit Hts-mediated Dlg delocalization at the NMJ. Such experiments will also serve as rescue assays since we can also determine whether blocking Dlg delocalization with the use of these non-phosphorylatable transgenes can supress Hts-dependent NMJ growth. In the event that both sites are required for Hts regulation of Dlg localization, Vincent Chui has created a *dlg* double non-phosphorylatable transgene, *UAS-dlg-S48A+S797A*, where both serines are altered to alanines (see ''The regulation of Hu-li tai shao (Hts) at the *Drosophila* neuromuscular junction'' submitted to the SFU Library in 2011). If Hts can still disrupt the postsynaptic targeting of all three Dlg non-phosphorylatable proteins, this may indicate that Hts regulates other kinases that target different Dlg phosphorylation sites, or that Hts regulates Dlg localization through means other than phosphorylation.

2.5.3. Hts elevates PAR-1 and CaMKII protein levels

We show that postsynaptic overexpression of Hts leads to elevations in PAR-1 and CaMKII protein levels throughout muscle during larval NMJ development. However, the mechanism in which Hts, a membrane-cytoskeletal protein, promotes the accumulation of synaptic proteins remains unknown. Future studies will involve determining whether this process is due to transcriptional or translational control, or regulation of transcript or protein transportation, localization or stability. Since we provide evidence that Hts can also elevate PAR-1 and CaMKII protein levels in epithelial cells during dorsal closure, the mode of regulation is one that is most likely conserved in both neuronal and epithelial tissues.

A recent study has revealed that mammalian α-adducin can shuttle between the nucleus and cytoplasm due to the presence of a **nuclear localization signal** (**NLS**) in the MARCKS domain and a **nuclear export signal** (**NES**) in the neck region, respectively (Chen et al., 2011). We have confirmed that both the NLS and NES sequences are conserved in Hts. One potential role for nuclear Hts could be to serve as a transcriptional coactivator. Currently, RNA *in situ* hybridisations are being done to determine whether Hts can regulate PAR-1 and CaMKII transcript levels.

2.5.4. Hts regulation of Dlg postsynaptic targeting to the larval NMJ is partially suppressed via phosphorylation of the MARCKS domain

Mammalian studies have shown that PKC can phosphorylate adducin in the MARCKS domain, thereby inhibiting adducin's actin-capping and spectrin-recruiting activities (Matsuoka et al., 1998). Through transgenic analysis involving non-phosphorylatable and phospho-mimetic *hts* transgenes, we provide evidence that phosphorylation of Hts at a conserved serine residue in the MARCKS domain partially supresses its ability to regulate Dlg localization at the larval NMJ. Nevertheless, phospho-mimetic Hts can still efficiently disrupt Dlg postsynaptic targeting, albeit not to the same extent as wild-type or non-phosphorylatable Hts. One possible explanation is that phospho-mimetic Hts retains some activity and we are expressing it well above physiological levels with the *mef2-Gal4* driver. Another possible, and related, explanation is that there may be other regulatory sites that are present outside of the MARCKS domain that are critical for inhibiting Hts function.

Several studies have shown that the mammalian adducins are substrates for multiple kinases (reviewed in Matsuoka et al., 2000). **Protein kinase A** (**PKA**) reduces adducin's affinity for actin-spectrin complexes by phosphorylating α- and β-adducin in the MARCKS domain, but has additional target sites at serines 408, 436 and 481 which are present only in the neck region of α-adducin (Matsuoka et al., 1996). Conversely, **Rho-kinase** (**Rok**) phosphorylates α-adducin at threonines 445 and 480 in the neck

region which promotes adducin's binding to F-actin and spectrin (Kimura et al., 1998; Fukata et al., 1999). Rok-dependent phosphorylation can be reversed by myosin phosphatase, the only adducin phosphatase identified to date (Kimura et al., 1998). Fyn has also been shown to promote adducin function by translocating adducin from the cytoplasm to the membrane through phosphorylation of tyrosine 489 found only in the C-terminal domain of β-adducin (Shima et al., 2001; Gotoh et al., 2006). Future studies will involve investigating whether these kinases act upstream of Hts-mediated NMJ growth. This can be accomplished, in part, by expressing transgenic RNAi against each kinase and assessing Hts localization at the larval NMJ.

2.5.5. Identifying new participants in Hts-mediated NMJ growth

We show that postsynaptic overexpression of Hts results in overdeveloped larval NMJs with significant increases in bouton number, branch number and branch length. We attribute this to observed increases in PAR-1 and CaMKII kinase levels throughout the muscle which promote Dlg phosphorylation, thereby disrupting Dlg localization at the postsynaptic membrane. However, previous studies have shown that overexpression of either PAR-1 or constitutively active CaMKII in the muscle causes a marked reduction in NMJ branching complexity (Koh et al., 1999; Zhang et al., 2008). Such discrepancies in phenotypes between Hts overexpression versus PAR-1 and CaMKII overexpression suggest that Hts is acting through other synaptic components to regulate larval NMJ development. Searching through the literature has revealed two potential candidates: **Draper** (**Drpr**) and **Phosphatidylinositol 4,5-bisphosphate** (**PIP_2**).

The CuraGen Corporation (New Haven, Connecticut) performed a proteome-wide yeast-two hybrid screen in *Drosophila* which picked up a protein-protein interaction between Hts and Drpr (Giot et al., 2003). Drpr, which is homologous to CED-1 in *C. elegans* and MEGF10 and MEGF11 in mammals, is an engulfment receptor involved in the clearing of apoptotic cells and pathogens. Interestingly, Drpr has been

implicated in the engulfment of dying germ cells by the surrounding follicular epithelium in egg chambers (Etchegaray et al., 2012).

The adult nervous system, whether in vertebrates or invertebrates, emerges from a developmental precursor which contains superfluous neuronal connections. That is, the developing nervous system is only a transient template and requires significant remodeling before the adult pattern can be achieved. To refine the neuronal network during development, selected branches and/or synapses are eliminated as others are left intact on the parent neuron in a process known as axonal pruning (reviewed in Waimey and Cheng, 2006). Previous studies have shown that Drpr is essential for the glial engulfment of synaptic debris shed from the NMJ, and also plays a role in NMJ growth though the mechanism has not been identified (Fuentes-Mendel et al., 2009).

We have been working in collaboration with Mannan Wang to determine whether Hts and Drpr interact during larval NMJ development. Mannan has so far shown that Hts and Drpr co-localize at the postsynaptic membrane of wild-type NMJs (see the thesis entitled ''Muscle-associated *Drosophila* adducin regulates larval neuromuscular junction development and the location of Draper to the synapse'' which will be submitted to the SFU Library in 2013). There, Hts negatively regulates Drpr postsynaptic targeting through an as of yet unidentified mechanism. We are currently assessing, by means of epistasis analysis, whether Hts can act through Drpr to control larval NMJ growth. Interestingly, embryos overexpressing Drpr in epidermal stripes via the segmental *prd-Gal4* driver display dorsal closure defects. In segments where Drpr is not overexpressed, the opposing epidermal flanks still meet at the dorsal midline upon dorsal closure completion. However, in segments within the same embryo where Drpr is overexpressed, the opposing epidermal flanks fail to come together. This results in what Dr. Harden likes to call the ''too small shirt'' phenotype. A recent study has revealed that the Drpr-like MEGF10 and MEGF11 proteins undergo homophilic

interactions which result in intercellular repulsion between mouse retinal neurons (Kay et al., 2012). Thus, one possible explanation for our observed dorsal closure defects is that Drpr overexpression in the embryonic epidermis results in homophilic repulsion between the opposing epidermal flanks as they approach each other at the dorsal midline.

Multiple studies have demonstrated that the mammalian MARCKS protein, or more specifically its MARCKS effector domain, can bind to and sequester PIP_2 in artificial lipid vesicles (Glaser et al., 1996; Denisov et al., 1998; Arbuzova et al., 2000; Wang et al., 2001; Rauch et al., 2002; Wang et al., 2002; Zhang et al., 2003; Gambhir et al., 2004; Dietrich et al., 2009). This interaction has been linked to the regulation of the actin cytoskeleton during the growth and branching of dendrites in rat brains, as well as the directed migration of bovine aortic endothelial cells (Li et al., 2008; Kalwa and Michel, 2011). Interestingly, it has been proposed that aberrant MARCKS regulation of PIP_2 signalling may be implicated in the formation of amyloid plaques in Alzheimer's disease (reviewed in Su et al., 2010).

Phosphatidylinositols are negatively charged phospholipids with a minor head group component on the cytosolic side of eukaryotic cell membranes (reviewed in Slabbaert et al., 2012). Reversible phosphorylation of the head group at positions D-3, D-4 and D-5 creates seven different phosphoinositides, where each has a unique subcellular distribution in subsets of membranes. PIP_2 is phosphorylated at positions D-4 and D-5 and serves as a substrate for a number of important signalling proteins. PIP_2 has previously been implicated in NMJ growth through WASP signalling (Khuong et al., 2010).

Work done with Byoungjoo Yoo, a research technician under Dr. Harden, has shown through the use of commercially available PIP strip membranes which are spotted with various phosphorylated phosphatidylinositol species that purified GST-Hts can bind to multiple phosphoinositides. One of these phosphoinositides is PIP_2. Future

work will involve determining whether this Hts-PIP_2 interaction exists *in vivo* at the larval NMJ. Encouragingly, Vincent Chui has preliminary data that indicate that Hts colocalizes with $PLC_{\delta 1}$-PH-GFP, a reporter containing the pleckstrin homology domain of phospholipase $C_{\delta 1}$ which is known to bind to PIP2, at the postsynaptic membrane (Varnai and Balla, 2008; Verstreken et al., 2009). We plan to follow up this result by evaluating whether Hts is required for PIP_2 localization at the larval NMJ by assessing $PLC_{\delta 1}$-PH-GFP distribution in *hts* mutant and overexpression analyses. Likewise, we will also assess whether PIP_2, in addition to the other phosphoinositides that were shown to bind to Hts on the PIP strip, are required for Hts localization and/or function at the larval NMJ. This will be done with the use of transgenic RNAi against the kinases and phosphatases that form the phosphoinositides we are interested in (reviewed in Slabbaert et al., 2012).

In the hopes of potentially discovering novel Hts interacting partners during larval NMJ development in the future, we propose performing a genetic screen to identify modifiers of a Hts-induced adult eye phenotype. Overexpression of Hts in the eye by crossing *GS13858* to a Gal4 driver under the control of the ***Glass Multimer Reporter*** (***GMR***) promoter caused a moderate rough eye phenotype in adult flies. This phenotype is unlikely to be an artifact as Hts has been implicated in eye development where it regulates photoreceptor axon guidance (Ohler et al., 2011). The rough eye phenotype will be used to conduct the genetic modifier screen instead of the defects we observe at the larval NMJ since the adult eye is dispensable for viability and is far easier to score. Results from genetic screens that involve the adult eye have often been successfully extrapolated to study many different aspects of developmental neurobiology, as it is a component of the peripheral nervous system (reviewed in St Johnston, 2002; reviewed in Sang and Jackson, 2005). Therefore, Hts interactions that are discovered in the adult eye may be conserved at the larval NMJ.

The Bloomington Stock Center (Indiana University, Indiana) has assembled a collection of fly lines bearing deficiencies that span most of the *Drosophila* genome (Cook et al., 2012). Each deficiency contains a large, molecularly defined deletion of genomic DNA that removes a number of genes. At present, the stock center provides a ''deficiency kit'' consisting of 468 fly lines with overlapping deficiencies that span the four chromosomes at 98% euchromatic coverage. In the future, our lab hopes to identify dominant enhancers and suppressors of the Hts-induced rough eye phenotype. This will be accomplished by screening adult flies that overexpress *GS13858* with *GMR-Gal4* in a background that is heterozygous for each individual deficiency. For deficiencies that contain putative modifiers, smaller deficiencies within those intervals will be ordered from the stock center to narrow down the regions responsible for the modification. Once narrowed down to just a few candidate genes, mutations for each gene will be tested to determine which gene interacts with Hts in the adult eye. The possibility of discovering novel Hts interacting partners may open up new avenues of research for this project, as well as give us a more complete understanding as to how Hts regulates larval NMJ development.

3. Concluding Remarks

In this thesis, we identify and characterize novel Dlg regulators during epithelial and synaptic plasticity events in *Drosophila* development. In one chapter, we provide genetic evidence that Pak and Pak3 recruit the Dlg-containing Scrib complex to the leading edge membrane of DME cells upon dorsal closure completion. In the other chapter, we show that Hts disrupts Dlg localization at the postsynaptic membrane through indirect phosphorylation. Many of the proteins that are mentioned throughout this work are actually found in both epithelial cells and neuronal cells suggesting the existence of conserved molecular complexes. Therefore, the results we obtained from one project may be relevant to the other. Future studies will involve studying Pak/Pak3 regulation at the NMJ and Hts regulation in epithelia in what we like to call the ''the cross-over studies''. Interestingly, mammalian adducins have been implicated in the regulation of cell-cell adhesion in epithelial cells (Naydenov and Ivanov, 2010; Chen et al., 2011; Naydenov and Ivanov, 2012). Furthermore, Pak3 has been shown to regulate synaptic structure and function in *Drosophila*, and several studies link Pak to multiple synaptic roles including axonal guidance (reviewed in Bokoch, 2003; Ozdowski et al., 2011).

References

Arbuzova A., Wang L., Wang J., Hangyas-Mihalyne G., Murray D., Honig B. and McLaughlin S. (2000). Membrane binding of peptides containing both basic and aromatic residues. Experimental studies with peptides corresponding to the scaffolding region of caveolin and the effector region of MARCKS. Biochemistry 39, 10330-9.

Arquier N., Perrin L., Manfruelli P. and Semeriva M. (2001). The Drosophila tumor suppressor gene lethal(2)giant larvae is required for the emission of the Decapentaplegic signal. Development 128, 2209-20.

Ashburner M. and Roote J. (2007). Maintenance of a Drosophila laboratory: general procedures. CSH Protoc, doi:10.1101/pdb.ip35.

Ataman B., Budnik V. and Thomas U. (2006). Scaffolding proteins at the Drosophila neuromuscular junction. Int Rev Neurobiol 75, 181-216.

Augustinack J.C., Schneider A., Mandelkow E.M. and Hyman B.T. (2002). Specific tau phosphorylation sites correlate with severity of neuronal cytopathology in Alzheimer's disease. Acta Neuropathol 103, 26-35.

Baek S.H., Cho H.W., Kwon Y.C., Lee J.H., Kim M.J., Lee H. and Choe K.M. (2012). Requirement for Pak3 in Rac1-induced organization of actin and myosin during Drosophila larval wound healing. FEBS Lett 586, 772-7.

Bahri S., Wang S., Conder R., Choy J., Vlachos S., Dong K., Merino C., Sigrist S., Molnar C., Yang X., Manser E. and Harden N. (2010). The leading edge during dorsal closure as a model for epithelial plasticity: Pak is required for recruitment of the Scribble complex and septate junction formation. Development 137, 2023-32.

Baines A.J. (2010). The spectrin-ankyrin-4.1-adducin membrane skeleton: adapting eukaryotic cells to the demands of animal life. Protoplasma 244, 99-131.

Banerjee S., Sousa A.D. and Bhat M.A. (2006). Organization and function of septate junctions: an evolutionary perspective. Cell Biochem Biophys 46, 65-77.

Barkalow K.L., Italiano J.E. Jr., Chou D.E., Matsuoka Y., Bennett V. and Hartwig J.H. (2003). α-Adducin dissociates from F-actin and spectrin during platelet activation. J Cell Biol 161, 557-70.

Bateman J.R., Lee A.M. and Wu C.T. (2006). Site-specific transformation of Drosophila via ϕC31 integrase-mediated cassette exchange. Genetics 173, 769-77.

Beckett K. and Baylies M.K. (2006). The development of the Drosophila larval body wall muscles. Int Rev Neurobiol 75, 55-70.

Bednarek E. and Caroni P. (2011). β-Adducin is required for stable assembly of new synapses and improved memory upon environmental enrichment. Neuron 69, 1132-46.

Belacortu Y. and Paricio N. (2011). Drosophila as a model of wound healing and tissue regeneration in vertebrates. Dev Dyn 240, 2379-404.

Bergstralh D.T. and St Johnston D. (2012). Epithelial cell polarity: what flies can teach us about cancer. Essays Biochem 53, 129-40.

Betschinger J., Mechtler K. and Knoblich J.A. (2003). The Par complex directs asymmetric cell division by phosphorylating the cytoskeletal protein Lgl. Nature 422, 326-30.

Beumer K., Matthies H.J., Bradshaw A. and Broadie K. (2002). Integrins regulate DLG/FAS2 via a CaM kinase II-dependent pathway to mediate synapse elaboration and stabilization during postembryonic development. Development 129, 3381-9.

Bogdanik L., Framery B., Frolich A., Franco B., Mornet D., Bockaert J., Sigrist S.J., Grau Y. and Parmentier M.L. (2008). Muscle dystroglycan organizes the postsynapse and regulates presynaptic neurotransmitter release at the Drosophila neuromuscular junction. PLoS One 3, e2084.

Bokoch G.M. (2003). Biology of the p21-activated kinases. Annu Rev Biochem 72, 743-81.

Brent J.R., Werner K.M. and McCabe B.D. (2009). Drosophila larval NMJ dissection. J Vis Exp, doi:10.3791/1107.

Brower D.L., Wilcox M., Piovant M., Smith R.J. and Reger L.A. (1984). Related cell-surface antigens expressed with positional specificity in Drosophila imaginal discs. Proc Nat Acad Sci U S A 81, 7485-9.

Budnik V., Koh Y.H., Guan B., Hartmann B., Hough C., Woods D. and Gorczyca M.. (1996). Regulation of synapse structure and function by the Drosophila tumor suppressor gene dlg. Neuron 17, 627-40.

Cammarota M., Bevilaqua L.R., Viola H., Kerr D.S., Reichmann B., Teixeira V., Bulla M., Izquierdo I. and Medina J.H. (2002). Participation of CaMKII in neuronal plasticity and memory formation. Cell Mol Neurobiol 22, 259-67.

Chen K., Merino C., Sigrist S.J. and Featherstone D.E. (2005). The 4.1 protein coracle mediates subunit-selective anchoring of Drosophila glutamate receptors to the postsynaptic actin cytoskeleton. J Neurosci 25, 6667-75.

Chen C.L., Lin Y.P., Lai Y.C. and Chen H.C. (2011). α-Adducin translocates to the nucleus upon loss of cell-cell adhesions. Traffic 12, 1327-40.

Conder R., Yu H., Ricos M., Hing H., Chia W., Lim L. and Harden N. (2004). dPak is required for integrity of the leading edge cytoskeleton during Drosophila dorsal closure but does not signal through the JNK cascade. Dev Biol 276, 378-90.

Conder R., Yu H., Zahedi B. and Harden N. (2007). The serine/threonine kinase dPak is required for polarized assembly of F-actin bundles and apical-basal polarity in the Drosophila follicular epithelium. Dev Biol 305, 470-82.

Cook R.K., Christensen S.J., Deal J.A., Coburn R.A., Deal M.E., Gresens J.M., Kaufman T.C. and Cook K.R. (2012). The generation of chromosomal deletions to provide extensive coverage and subdivision of the Drosophila melanogaster genome. Genome Biol 13, R21.

Dan I., Watanabe N.M. and Kusumi A. (2005). The Ste20 group kinases as regulators of MAP kinase cascades. Trends Cell Biol 11, 220-30.

David D.J., Tishkina A. and Harris T.J. (2010). The PAR complex regulates pulsed actomyosin contractions during amnioserosa apical constriction in Drosophila. Development 137, 1645-55.

Deng W. and Lin H. (1997). Spectrosomes and fusomes anchor mitotic spindles during asymmetric germ cell divisions and facilitate the formation of a polarized microtubule array for oocyte specification in Drosophila. Dev Biol 189, 79-94.

Denisov G., Wanaski S., Luan P., Glaser M. and McLaughlin S. (1998). Binding of basic peptides to membranes produces lateral domains enriched in the acidic lipids phosphatidylserine and phosphatidylinositol 4,5-bisphosphate: an electrostatic model and experimental results. Biophys J 74, 731-44.

Dietrich U., Kruger P., Gutberlet T. and Kas J.A. (2009). Interaction of the MARCKS peptide with PIP2 in phospholipid monolayers. Biochim Biophys Acta 1788, 1474-81.

Dietzl G., Chen D., Schnorrer F., Su K.C., Barinova Y., Fellner M., Gasser B., Kinsey K., Oppel S., Scheiblauer S., Couto A., Marra V., Keleman K. and Dickson B.J. (2007). A genome-wide transgenic RNAi library for conditional gene inactivation in Drosophila. Nature 448, 151-6.

Ding D., Parkhurst S.M. and Lipshitz H.D. (1993). Different genetic requirements for anterior RNA localization revealed by the distribution of Adducin-like transcripts during Drosophila oogenesis. Proc Nat Acad Sci U S A 90, 2512-6.

Drees F., Pokutta S., Yamada S., Nelson W.J. and Weis W.I. (2005). α-catenin is a molecular switch that binds E-cadherin-β-catenin and regulates actin-filament assembly. Cell 123, 903-15.

Drewes G., Ebneth A., Preuss U., Mandelkow E.M. and Mandelkow E. (1997). MARK, a novel family of protein kinases that phosphorylate microtubule-associated proteins and trigger microtubule disruption. Cell 89, 297-308.

Duffy J.B. (2002). GAL4 system in Drosophila: a fly geneticist's Swiss army knife. Genesis 34, 1-15.

Eisen A. (2009). Amyotrophic lateral sclerosis: a 40-year personal perspective. J Clin Neurosci 16, 505-12.

Ellenbroek S.I., Iden S. and Collard J.G. (2012). Cell polarity proteins and cancer. Semin Cancer Biol 22, 208-15.

Elsum I., Yates L., Humbert P.O. and Richardson H.E. (2012). The Scribble-Dlg-Lgl polarity module in development and cancer: from flies to man. Essays Biochem 53, 141-68.

Etchegaray J.I., Timmons A.K., Klein A.P., Pritchett T.L., Welch E., Meehan T.L., Li C. and McCall K. (2012). Draper acts through the JNK pathway to control synchronous engulfment of dying germline cells by follicular epithelial cells. Development 139, 4029-39.

Fehon R.G., Dawson I.A. and Artavanis-Tsakonas S. (1994). A Drosophila homologue of membrane-skeleton protein 4.1 is associated with septate junctions and is encoded by the coracle gene. Development 120, 545-57.

Fuentes-Medel Y., Logan M.A., Ashley J., Ataman B., Budnik V. and Freeman M.R. (2009). Glia and muscle sculpt neuromuscular arbors by engulfing destabilized synaptic boutons and shed presynaptic debris. PLoS Biol 7, e1000184.

Fukata Y., Oshiro N., Kinoshita N., Kawano Y., Matsuoka Y., Bennett V., Matsuura Y. and Kaibuchi K. (2009). Phosphorylation of adducin by Rho-kinase plays a crucial role in cell motility. J Cell Biol 45, 347-61.

Gambhir A., Hangyas-Mihalyne G., Zaitseva I., Cafiso D.S., Wang J., Murray D., Pentyala S.N., Smith S.O. and McLaughlin S. (2004). Electrostatic sequestration of PIP2 on phospholipid membranes by basic/aromatic regions of proteins. Biophys J 86, 2188-207.

Gibson M.C. and Perrimon N. (2003). Apicobasal polarization: epithelial form and function. Curr Opin Cell Biol 15, 747-52.

Gilligan D.M., Sarid R. and Weese J. (2002). Adducin in platelets: activation-induced phosphorylation by PKC and proteolysis by calpain. Blood 99, 2418-26.

Giot L., Bader J.S., Brouwer C., Chaudhuri A., Kuang B., Li Y., Hao Y.L., Ooi C.E., Godwin B., Vitols E., Vijayadamodar G., Pochart P., Machineni H., Welsh M., Kong Y., Zerhusen B., Malcolm R., Varrone Z., Collis A., Minto M., Burgess S., McDaniel L., Stimpson E., Spriggs F., Williams J., Neurath K., Ioime N., Agee M., Voss E., Furtak K., Renzulli R., Aanensen N., Carrolla S., Bickelhaupt E., Lazovatsky Y., DaSilva A., Zhong J., Stanyon C.A., Finley R.L. Jr., White K.P., Braverman M., Jarvie T., Gold S., Leach M., Knight J., Shimkets R.A., McKenna M.P., Chant J. and Rothberg J.M. (2003). A protein interaction map of Drosophila melanogaster. Science 302, 1727-36.

Glaser M., Wanaski S., Buser C.A., Boguslavsky V., Rashidzada W., Morris A., Rebecchi M., Scarlata S.F., Runnels L.W., Prestwich G.D., Chen J., Aderem A., Ahn J. and McLaughlin S. (1996). Myristoylated alanine-rich C kinase substrate (MARCKS) produces reversible inhibition of phospholipase C by sequestering phosphatidylinositol 4,5-bisphosphate in lateral domains. J Biol Chem 271, 26187-93.

Goldstein B. and Macara I.G. (2007). The PAR proteins: fundamental players in animal cell polarization. Dev Cell 13, 609-22.

Gorczyca M. and Budnik V. (2006). Anatomy of the larval body wall muscles and NMJs in the third instar larval stage. Int Rev Neurobiol 75, 367-73.

Gorfinkiel N. and Arias A.M. (2007). Requirements for adherens junction components in the interaction between epithelial tissues during dorsal closure in Drosophila. J Cell Sci 120, 3289-98.

Gorfinkiel N., Schamberg S. and Blanchard G.B. (2011). Integrative approaches to morphogenesis: lessons from dorsal closure. Genesis 49, 522-33.

Gotoh H., Okumura N., Yagi T., Okumura A., Shima T., Nagai K. (2006). Fyn-induced phosphorylation of beta-adducin at tyrosine 489 and its role in their subcellular localization. Biochem Biophys Res Commun 346, 600-5.

Grevengoed E.E., Loureiro J.J., Jesse T.L. and Peifer M. (2001). Abelson kinase regulates epithelial morphogenesis in Drosophila. J Cell Biol 155, 1185-98.

Griffith L.C. (2004a). Calcium/calmodulin-dependent protein kinase II: an unforgettable kinase. J Neurosci 24, 8391-3.

Griffith L.C. (2004b). Regulation of calcium/calmodulin-dependent protein kinase II activation by intramolecular and intermolecular interactions. J Neurosci 24, 8394-8.

Griffith L.C. and Budnik V. (2006). Plasticity and second messengers during synapse development. Int Rev Neurobiol 75, 237-65.

Gruenbaum L.M., Gilligan D.M., Picciotto M.R., Marinesco S. and Carew T.J. (2003). Identification and characterization of Aplysia adducin, an Aplysia cytoskeletal protein homologous to mammalian adducins: increased phosphorylation at a protein kinase C consensus site during long-term synaptic facilitation. J Neurosci 23, 2675-85.

Harden N., Lee J., Loh H.Y., Ong Y.M., Tan I., Leung T., Manser E. and Lim L. (1996). A Drosophila homolog of the Rac- and Cdc42-activated serine/threonine kinase PAK is a potential focal adhesion and focal complex protein that colocalizes with dynamic actin structures. Mol Cell Biol 16, 1896-908.

Harden N. (2002). Signaling pathways directing the movement and fusion of epithelial sheets: lessons from dorsal closure in Drosophila. Differentiation 70, 181-203.

Harris T.J., Sawyer J.K. and Peifer M. (2009). How the cytoskeleton helps build the embryonic body plan: models of morphogenesis from Drosophila. Curr Top Dev Biol 89, 55-85.

Harris T.J. and Tepass U. (2010). Adherens junctions: from molecules to morphogenesis. Nat Rev Mol Cell Biol 11, 502-14.

Harris T.J. (2012). Adherens junction assembly and function in the Drosophila embryo. Int Rev Cell Mol Biol 293, 45-83.

Hartsock A. and Nelson W.J. (2008). Adherens and tight junctions: structure, function and connections to the actin cytoskeleton. Biochim Biophys Acta 1778, 660-9.

Heisenberg C.P. (2009). Dorsal closure in Drosophila: cells cannot get out of the tight spot. Bioessays 31, 1284-7.

Hing H., Xiao J., Harden N., Lim L. and Zipursky S.L. (1999). Pak functions downstream of Dock to regulate photoreceptor axon guidance in Drosophila. Cell 97, 853-63.

Hu J.H. and Krieger C. (2002). Protein phosphorylation networks in motor neuron death. Prog Drug Res 59, 71-109.

Hu J.H., Zhang H., Wagey R., Krieger C. and Pelech S.L. (2003). Protein kinase and protein phosphatase expression in amyotrophic lateral sclerosis spinal cord. J Neurochem 85, 432-42.

Humbert P., Russell S. and Richardson H. (2003). Dlg, Scribble and Lgl in cell polarity, cell proliferation and cancer. Bioessays 25, 542-53.

Jacinto A., Wood W., Balayo T., Turmaine M., Martinez-Arias A. and Martin P. (2000). Dynamic actin-based epithelial adhesion and cell matching during Drosophila dorsal closure. Curr Biol 10, 1420-6.

Jacinto A., Woolner S. and Martin P. (2002a). Dynamic analysis of dorsal closure in Drosophila: from genetics to cell biology. Dev Cell 3, 9-19.

Jacinto A., Wood W., Woolner S., Hiley C., Turner L., Wilson C., Martinez-Arias A. and Martin P. (2002b). Dynamic analysis of actin cable formation during Drosophila dorsal closure. Curr Biol 12, 1245-50.

Jaffe A.B. and Hall A. (2005). Rho GTPases: biochemistry and biology. Annu Rev Cell Dev Biol 21, 247-69.

Kaltschmidt J.A., Lawrence N., Morel V., Balayo T., Fernandez B.G., Pelissier A., Jacinto A. and Martinez-Arias A. (2002). Planar polarity and actin dynamics in the epidermis of Drosophila. Nat Cell Biol 4, 937-44.

Kalwa H. and Michel T. (2011). The MARCKS protein plays a critical role in phosphatidylinositol 4,5-bisphosphate metabolism and directed cell movement in vascular endothelial cells. J Biol Chem 286, 2320-30.

Kay J.N., Chu M.W. and Sanes JR. (2012). MEGF10 and MEGF11 mediate homotypic interactions required for mosaic spacing of retinal neurons. Nature 483, 465-9.

Khuong T.M., Habets R.L., Slabbaert J.R. and Verstreken P. (2010). WASP is activated by phosphatidylinositol-4,5-bisphosphate to restrict synapse growth in a pathway parallel to bone morphogenetic protein signaling. Proc Natl Acad Sci U S A 107, 17379-84.

Kimura K., Fukata Y., Matsuoka Y., Bennett V., Matsuura Y., Okawa K., Iwamatsu A. and Kaibuchi K. (1998). Regulation of the association of adducin with actin filaments by Rho-associated kinase (Rho-kinase) and myosin phosphatase. J Biol Chem 273, 5542-8.

Koh Y.H., Popova E., Thomas U., Griffith L.C. and Budnik V. (1999). Regulation of DLG localization at synapses by CaMKII-dependent phosphorylation. Cell 98, 353-63.

Krieger C., Hu J.H. and Pelech S.. (2003). Aberrant protein kinases and phosphoproteins in amyotrophic lateral sclerosis. Trends Pharmacol Sci 24, 535-41.

Labouesse M. (2006). Epithelial junctions and attachments. WormBook, doi:10.1895/wormbook.1.56.1.

Lahey T., Gorczyca M., Jia X.X. and Budnik V. (1994). The Drosophila tumor suppressor gene dlg is required for normal synaptic bouton structure. Neuron 13, 823-35.

Lamb R.S., Ward R.E., Schweizer L. and Fehon R.G. (1998). Drosophila coracle, a member of the protein 4.1 superfamily, has essential structural functions in the septate junctions and developmental functions in embryonic and adult epithelial cells. Mol Biol Cell 9, 3505-19.

Laplante C. and Nilson L.A. (2011). Asymmetric distribution of Echinoid defines the epidermal leading edge during Drosophila dorsal closure. J Cell Biol 192, 335-48.

Lawrence N. and Morel V. (2003). Dorsal closure and convergent extension: two polarised morphogenetic movements controlled by similar mechanisms? Mech Dev 120, 1385-93.

Li H., Chen G., Zhou B. and Duan S. (2008). Actin filament assembly by myristoylated alanine-rich C kinase substrate-phosphatidylinositol-4,5-diphosphate signaling is critical for dendrite branching. Mol Biol Cell 19, 4804-13.

Lin H., Yue L. and Spradling A.C. (1994). The Drosophila fusome, a germline-specific organelle, contains membrane skeletal proteins and functions in cyst formation. Development 120, 947-56.

Lue R.A., Marfatia S.M., Branton D. and Chishti A.H. (1994). Cloning and characterization of hdlg: the human homologue of the Drosophila discs large tumor suppressor binds to protein 4.1. Proc Natl Acad Sci U S A 91, 9818-22.

Manser E., Loo T.H., Koh C.G., Zhao Z.S., Chen X.Q., Tan L., Tan I., Leung T. and Lim L. (1998). PAK kinases are directly coupled to the PIX family of nucleotide exchange factors. Mol Cell 1, 183-92.

Martin P. and Wood W. (2002). Epithelial fusions in the embryo. Curr Opin Cell Biol 14, 569-74.

Martin P. and Parkhurst S.M. (2004). Parallels between tissue repair and embryo morphogenesis. Development 131, 3021-34.

Matsuoka Y., Hughes C.A. and Bennett V. (1996). Adducin regulation. Definition of the calmodulin-binding domain and sites of phosphorylation by protein kinases A and C. J Biol Chem Sci 271, 25157-66.

Matsuoka Y., Li X. and Bennett V. (1998). Adducin is an in vivo substrate for protein kinase C: phosphorylation in the MARCKS-related domain inhibits activity in promoting spectrin-actin complexes and occurs in many cells, including dendritic spines of neurons. J Cell Biol 142, 485-97.

Matsuoka Y., Li X. and Bennett V. (2000). Adducin: structure, function and regulation. Cell Mol Life Sci 57, 884-95.

Mendoza C., Olguin P., Lafferte G., Thomas U., Ebitsch S., Gundelfinger E.D., Kukuljan M. and Sierralta J. (2003). Novel isoforms of Dlg are fundamental for neuronal development in Drosophila. J Neurosci 23, 2093-101.

Mendoza-Topaz C., Urra F., Barria R., Albornoz V., Ugalde D., Thomas U., Gundelfinger E.D., Delgado R., Kukuljan M., Sanxaridis P.D., Tsunoda S., Ceriani M.F., Budnik V. and Sierralta J. (2008). DLGS97/SAP97 is developmentally upregulated and is required for complex adult behaviors and synapse morphology and function. J Neurosci 28, 304-14.

Mentzel B. and Raabe T. (2005). Phylogenetic and structural analysis of the Drosophila melanogaster p21-activated kinase DmPAK3. Gene 349, 25-33.

Millard T.H. and Martin P. (2008). Dynamic analysis of filopodial interactions during the zippering phase of Drosophila dorsal closure. Development 135, 621-6.

Morel V. and Arias A.M. (2004). Armadillo/β-catenin-dependent Wnt signalling is required for the polarisation of epidermal cells during dorsal closure in Drosophila. Development 131, 3273-83.

Narasimha M. and Brown N.H. (2004). Novel functions for integrins in epithelial morphogenesis. Curr Biol 14, 381-5.

Narasimha M., Uv A., Krejci A., Brown N.H. and Bray S.J. (2008). Grainy head promotes expression of septate junction proteins and influences epithelial morphogenesis. J Cell Sci 121, 747-52.

Naydenov N.G. and Ivanov A.I. (2010). Adducins regulate remodeling of apical junctions in human epithelial cells. Mol Biol Cell 21, 3506-17.

Naydenov N.G. and Ivanov A.I. (2011). Spectrin-adducin membrane skeleton: A missing link between epithelial junctions and the actin cytoskeleton? Bioarchitecture 1, 186-191.

Newsome T.P., Asling B. and Dickson B.J. (2000a). Analysis of Drosophila photoreceptor axon guidance in eye-specific mosaics. Development 127, 851-60.

Newsome T.P., Schmidt S., Dietzl G., Keleman K., Asling B., Debant A. and Dickson B.J. (2000b). Trio combines with dock to regulate Pak activity during photoreceptor axon pathfinding in Drosophila. Cell 101, 283-94.

Nieto M.A. (2011). The ins and outs of the epithelial to mesenchymal transition in health and disease. Annu Rev Cell Dev Biol 27, 347-76.

Nishimura I., Yang Y. and Lu B. (2004). PAR-1 kinase plays an initiator role in a temporally ordered phosphorylation process that confers tau toxicity in Drosophila. Cell 116, 671-82.

Nola S., Sebbagh M., Marchetto S., Osmani N., Nourry C., Audebert S., Navarro C., Rachel R., Montcouquiol M., Sans N., Etienne-Manneville S., Borg J.P. and Santoni M.J. (2008). Scrib regulates PAK activity during the cell migration process. Hum Mol Genet 17, 3552-65.

Oda H., Uemura T., Harada Y., Iwai Y. and Takeichi M. (1994). A Drosophila homolog of cadherin associated with armadillo and essential for embryonic cell-cell adhesion. Dev Biol 165, 716-26.

Ohler S., Hakeda-Suzuki S. and Suzuki T. (2011). Hts, the Drosophila homologue of Adducin, physically interacts with the transmembrane receptor Golden goal to guide photoreceptor axons. Dev Dyn 240, 135-48.

Oliva C., Escobedo P., Astorga C., Molina C. and Sierralta J. (2012). Role of the MAGUK protein family in synapse formation and function. Dev Neurobiol 72, 57-72.

Ozdowski E.F., Gayle S., Bao H., Zhang B. and Sherwood N.T. (2011). Loss of Drosophila melanogaster p21-activated kinase 3 suppresses defects in synapse structure and function caused by spastin mutations. Genetics 189, 123-35.

Parks A.L., Cook K.R., Belvin M., Dompe N.A., Fawcett R., Huppert K., Tan L.R., Winter C.G., Bogart K.P., Deal J.E., Deal-Herr M.E., Grant D., Marcinko M., Miyazaki W.Y., Robertson S., Shaw K.J., Tabios M., Vysotskaia V., Zhao L., Andrade R.S., Edgar K.A., Howie E., Killpack K., Milash B., Norton A., Thao D., Whittaker K., Winner M.A., Friedman L., Margolis J., Singer M.A., Kopczynski C., Curtis D., Kaufman T.C., Plowman G.D., Duyk G. and Francis-Lang HL. (2004). Systematic generation of high-resolution deletion coverage of the Drosophila melanogaster genome. Nat Genet 36, 288-92.

Parnas D., Haghighi A.P., Fetter R.D., Kim S.W. and Goodman C.S. (2001). Regulation of postsynaptic structure and protein localization by the Rho-type guanine nucleotide exchange factor dPix. Neuron 32, 415-24.

Parton R.M., Valles A.M., Dobbie I.M. and Davis I. (2010). Collection and mounting of Drosophila embryos for imaging. Cold Spring Harb Protoc, doi:10.1101/pdb.prot5403.

Paschinger K., Rendic D. and Wilson I.B. (2009). Revealing the anti-HRP epitope in Drosophila and Caenorhabditis. Glycoconj J 26, 385-95.

Peter A., Schottler P., Werner M., Beinert N., Dowe G., Burkert P., Mourkioti F., Dentzer L., He Y., Deak P., Benos P.V., Gatt M.K., Murphy L., Harris D., Barrell B., Ferraz C., Vidal S., Brun C., Demaille J., Cadieu E., Dreano S., Gloux S., Lelaure V., Mottier S., Galibert F., Borkova D., Minana B., Kafatos F.C., Bolshakov S., Siden-Kiamos I., Papagiannakis G., Spanos L., Louis C., Madueno E., de Pablos B., Modolell J., Bucheton A., Callister D., Campbell L., Henderson N.S., McMillan P.J., Salles C., Tait E., Valenti P., Saunders R.D., Billaud A., Pachter L., Klapper R., Janning W., Glover D.M., Ashburner M., Bellen H.J., Jackle H. and Schafer U. (2002). Mapping and identification of essential gene functions on the X chromosome of Drosophila. EMBO Rep 3, 34-8.

Petrella L.N., Smith-Leiker T. and Cooley L. (2007). The Ovhts polyprotein is cleaved to produce fusome and ring canal proteins required for Drosophila oogenesis. Development 134, 703-12.

Pickering K., Alves-Silva J., Goberdhan D. and Millard T.H. (2013). Par3/Bazooka and phosphoinositides regulate actin protrusion formation during Drosophila dorsal closure and wound healing. Development 140, 800-9.

Pielage J., Bulat V., Zuchero J.B., Fetter R.D. and Davis G.W. (2011). Hts/Adducin controls synaptic elaboration and elimination. Neuron 69, 1114-31.

Pokutta S. and Weis W.I. (2000). Structure of the dimerization and β-catenin-binding region of α-catenin. Mol Cell 5, 533-43.

Porro F., Rosato-Siri M., Leone E., Costessi L., Iaconcig A., Tongiorgi E. and Muro A.F. (2010). β-adducin (Add2) KO mice show synaptic plasticity, motor coordination and behavioral deficits accompanied by changes in the expression and phosphorylation levels of the α- and γ-adducin subunits. Genes Brain Behav 9, 84-96.

Rabenstein R.L., Addy N.A., Caldarone B.J., Asaka Y., Gruenbaum L.M., Peters L.L., Gilligan D.M., Fitzsimonds R.M. and Picciotto M.R. (2005). Impaired synaptic plasticity and learning in mice lacking β-adducin, an actin-regulating protein. J Neurosci 25, 2138-45.

Ramachandran P. and Budnik V. (2010a). Dissection of Drosophila larval body-wall muscles. Cold Spring Harb Protoc, doi:10.1101/pdb.prot5469.

Ramachandran P. and Budnik V. (2010b). Immunocytochemical staining of Drosophila larval body-wall muscles. Cold Spring Harb Protoc, doi:10.1101/pdb.prot5470.

Rasse T.M., Fouquet W., Schmid A., Kittel R.J., Mertel S., Sigrist C.B., Schmidt M., Guzman A., Merino C., Qin G., Quentin C., Madeo F.F., Heckmann M. and Sigrist S.J. (2005). Glutamate receptor dynamics organizing synapse formation in vivo. Nat Neurosci 8, 898-905.

Rauch M.E., Ferguson C.G., Prestwich G.D. and Cafiso D.S. (2002). Myristoylated alanine-rich C kinase substrate (MARCKS) sequesters spin-labeled phosphatidylinositol 4,5-bisphosphate in lipid bilayers. J Biol Chem 277, 14068-76.

Redd M.J., Cooper L., Wood W., Stramer B. and Martin P. (2004). Wound healing and inflammation: embryos reveal the way to perfect repair. Philos Trans R Soc Lond B Biol Sci 359, 777-84.

Reed B.H., McMillan S.C. and Chaudhary R. (2009). The preparation of Drosophila embryos for live-imaging using the hanging drop protocol. J Vis Exp, doi:10.3791/1206.

Rimm D.L., Koslov E.R., Kebriaei P., Cianci C.D. and Morrow J.S. (1995). α1(E)-catenin is an actin-binding and -bundling protein mediating the attachment of F-actin to the membrane adhesion complex. Proc Nat Acad Sci U S A 92, 8813-7.

Roberts S., Delury C. and Marsh E. (2012). The PDZ protein discs-large (DLG): the 'Jekyll and Hyde' of the epithelial polarity proteins. FEBS J 279, 3549-58.

Robinson D.N., Cant K. and Cooley L. (1994). Morphogenesis of Drosophila ovarian ring canals. Development 120, 2015-25.

Rothwell W.F. and Sullivan W. (2007a). Drosophila embryo collection. CSH Protoc, doi:10.1101/pdb.prot4825.

Rothwell W.F. and Sullivan W. (2007b). Drosophila embryo dechorionation. CSH Protoc, doi:10.1101/pdb.prot4826.

Rothwell W.F. and Sullivan W. (2007c). Fixation of Drosophila embryos. CSH Protoc, doi:10.1101/pdb.prot4827.

Rubin G.M., Hong L., Brokstein P., Evans-Holm M., Frise E., Stapleton M. and Harvey D.A. (2000). A Drosophila complementary DNA resource. Science 287, 2222-4.

Sang T.K. and Jackson G.R. (2005). Drosophila models of neurodegenerative disease. NeuroRx 2, 438-46.

Schuster C.M., Davis G.W., Fetter R.D. and Goodman C.S. (1996a). Genetic dissection of structural and functional components of synaptic plasticity. I. Fasciclin II controls synaptic stabilization and growth. Neuron 17, 641-54.

Schuster C.M., Davis G.W., Fetter R.D. and Goodman C.S. (1996b). Genetic dissection of structural and functional components of synaptic plasticity. II. Fasciclin II controls presynaptic structural plasticity. Neuron 17, 655-71.

Seidel B., Zuschratter W., Wex H., Garner C.C. and Gundelfigner E.D. (1995). Spatial and sub-cellular localization of the membrane cytoskeleton-associated protein α-adducin in the rat brain. Brain Res 700, 13-24.

Shan X., Hu J.H., Cayabyab F.S. and Krieger C. (2005). Increased phospho-adducin immunoreactivity in a murine model of amyotrophic lateral sclerosis. Neuroscience 134, 833-46.

Shen W., Chen X., Cormier O., Cheng D.C., Reed B. and Harden N. (2013). Modulation of morphogenesis by Egfr during dorsal closure in Drosophila. PLoS One 8, e60180.

Shima T., Okumura N., Takao T., Satomi Y., Yagi T., Okada M. and Nagai K. (2001). Interaction of the SH2 domain of Fyn with a cytoskeletal protein, beta-adducin. J Biol Chem 276, 42233-40.

Shin K., Fogg V.C. and Margolis B. (2006). Tight junctions and cell polarity. Annu Rev Cell Dev Biol 22, 207-35.

Simpson R.J. (2006). SDS-PAGE of proteins. CSH Protoc, doi:10.1101/pdb.prot4313.

Slabbaert J.R., Khuong T.M. and Verstreken P. (2012). Phosphoinositides at the neuromuscular junction of Drosophila melanogaster: a genetic approach. Methods Cell Biol 108, 227-47.

Spradling A.C., Stern D., Beaton A., Rhem E.J., Laverty T., Mozden N., Misra S. and Rubin G.M. (1999). The Berkeley Drosophila Genome Project gene disruption project: Single P-element insertions mutating 25% of vital Drosophila genes. Genetics 153, 135-77.

St Johnston D. (2002). The art and design of genetic screens: Drosophila melanogaster. Nat Rev Genet 3, 176-88.

Stapleton M., Liao G., Brokstein P., Hong L., Carninci P., Shiraki T., Hayashizaki Y., Champe M., Pacleb J., Wan K., Yu C., Carlson J., George R., Celniker S. and Rubin G.M. (2002). The Drosophila gene collection: identification of putative full-length cDNAs for 70% of D. melanogaster genes. Genome Res 12, 1294-300.

Stern D.L. and Sucena E. (2011). Preparation of cuticles from unhatched first-instar Drosophila larvae. Cold Spring Harb Protoc, doi:10.1101/pdb.prot065532.

Su R., Han Z.Y., Fan J.P. and Zhang Y.L. (2010). A possible role of myristoylated alanine-rich C kinase substrate in endocytic pathway of Alzheimer's disease. Neurosci Bull 26, 338-44.

Swedlow J. (2011). Immunolabeling of Drosophila embryos and tissues. Cold Spring Harb Protoc, doi:10.1101/pdb.prot5657.

Takada Y., Ye X. and Simon S. (2007). The integrins. Genome Biol 8, 215-9.

Tao Y. and Schulz R.A. (2007). Heart development in Drosophila. Semin Cell Dev Biol 18, 3-15.

Telonis-Scott M., Kopp A., Wayne M.L., Nuzhdin S.V. and McIntyre L.M. (2009). Sex-specific splicing in Drosophila: widespread occurrence, tissue specificity and evolutionary conservation. Genetics 181, 421-34.

Tepass U., Tanentzapf G., Ward R. and Fehon R. (2001). Epithelial cell polarity and cell junctions in Drosophila. Annu Rev Genet 35, 747-84.

Thomas U., Kim E., Kuhlendahl S., Koh Y.H., Gundelfinger E.D., Sheng M., Garner C.C. and Budnik V. (1997). Synaptic clustering of the cell adhesion molecule fasciclin II by discs-large and its role in the regulation of presynaptic structure. Neuron 19, 787-99.

Thomas U., Kobler O. and Gundelfinger E.D. (2010). The Drosophila larval neuromuscular junction as a model for scaffold complexes at glutamatergic synapses: benefits and limitations. J Neurogenet 24, 109-19.

Ting S.B., Caddy J., Wilanowski T., Auden A., Cunningham J.M., Elias P.M., Holleran W.M. and Jane S.M. (2005). The epidermis of grhl3-null mice displays altered lipid processing and cellular hyperproliferation. Organogenesis 2, 33-5.

Toba G., Ohsako T., Miyata N., Ohtsuka T., Seong K.H. and Aigaki T. (1999). The gene search system. A method for efficient detection and rapid molecular identification of genes in Drosophila melanogaster. Genetics 151, 725-37.

Tomancak P., Piano F., Riechmann V., Gunsalus K.C., Kemphues K.J. and Ephrussi A. (2000). A Drosophila melanogaster homologue of Caenorhabditis elegans par-1 acts at an early step in embryonic-axis formation. Nat Cell Biol 2, 458-60.

Valenta T., Hausmann G. and Basler K. (2012). The many faces and functions of β-catenin. EMBO J 31, 2714-36.

Varnai P. and Balla T. (2008). Live cell imaging of phosphoinositides with expressed inositide binding protein domains. Methods 46, 167-76.

Verstreken P., Ohyama T., Haueter C., Habets R.L., Lin Y.Q., Swan L.E., Ly C.V., Venken K.J., De Camilli P. and Bellen H.J. (2009). Tweek, an evolutionarily conserved protein, is required for synaptic vesicle recycling. Neuron 63, 203-15.

Vukojevic V., Gschwind L., Vogler C., Demougin P., de Quervain D.J., Papassotiropoulos A. and Stetak A. (2012). A role for α-adducin (ADD-1) in nematode and human memory. EMBO J 31, 1453-66.

Wagey R.T. and Krieger C. (1998). Abnormalities of protein kinases in neurodegenerative diseases. Prog Drug Res 51, 133-83.

Waimey K.E. and Cheng H.J. (2006). Axon pruning and synaptic development: how are they per-plexin? Neuroscientist 12, 398-409.

Wang J., Arbuzova A., Hangyas-Mihalyne G. and McLaughlin S. (2001). The effector domain of myristoylated alanine-rich C kinase substrate binds strongly to phosphatidylinositol 4,5-bisphosphate. J Biol Chem 276, 5012-9.

Wang J., Gambhir A., Hangyas-Mihalyne G., Murray D., Golebiewska U. and McLaughlin S. (2002). Lateral sequestration of phosphatidylinositol 4,5-bisphosphate by the basic effector domain of myristoylated alanine-rich C kinase substrate is due to nonspecific electrostatic interactions. J Biol Chem 277, 34401-12.

Wang S., Yang J., Tsai A., Kuca T., Sanny J., Lee J., Dong K., Harden N. and Krieger C. (2011). Drosophila adducin regulates Dlg phosphorylation and targeting of Dlg to the synapse and epithelial membrane. Dev Biol 357, 392-403.

Whittaker K.L., Ding D., Fisher W.W. and Lipshitz H.D. (1999). Different 3' untranslated regions target alternatively processed hu-li tai shao (hts) transcripts to distinct cytoplasmic locations during Drosophila oogenesis. J Cell Sci 112, 3385-98.

Wodarz A. and Nathke I. (2007). Cell polarity in development and cancer. Nat Cell Biol 9, 1016-24.

Woods D.F. and Bryant P.J. (1991). The discs-large tumor suppressor gene of Drosophila encodes a guanylate kinase homolog localized at septate junctions. Cell 66, 451-64.

Woods D.F., Hough C., Peel D., Callaini G. and Bryant P.J. (1996). Dlg protein is required for junction structure, cell polarity, and proliferation control in Drosophila epithelia. J Cell Biol 134, 1469-82.

Wu X., Tanwar P.S. and Raftery L.A. (2008). Drosophila follicle cells: morphogenesis in an eggshell. Semin Cell Dev Biol 19, 271-82.

Yamada S., Pokutta S., Drees F., Weis W.I. and Nelson W.J. (2005). Deconstructing the cadherin-catenin-actin complex. Cell 123, 889-901.

Yamanaka T. and Ohno S. (2008). Role of Lgl/Dlg/Scribble in the regulation of epithelial junction, polarity and growth. Front Biosci 13, 6693-707.

Yue L. and Spradling A.C. (1992). hu-li tai shao, a gene required for ring canal formation during Drosophila oogenesis, encodes a homolog of adducin. Genes Dev 6, 2443-54.

Zaccai M. and Lipshitz H.D. (1996a). Role of Adducin-like (hu-li tai shao) mRNA and protein localization in regulating cytoskeletal structure and function during Drosophila oogenesis and early embryogenesis. Dev Genet 19, 249-57.

Zaccai M. and Lipshitz H.D. (1996b). Differential distributions of two adducin-like protein isoforms in the Drosophila ovary and early embryo. Zygote 4, 159-66.

Zahedi B., Shen W., Xu X., Chen X., Mahey M. and Harden N. (2008). Leading edge-secreted Dpp cooperates with ACK-dependent signaling from the amnioserosa to regulate myosin levels during dorsal closure. Dev Dyn 237, 2936-46.

Zeitler J., Hsu C.P., Dionne H. and Bilder D. (2004). Domains controlling cell polarity and proliferation in the Drosophila tumor suppressor Scribble. J Cell Biol 167, 1137-46.

Zeng Y.A., Rahnama M., Wang S., Lee W. and Verheyen E.M. (2008). Inhibition of Drosophila Wg signaling involves competition between Mad and Armadillo/β-catenin for dTcf binding. PLoS One 3, e3893.

Zhang W., Crocker E., McLaughlin S. and Smith S.O. (2003). Binding of peptides with basic and aromatic residues to bilayer membranes: phenylalanine in the myristoylated alanine-rich C kinase substrate effector domain penetrates into the hydrophobic core of the bilayer. J Biol Chem 278, 21459-66.

Zhang Y., Guo H., Kwan H., Wang J.W., Kosek J. and Lu B. (2007). PAR-1 kinase phosphorylates Dlg and regulates its postsynaptic targeting at the Drosophila neuromuscular junction. Neuron 53, 201-15.

Zhang B. and Stewart B. (2010). Electrophysiological recording from Drosophila larval body-wall muscles. Cold Spring Harb Protoc, doi:10.1101/pdb.prot5487.

Zinsmaier K.E., Eberle K.K., Buchner E., Walter N. and Benzer S. (1994). Paralysis and early death in cysteine string protein mutants of Drosophila. Science 263, 977-80.

Zito K., Fetter R.D., Goodman C.S. and Isacoff E.Y. (1994). Synaptic clustering of Fasciclin II and Shaker: essential targeting sequences and role of Dlg. Neuron 19, 1007-16.

Appendices

Appendix A – Movies

Please see the attached CD-ROM.

MOVIE 1: Dorsal closure of the *Drosophila* embryo.

Dorsal view of an embryo expressing *UAS-dlgA-GFP* throughout the epidermis with *ptc-Gal4* (refer to Figure 1). Following germband retraction, a hole is present in the dorsal epidermis of the embryo. Dorsal closure occurs when the epidermal flanks that surround both sides of the hole migrate towards each other, up and over the amnioserosa tissue (not marked) occupying the hole. The advancing flanks eventually meet at the dorsal midline and fuse together, closing the hole shut to form a continuous epidermis. Consequently, the amnioserosa is internalized and degraded. The time interval between frames is one minute, with the frame rate of the movie set to 12 frames per second (i.e. one second in the movie represents 12 minutes in real time).

Filename: Movie 01.mp4

MOVIE 2: Live image analysis of Pak-GFP distribution during dorsal closure.

Dorsolateral view of an embryo expressing *UAS-pak-GFP* in epidermal stripes with *prd-Gal4* (refer to Figure 6). Pak-GFP accumulates along the leading edge membrane of DME cells during dorsal closure. Upon dorsal closure completion, Pak-GFP accumulation is lost after the opposing epidermal flanks meet at the dorsal midline. The time interval between frames is two minutes, with the frame rate of the movie set to five frames per second (i.e. one second in the movie represents ten minutes in real time).

Filename: Movie 02.mp4

MOVIE 3: Live image analysis of DlgA-GFP recruitment to the leading edge membrane of DME cells in a wild-type embryo at the end of dorsal closure.

Dorsal view of an embryo expressing *UAS-dlgA-GFP* throughout the epidermis with *ptc-Gal4* in a wild-type background (see Figure 12). DlgA-GFP is restored at the dorsal midline, first appearing shortly after opposing DME cells make contact with each other, usually several cells back from the canthi. The time interval between frames is one minute, with the frame rate of the movie set to five frames per second (i.e. one second in the movie represents five minutes in real time).

Filename: Movie 03.mp4

MOVIE 4: Live image analysis of DlgA-GFP recruitment to the leading edge membrane of DME cells in a *pak*^{14}*pak3*^{76a} mutant embryo at the end of dorsal closure.

Dorsal view of an embryo expressing *UAS-dlgA-GFP* throughout the epidermis with *ptc-Gal4* in a *pak*^{14}*pak3*^{76a} mutant background (see Figure 12). DlgA-GFP is not restored at the dorsal midline, even though the dorsal hole is completely closed and the opposing epidermal flanks are clearly in contact with each other. The time interval between frames is one minute, with the frame rate of the movie set to five frames per second (i.e. one second in the movie represents five minutes in real time).

Filename: Movie 04.mp4

MOVIE 5: Mobility of a wild-type pharate adult.

A wild-type pharate adult removed from its pupal case and placed on a grape juice agar plate. Wild-type pharate adults are quite active as they must be able to emerge from their pupal cases to feed. The pharate adult was filmed with a digital microscope camera.

Filename: Movie 05.mp4

MOVIE 6: Mobility of a pharate adult with muscle-specific knockdown of Hts.

A pharate adult, with *UAS-hts-RNAi* expression in the muscle with *mef2-Gal4*, removed from its pupal case and placed on a grape juice agar plate. *mef2>hts-RNAi* mutants fail to eclose from their pupal cases and die. Newly formed pharate adults that are dissected out of their pupal cases are still alive but move feebly, indicating that they are too weak to emerge from their pupal cases on their own. The pharate adult was filmed with a digital microscope camera.

Filename: Movie 06.mp4

Appendix B – Reagents

All recipes are for working solutions, i.e. ready to use. Chemicals are dissolved in water unless otherwise stated. Solutions are stored at room temperature unless otherwise stated.

50% Bleach

- 50% Clorox bleach
- 50% 0.01% Triton X-100 (made from Sigma-Aldrich – T8787)

Make fresh each time. Do not add detergent when dechorionating embryos for live imaging.

1% Bovine Serum Albumin (BSA)

- 1% BSA (BioShop Canada – ALB001)
- PBS
- 0.1% Triton X-100 (Sigma-Aldrich – T8787)

Store at 4°C. Make fresh every three to four months.

2.5% Bovine Serum Albumin (BSA)

- 2.5% BSA (BioShop Canada – ALB001)
- TBS
- 0.1% Tween 20 (Fisher Scientific – BP337)

Store at 4°C. Make fresh every three to four months.

5% Bovine Serum Albumin (BSA)

- 5% BSA (BioShop Canada – ALB001)
- TBS
- 0.1% Tween 20 (Fisher Scientific – BP337)

Store at 4°C. Make fresh every three to four months.

Grape Juice Agar Plates

- 75g Agar (Anachemia Science – 02116-380)
- 83.5g Sugar
- 5g Tegosept (Sigma-Aldrich – H5501)
- 830mL Welch's grape juice

Dissolve agar and sugar in 2.5L of water. Autoclave. Cool to approximately 60°C, i.e. hand hot, before adding tegosept and grape juice. Pour into 60×15mm plastic petri dishes (the recipe is for approximately 200 plates). Store inverted at 4°C.

Hoyer's Medium

- 30g Gum arabic (Sigma-Aldrich – G9752)
- 200g Chloral hydrate (Sigma-Aldrich – C8383)
- 16mL Glycerol (Caledon Laboratories – 5350-1)

Dissolve gum arabic, then chloral hydrate, in 50mL of water before adding glycerol. Centrifuge at 12,000×g for three hours. Pour into glass amber drop dispensing bottles, taking care not to transfer black precipitates that were pelleted after centrifugation.

Lysis Buffer I

- 475mM Tris (Caledon Laboratories – 8980-1)
- 0.5% Triton X-100 (Sigma-Aldrich – T8787)

Add one protease inhibitor cocktail tablet (Roche Applied Science – 11 697 498 001) for every 50mL of solution. Filter sterilize. Store at -20°C.

Lysis Buffer II

- 50% Lysis Buffer I
- 50% 1M NaCl (made from Caledon Laboratories – 7560-1)

Filter sterilize. Store at -20°C.

2.5% Milk

- 2.5% Skim milk powder
- TBS
- 0.1% Tween 20 (Fisher Scientific – BP337)

Store at 4°C. Make fresh every one to two weeks.

5% Milk

- 5% Skim milk powder
- TBS
- 0.1% Tween 20 (Fisher Scientific – BP337)

Store at 4°C. Make fresh every one to two weeks.

4% Paraformaldehyde (PFA)

- 4% PFA (Anachemia Science – 66194-300)
- 1mM NaOH (EMD Millipore – SX0590)
- PBS

Dissolve PFA in water before adding PBS. To completely dissolve PFA, heat the solution to 65°C and adjust the pH with NaOH. Store at 4°C. Make fresh every three to four months.

Phosphate Buffer Saline (PBS)

- 3mM NaH_2PO_4 (Caledon Laboratories – 8180-1)
- 7mM Na_2HPO_4 (Caledon Laboratories – 8120-1)
- 1.3M NaCl (Caledon Laboratories – 7560-1)

Adjust pH to 7.0 with NaOH. Autoclave.

Phosphate Buffer Saline with Triton (PBT)

- PBS
- 0.1% Triton X-100 (Sigma-Aldrich – T8787)

Running Buffer

- 25mM Tris (Caledon Laboratories – 8980-1)
- 192mM Glycine (BioShop Canada – GLN001)
- 0.1% SDS (Sigma-Aldrich – L5750)

Stripping Solution

- TBS
- 2% SDS (Sigma-Aldrich – L5750)
- 0.7% β-mercaptoethanol (BioShop Canada – MER002)

Tris Buffer Saline (TBS)

- 50mM Tris (Caledon Laboratories – 8980-1)
- 150mM NaCl (Caledon Laboratories – 7560-1)

Adjust pH to 7.5 with HCl. Store at 4°C.

Tris Buffer Saline with Tween (TBST)

- TBS
- 0.1% Tween 20 (Fisher Scientific – BP337)

Store at 4°C.

Transfer Buffer

- 25mM Tris (Caledon Laboratories – 8980-1)
- 192mM Glycine (BioShop Canada – GLN001)
- 25% Methanol (Caledon Laboratories – 6700-1)

Yeast Paste

- 50% White vinegar

Add active dry yeast. Mix until the paste is the consistency of peanut butter. Store at 4°C.

Appendix C – Subcloning

Digested PCR fragments were subcloned into pGEX-4T-1 (GE Healthcare – 28-9545-49) and pET-28a(+) (Novagen – 69864-3) vectors.

***pak* (LD20767)**

Forward Primer:
5' CGTAGAATTCATGTCCAGCGAGGAAGACAAACC 3'

Reverse Primer:
5' TAATCTCGAGTCAGTTGCCCTTGGTAGCCTCC 3'

Internal Sequencing Primer:
5' TAACCTGATTGGCGTCCAGTTGG 3' +564

ATGTCCAGCGAGGAAGACAAACCGCCGGCGCCGCCTGTGCGTCTCACCAGCAACCGGGGCGGCAATGAACG
ATCGGGAGGAGGAGTGGGCGTCGGTGGCGGAGGACTGGGAGGTGGCGGTATGGGAGATGTACCGCCCGACA
TGCGTCCGCTGCCCAAGGAACCCGACGACTCCGATCGGAAGAAGAAAACGCTGAAGAGCAAGATCAAAGGA
TCGAAGCCCTCGCACACGGACTCCAAGCCGAACATCTCCTATCCCACGAACTTTGAGCACACGGTCCATGT
GGGATTCGATGCTGTCACCGGCGAGTTTACCGGCATGCCGGAGGCATGGGCGCGACTCCTGATGAACTCCA
ACATCAGCAAGCAGGAGCAGAAGAAGAATCCCCAGGCCGTGCTGGATGTGCTCAAGTGGTTCGACAACACT
ACCAAACAGAGGCCAAGTTCCAAGTACATGACAAATGCCATTACGACGCATTCAGGTTCATCGCTCAGCCG
CGTCAGCAGCAGCAGTCCGAGCAGCACGCCAACAGACTCGGAGCTGCACGGCTCCAACAGCGGAGGTAACC
TGATTGGCGTCCAGTTGGGCAGTATGACTCTGGGTCCCAACGCCAACAACGTGGCCGTTGCTGGGCAAATT
CTGGGCAACCACTACCAACAGCAGCAGCAGCACCTCCTTCAGCAGCAGCAGCCACTTTTGCATCAGAACCA
CAACCAGCATCACATGGGCATAAGTCAATCGCACTCGTACAACTTTGTCGGACACACGGTCTCCTCATCCA
CATCGCAACATTCATCCGCTAACGAGGACGATATGCTGGGACCACAGCACCCGCAGCAACAGCCGCCACCT
CCACCGGTGGCCTCTAGGCCTGAGCGCACGAAATCCATCTACACGCGGCCAATCGAGGATCTACAGCCAGC
CATCATCCCAATGCCAGTGGCGCCAGCAACCACGCCTGCAACGCCGCTGCAAAATCATAGGACGCCAGGCG
GAATATCAGCACCAGCGGCATCGCCAATGATGCACAACAATGCCACGACGACGCTGGACAAGAATAAAAAC
AATGCAAATCTGTACACACCGGAACCCACGGTAGCCCAAGTGTCAGCCGGTGGCCCAAGTTCTCAAGTGGC
TGGAAACCAAATCGCCGTGCCCCAGGCAGCTGTGGCTCCGGCTGCAACGCCCAACACGAGGGCAGCCAACG
CCAAGAAGAAAAAGATGTCCGACGAGGAGATCTTGGAGAAACTGCGCACCATTGTCTCTGTGGGCGATCCA
AATCGAAAGTACACCAAGATGGAGAAGATTGGCCAGGGTGCCTCTGGCACAGTGTATACTGCAATTGAATC
CTCGACCGGCATGGAGGTGGCCATCAAGCAGATGAACCTGTCACAGCAGCCTAAAAAGGAGCTCATCATCA
ACGAGATCCTTGTGATGCGGGAGAACAAACACCCAAATGTAGTCAACTATCTTGACAGCTACCTCGTGTCT
GAGGAACTGTGGGTGGTCATGGAGTACCTGCCCGGCGGCTCTCTTACCGACGTCGTCACCGAGACCTGCAT
GGACGAGGGCCAGATCGCAGCTGTTTGCCGAGAAGTGCTGCAAGCTCTGGAGTTCCTTCACGCCAACCAGG
TTATCCATCGCGACATCAAGAGTGATAACATTCTGCTGGGCCTTGACGGCTCTGTCAAGCTGACTGACTTT
GGTTTCTGTGCGCAAATATCGCCGGAGCAATCCAAACGCACAACGATGGTAGGCACACCCTACTGGATGGC
TCCCGAGGTCGTCACCCGGAAACAGTACGGACCCAAGGTGGACCTTTGGTCTTTGGGCATTATGGCCATAG
AAATGGTCGAGGGCGAACCGCCGTACCTAAACGAGAATCCGCTTAAAGCCTTGTACCTCATTGCCACCAAT
GGCAAGCCAGAGATTAAAGAAAAAGACAAGCTGTCCTCAGCATTTCAGGACTTCCTCGACCAGTGTCTGGA
GGTGGAGGTGGATCGGCGAGCAAGCGCATTGGACTTGCTAAAGCATCCCTTCCTAAAACTGGCCCGTCCAT
TGGCCAGTCTGACTCCCTTGATCATGGCCGCAAAGGAGGCTACCAAGGGCAACTGA

***pak3* (LD10376)**

Forward Primer:
5' CGTAGAATTCATGAGCTTCACCAAGTGG 3'

Reverse Primer:
5' TATACTCGAGCTATACGTTGCGTCGGAGC 3'

Internal Sequencing Primer:
5' ACACAGAAGTTCTCACGCACTTCG 3' +637

ATGAGCTTCACCAAGTGGTTCAAGAAGAAGGGCGGAGATGGGGGATCGATCTCAGAGATCGGTGCACCCAC
AAACTTCCAACGGCACTTCCATGTCTCGCGCAACCAGGAAACCGGCGACCTGGAGGGGCTTCCAGCTCCAT
GGGTGCGCCTAATGAACTCACAGATCACTCGCGATGAGCAGGACAAGAATCCAGATGCTGCCTACCATGCC
GTTAAGTACTACAACTATTCGATTAAGAAGAAAGAGAACGAGGTCTTCAAGCCCTTCATCACCGAAGATGT
GATCCACGAGGAGTCCAAGGAGATAGAAAACTATGTCAACTACAAAAACAAGCACAAGTCTCAGGATCCCG
AAAAGTCCGACGACGATGGCAGTTCGACGGCCACGGAGACGGAAAGTAGCAGCGGTTGTGGCTCCTCGGCA
GGTAATAGTAACAGCAGCAGCATCAACGACAGCAGCCAGCAGTCGACGGTGCCGCTGGACGCCCTAGAGGA
GGTGTTCAAGGAGCTCAAGACCAATCTGGAGCACCGCGAAACGCTGAAGGCCGCACCGCAAGAGCCTCCAC
CAGTACCGCCCAAGAAATCGCCCCACACCATACCGCCCAAACCGCAAATCAAGCCCAAACCTCGTGTCACA
CAGAAGTTCTCACGCACTTCGGATATACGTCGAGATGAGGACTCCGACAACCAGCACAAGATCAACACAGA
CACAATCATCATCAAGCCAGCCGTAGGGGCCCAGGATGCTGGAGCGGATGATAATCCCGACGAGACGATAC
TGCGCCGCTCCAAGGAGAAGAGGGCCCAGAAAACCGATGCCGAAATCTACGTTGAGCTGCGGGCAATTTGC
AATTCAGATGACCCAAGGGAACGCTACAAGACCACCCAGGAGGTGGGCAAGGGAGCTTCTGGCATAGTTTT
CATAGCCGCCGATTTGCAGAACGAATCGCAGGTGGCCGTCAAGACCATCGATATGAAGAACCAGTCCTCGA
AGGATCTCATACTCACAGAAATCCGAGTGCTCAAGGACTTCAACCACAAGAATCTGGTAAACTTTCTGGAT
GCCTACCTTCTGGAGCCCGAGGACCAACTGTGGGTAGTCATGGAGTACATGGATGGCGGCCCATTGACTGA
CGTCGTTACCGAGACTGTGATGAAGGAGCGCCAGATTGCCTGCGTCTGCCGCGAGACACTCTACGCTATTA
GTTTTCTGCACGCTAAGGGCATTATCCACCGGGACATCAAGTCAGACAACGTGCTGCTGGGCATGGATGGC
AGTGTTAAGGTGACGGACTTTGGGTTCTGCGCCAACATCGAGGGCGATGAGAAGCGCCAGACAATGGTGGG
AACGCCGTACTGGATGGCGCCCGAAGTGGTCACGCGCAAGAAGTACGGCAAGAAGGTGGACATCTGGTCTA
TCGGCATCATGGCCATCGAGATGATCGAAGGCCAGCCACCCTACCTATACGAGACTCCACTCCGCGCCCTC
TACCTGATCGCCGCCAACGGTCGGCCGGATATCAAGAGCTGGGATAAGCTGAGTCCCAACCTTCAAGACTT
TCTCGATCGCTGTCTCCAGGTGGAGGTGGACCGAAGGGCCACCGCCGACGAGTTGCTCAGCCATCCGTTCC
TCAACGACTGCAGCGAGGTCAAGGCCCTCGTGCCCAACATCAAGGCGGCCAAGAAGGTGCTCCGACGCAAC
GTATAG

***hts* (SD02552)**

Forward Primer:
5' CGTAGAATTCATGACTGAAGTTGAGCAACC 3'

Reverse Primer (Full Length):
5' GGTTCTCGAGTTGGTCAAGATTGCTACTCC 3'

Reverse Primer (ΔMARCKS):
5' TATTCTCGAGTTACTTGTCTTTCTTGGGGGATCC 3'

Internal Sequencing Primer:
5' AAGAGTCACTTTGTCCTCCATTCG 3' +571

ATGACTGAAGTTGAGCAACCGCCACAGAATGGCATAGATCCCACTGCCGGCGAAGATGATGACAATAGCAA
AGCACGTCCCGCGGATATTGAACAGGATATGCGCGAAATGGAGCGTCGCAAGCGAGTCGAGGCTATAATGG
GCTCGAAACTGTTCCGCGAGGAGCTGGAGCGTATCGTGGACTCGGCGCGCGATGGAGGTGCTGGCGCTAGT
GGAATCCTGCAGCTGTCGGACATTGTGGGCGTACCAGTGTCCAGGGTGGGCAGCGTCTTCAAGAGCAGCAA
CTGCATGGTGCCAATCAACGATATACGCGGCGTCGAGTCCATGGGCTATGCCAAGGGCGAGAAGATACTCC
GGTGCAAGCTGGCCGCCACATTCCGTCTGCTCGATCTGTACGGCTGGACCCAGGGTCTGGGGGCACAGATC
ACCGCCCGACTCAAGGTCGATCAGGAGTACTTCCTGGTTAACCCATACGGCCTGCTTTACCACGAGATCAC
TGCCTCAGCGCTGAACAAGGTGGATATGCAAGGACAGATTGTGGAGCAGGGCACCACCAACTTTGGCGGCA
ACAAGAGTCACTTTGTCCTCCATTCGGTGGTACATGCTGCCCGTCCAGATATTCGATGCGCCATCTATATC
GGCTGCAGTCCAGTCGTGGCTATTTCCTCACTAAAGACGGGTCTATTGCCCTTGACCAAGGATGCCTGTGT
GCTGGGCGAGATCACCACTCACGCTTATACTGGTCTATTCGACGAGGAGGAGCGCAATCGATTGGTCCGCA
GCCTTGGTCCCAACTCCAAGGTGATTCTGTTAACTAATCACGGTGCTTTGTGCTGCGGAGAGACCATCGAG
GAAGCCTTCTTCGCCGCCTGTCACATTGTACAGGCGTGTGAGACGCAACTGAAGCTGTTGCCCGTCGGTTT
GGATAACTTGGTGCTGATTCCAGAGGAGTCGCGCAAGGCCATTTACGAGCAGTCGCGCCGGCCGCCGGAGG
ATCTGGAGAAGAAGTTTGCCGCCGTCGCCGCTGCCGAAGATGGTGCTGCTACTGCTGAAAAGGATGCAGCC
GAAGCAGTACCCAAGGTTGGCAGTCCGCCCAAGTGGCGTGTGGGTGGTGCTGAATTTGAGGCCTTGATGCG
CATGCTGGACAATGCTGGCTATCGCACTGGCTATATCTACCGTCATCCACTGATCAAATCGGATCCTCCCA
AGCCTAAGAACGATGTCGAACTACCGCCAGCTGTTTCATCACTGGGCTATCTTCTTGAGGAGGAGGAACTC
TTCCGTCAAGGGATCTGGAAGAAGGGAGATATTCGCAAAGGCGGCGATCGCAGTCGGTGGCTCAACTCGCC
AAACGTTTACCAAAAGGTCGAGGTTCTGGAGACCGGCACTCCGGATCCCAAGAAGATTACAAAGTGGGTGG
CTGAGGGTTCCCCCACCCACTCAACGCCAGTGAGGATAGAAGATCCACTCCAGTTTGTGCCTGCAGGAACC
AATCCAAGGGAATTTAAGCGTGTCCAGCAACTAATTAAGGACAACCGCCGGGCAGATAAGATTTCAGCCGG
ACCACAGTCGCATATTCTGGAGGGCGTGACATGGGACGAGGCGAGCCGACTCAAGGATGCAACGGTCTCGC
AGGCCGGCGATCATGTCGTCATGATGGGTGCTGCCTCCAAAGGAATCATTCAGCGTGGCTTCCAGCACAAT
GCCACTGTCTACAAGGCACCGTATGCTAAGAACCCATTCGATAACGTCACAGACGATGAACTCAATGAATA
CAAACGCACGGTGGAGCGCAAAAAGAAATCGGTGCATGGTGAATATACCGACACAGACTTTTCGGAATCCG
AAGCGGTCCTGCAGGCGGGGACAAAGAAATACCCACAAAGCGAACCCGAGACCGAGCACCAGGTCATTGAG
ATCCAAACACAGCAAGCGCCAGTGCCAAGGCAGGCGGAAGTCGTGCTGAGCGATGGTGAAAACGTACAAAA
TGGCGATCATTCGGAGGCACACTTGAGCACCTTCTCGCAGAGCAGTAAAGAGTTCCAGGATGTCTCCACGG
ACGGATCCCCCAAGAAAGACAAGAAGAAGAAGAAGGGTCTGCGCACACCATCGTTTTTGAAAAAGAAGAAG
GAGAAGAAGAAGGCCGAGGCCTAAGCTGACCATCAGCGTGATCCGTAGGAGTAGCAATCTTGACCAA

MARCKS domain

***dlg* (RE30311)**

Forward Primer:
5' CGTAGAATTCATGACAACGAGGAAAAAGAAGC 3'

Reverse Primer:
5' CGTGCTCGAGTCATAGAGATTCCTTGGAAGG 3'

Internal Sequencing Primers:
5' GCATCTATGTGACCAAGTTGATGG 3' +545
5' CAACAACACAATCAGCAACACC 3' +1002
5' AGAGGAGTACAATCGCTTCGAGG 3' +1701

ATGACAACGAGGAAAAAGAAGCGCGACGGCGGCGGCAGCGGCGGCGGATTCATCAAGAAAGTTTCGTCACT
CTTCAATCTGGATTCGGTGAATGGCGATGATAGCTGGTTATACGAGGACATTCAGCTGGAGCGCGGCAACT
CCGGATTGGGCTTTTCCATTGCCGGCGGTACGGATAATCCGCACATCGGCACCGACACCTCCATCTACATC
ACCAAGCTCATTTCCGGTGGAGCAGCTGCCGCCGATGGACGTCTGAGCATCAACGATATCATCGTATCGGT
GAACGATGTGTCCGTGGTGGATGTGCCACATGCCTCCGCCGTGGATGCCCTCAAGAAGGCGGGCAATGTTG
TTAAGCTGCATGTGAAGCGAAAACGTGGAACGGCCACCACCCCGGCAGCGGGATCGGCGGCAGGAGATGCT
CGGGATAGTGCGGCCAGCGGACCGAAGGTCATCGAAATCGATCTGGTCAAGGGCGGCAAGGGACTGGGCTT
CTCAATTGCCGGCGGCATTGGCAACCAGCACATCCCCGGCGACAATGGCATCTATGTGACCAAGTTGATGG
ACGGCGGAGCAGCGCAGGTGGACGGACGTCTCTCCATCGGAGATAAGCTGATTGCAGTGCGCACCAACGGG
AGCGAGAAGAACCTGGGGAACGTAACGCACGAACTGGCGGTGGCCACGTTGAAATCGATCACCGACAAGGT
GACGCTGATCATTGGAAAGACACAGCATCTGACCACCAGTGCGTCCGGCGGCGGAGGAGGAGGCCTTTCAT
CCGGACAACAATTGTCGCAGTCCCAATCGCAGTTGGCCACCAGCCAGAGCCAAAGTCAGGTGCATCAGCAG
CAGCATGCGACGCCGATGGTCAATTCGCAGTCGACAGGTGCGCTAAATAGTATGGGACAGACGGTTGTCGA
TTCACCATCAATACCACAAGCAGCCGCAGCAGTAGCAGCAGCAGCAAATGCATCTGCATCTGCATCAGTCA
TTGCAAGCAACAACACAATCAGCAACACCACAGTCACCACAGTCACGGCCACGGCCACAGCCAGCAACAGT
AGCAGCAAGTTGCCGCCGTCGCTTGGCGCTAACAGCAGCATTAGCATTAGCAATAGCAATAGCAATAGCAA
CAGCAATAATATCAACAACATTAATAGCATCAACAACAACAACAGTAGCAGCAGCAGCACGACGGCAACTG
TTGCAGCAGCAACACCAACAGCAGCATCAGCAGCAGCAGCAGCAGCATCATCTCCACCCGCCAACTCCTTC
TATAACAATGCTTCCATGCCCGCCCTGCCTGTCGAATCCAATCAAACAAACAACCGATCCCAATCACCCCA
GCCGCGCCAGCCCGGGTCGCGATACGCCTCTACAAATGTCCTAGCCGCCGTTCCACCAGGAACTCCACGCG
CTGTCAGCACCGAGGATATAACCAGAGAACCGCGCACCATCACCATCCAGAAGGGACCGCAGGGCCTGGGC
TTCAATATCGTTGGCGGCGAGGATGGCCAGGGTATCTATGTGTCCTTCATCCTGGCCGGCGGCCCAGCGGA
TCTCGGGTCGGAGTTGAAGCGTGGCGACCAGCTGCTCAGCGTGAACAATGTCAATCTCACGCACGCCACCC
ACGAAGAGGCAGCCCAGGCGCTCAAGACTTCTGGCGGTGTGGTGACCCTGTTGGCGCAGTACCGCCCAGAG
GAGTACAATCGCTTCGAGGCACGCATTCAAGAGTTGAAACAACAGGCTGCCCTCGGTGCCGGCGGATCGGG
AACGCTGCTGCGCACCACGCAAAAGCGATCGCTGTATGTGCGCGCCCTGTTTGACTACGATCCGAATCGGG
ATGATGGATTGCCCTCGCGAGGATTGCCCTTTAAGCACGGCGATATCCTGCACGTGACCAATGCCTCCGAC
GATGAATGGTGGCAGGCACGACGAGTTCTCGGCGACAACGAGGACGAGCAAATCGGTATTGTACCATCGAA
AAGGCGTTGGGAGCGCAAAATGCGAGCTAGGGACCGCAGCGTTAAGTTCCAGGGACATGCGGCAGCTAATA
ATAATCTGGATAAGCAATCGACATTGGATCGAAAGAAAAAGAATTTCACATTCTCGCGCAAATTTCCGTTT
ATGAAGAGTCGCGATGAGAAGAATGAAGATGGCAGCGACCAAGAGCCCAATGGAGTTGTGAGCAGCACCAG
CGAGATTGACATCAATAATGTCAACAACAACCAGTCAAATGAACCGCAACCCTTTATGCTTTGCTACACAC
AAGACGATGCCAATGCTGAAGGAGCTTCCGAGGAGAACGTGTTGTCCTACGAGGCCGTACAGCGTTTGTCC
ATCAACTACACGCGCCCGGTGATTATTCTGGGACCCCTGAAGGATCGCATCAACGATGACCTTATATCAGA
GTATCCCGACAAGTTCGGCTCTTGTGTGCCACACACCACCCGACCCAAGCGAGAGTACGAGGTGGATGGTA
GGGACTACCACTTTGTATCCTCTCGCGAGCAAATGGAACGGGATATTCAGAATCATCTGTTCATCGAGGCG
GGACAGTATAACGACAATCTGTACGGCACATCGGTGGCCAGCGTGCGCGAAGTGGCCGAGAAGGGTAAACA
CTGCATCCTGGACGTGTCCGGGAACGCCATCAAGCGACTCCAAGTTGCCCAGCTGTATCCCGTCGCCGTGT
TCATCAAGCCCAAGTCGGTGGATTCAGTGATGGAAATGAATCGTCGCATGACGGAGGAGCAGGCCAAGAAG
ACTTACGAGCGGGCGATTAAAATGGAGCAAGAATTCGGCGAATACTTTACGGGCGTTGTCCAAGGCGATAC

CATCGAGGAGATTTACAGCAAAGTGAAATCGATGATTTGGTCCCAGTCGGGACCAACCATTTGGGTACCTT
CCAAGGAATCTCTATGA

***scrib* (RE02389)**

Forward Primer:
5' CGTAGAATTCATGTTCAAGTGCATTCCCATCTTCAAGG 3'

Reverse Primer:
5' CGTAGCGGCCGCCTAATCACGGCGCAATGTTGCAATTTTCC 3'

Internal Sequencing Primers:
5' ATCACAATCAGCTGCAGC 3' +617
5' CCAGCAGGAATACCAGCC 3' +1254
5' TTACACAGAAGGGATACTCC 3' +1870
5' AGGATGGTAGTGTGTCCC 3' +2486
5' CGATTTGTGCGTTTGGTGTTGC 3' +3025
5' CGATTTGTGCGTTTGGTGTTGC 3' +3718

ATGTTCAAGTGCATTCCCATCTTCAAGGGCTGCAACCGGCAGGTGGAGTTCGTGGACAAGCGCCACTGCTC
CCTGCCGCAGGTGCCCGAGGAGATCCTGCGGTACTCCCGTACCCTGGAGGAGCTCTTCCTCGACGCCAACC
ACATCCGGGACTTGCCCAAGAATTTCTTCAGATTGCATCGCCTGAGAAAGCTGGGACTGAGTGACAATGAA
ATTGGCCGCCTGCCGCCGGATATACAAAACTTTGAAAATCTCGTTGAGCTCGACGTTTCACGCAATGATAT
ACCCGACATTCCCGACGATATCAAGCATCTGCAGAGCCTGCAGGTGGCTGATTTTAGTTCGAACCCGATAC
CCAAGTTGCCTTCGGGCTTCTCCCAGCTAAAGAACCTGACCGTCCTGGGACTCAACGACATGTCGCTCACC
ACATTGCCAGCGGATTTTGGCAGCCTGACTCAATTGGAATCCCTGGAGCTTCGCGAGAATCTGCTCAAGCA
TCTGCCCGAGACAATAAGCCAGCTGACGAAGCTGAAGCGTCTGGATCTGGGCGACAACGAGATCGAGGATC
TGCCACCCTATTTGGGTTATCTGCCGGGTCTGCACGAGCTTTGGTTGGATCACAATCAGCTGCAGCGATTG
CCGCCGGAGCTGGGACTCCTGACCAAACTGACCTACCTCGATGTCTCCGAAAATCGACTGGAGGAGCTGCC
CAACGAGATCAGCGGTCTGGTCAGCCTGACGGACCTCGATCTGGCCCAGAATCTACTCGAGGCACTGCCCG
ATGACATTGCCAAGCTGAGCAGACTGACTATCCTGAAGTTGGATCAGAATCGATTGCAGCGGTTGAACGAT
ACGCTAGGAAACTGCGAAAACATGCAGGAGCTGATTCTGACCGAGAACTTTCTCTCCGAGCTGCCCGCCTC
CATTGGCCAAATGATCAAGTTGAACAATCTGAACGTGGATCGCAATGCCCTGGAGTACCTGCCCCTGGAGA
TTGGCCAGTGTGCCAATCTGGGCGTGCTGAGTCTGCGGGACAACAAGCTGAAGAAGCTGCCGCCAGAGTTG
GGCAACTGCACCGTGCTGCATGTGCTCGATGTGAGCGGCAATCAGTTGCTGTATCTGCCCTACTCGCTGGT
CAATTTGCAGCTGAAGGCCGTCTGGCTGTCGGAGAATCAGTCGCAGCCGCTGCTCACCTTTCAACCGGACA
CGGATGCGGAAACGGGCGAACAGGTGTTGTCTTGCTATCTGCTGCCCCAGCAGGAATACCAGCCAATTACC
CCAGCCCGTGACCTGGAATCCGATTCTGAGCCGTTCGAGGAGCGCGAACCGTCGCGCACCGTGGTCAAGTT
CTCGGAGGAGGCCACCCAGGAGAAGGAGACGCCCTTCGTGCGCCAGAACACGCCGCATCCCAAGGATCTCA
AGGCCAAGGCGCAGAAGCTGAAGGTGGAGCGCAGTCGAAACGAGGAGCATGCCAATCTGGTCACCCTTCCG
GAGGAGAATGGCACCAAGTTAGCTGAGACCCCAACCGAGACCCGAACCATTGCAAACAATCACCAACAGCA
GCCACACCCAGTGCAGCAACCAATCGTTGGTGTAAATTCCAAGCAACCAGTGGTTGTGGGTGTAGTCACTC
CAACTACGACGACAGTCGCCCCAACCGGCGTACAGGGTGGCTCAGAGGGAGCCAGCTCCACGGCCAACAAT
GTAAAGGCAGCAACAGCAGCTGTGGTGGCTGAGTTAGCAGCCACTGTTGGTGGAAGTGATGAGGTCCAGGA
TGATGACGAGCAGGAGGATGAGTTTGAATCCGATCGCCGCGTGGGCTTTCAAGTGGAGGGCGAAGATGATG
ACTTTTACAAGAGGCCACCCAAATTACACAGAAGGGATACTCCGCATCACCTGAAGAATAAGCGTGTCCAG
CATTTAACCGACAAGCAGGCCAGTGAAATCTTGGCAAATGCCCTAGCCTCACAGGAGCGGAACGATACCAC
ACCGCAGCACTCGCTTTCCGGCAAAGTGACATCACCAATTGAGGAGGAGGAGCAGCTGGAGGTGGAACAGG
AGCAGCAACAGCAACAGCAGCAGCATCCCTTCGACTCCTCGCTCTCGCCCATTTCGGCTGGCAAAACAGCA
GAGGCTAGCACCGACCCAGACAACTTGGATGGCGTTACGGAGCTGCGTTTGGAGCAGTACGAAATCCACAT
CGAGCGCACTGCAGCCGGATTGGGTCTGAGTATTGCCGGTGGCAAGGGCTCAACACCCTTTAAGGGTGACG
ATGATGGCATCTTCATATCAAGGGTCACCGAGGCGGGACCCGCTGATCTGGCTGGTCTTAAAGTGGGCGAC
AAAGTTATCAAAGTCAACGGCATTGTTGTCGTGGATGCGGATCACTACCAGGCGGTGCAGGTGTTAAAAGC
CTGCGGTGCCGTACTTGTTTTGGTGGTACAGCGTGAGGTGACTCGCCTGATTGGCCACCCCGTGTTTAGCG
AGGATGGTAGTGTGTCCCAAATCTCGGTCGAGACGCGACCACTGGTGGCGGATGCCCCTCCAGCTGCATCC
ATTAGCCACGAGCGTTACATCCCGGCACCCATTGAAATTGTGCCCCAACAGCAGCATCTACAGCAACAGCA

ACAGCAGCCCATTCAGCAGGTGGCCCCAACGCATAGCTATTCGGGCAACGTGTTTGCCACACCCACTGCCG
CACAAACGGTGCAGCCTGCTGTGTCTGCTGCGCCCAATGGATTGCTACTGAATGGCAGGGAGGCGCCACTG
AGCTACATCCAGCTGCACACAACGCTCATCCGCGATCAGATTGGCCAAGGACTGGGCTTCAGCATTGCGGG
CGGAAAGGGGTCGCCGCCGTTCAAGGACGACTGCGATGGCATTTTCATATCCCGCATCACGGAGGGCGGAC
TAGCGTACCGCGATGGGAAAATTATGGTGGGCGACCGGGTGATGGCGATTAACGGCAACGATATGACTGAA
GCCCATCATGACGCAGCCGTCGCCTGTTTGACTGAACCGCAGCGATTTGTGCGTTTGGTGTTGCAGCGCGA
GTACAGAGGTCCACTGGAACCACCGACGAGTCCGCGAAGTCCGGCAGTGCTCAACTCTTTGAGCCCCTCTG
GATATTTGGCCAACCGACCAGCTAATTTCAGTCGATCGGTGGTGGAAGTTGAGCAGCCGTACAAGTACAAC
ACCCTGGCTACGACCACGCCCACACCGAAGCCCACTGTGCCAGCTAGTATTAGCAACAATAATAACACTCT
GCCCAGCAGCAAAACCAATGGATTTGCCACTGCTGCTGCTGCCACGATAGACAGTTCCACGGGTCAACCGG
TGCCCGCTCCCCGTCGTACCAACTCTGTTCCAATGGGAGATGGAGACATTGGGGCGGGTTCCACCACCAGT
GGGGATTCTGGCGAGGCACAGGAGGTTGTGCTGCCCAAGAACCAGGGCTCCCTGGGATTCAGCATCATCGG
CGGCACGGATCATTCCTGTGTGCCCTTCGGCACTCGAGAGCCTGGCATATTCATATCGCACATTGTGCCCG
GCGGGATTGCCTCCAAGTGCGGCAAGCTGCGCATGGGCGATCGCATATTGAAAGTCAACGAGGCGGATGTT
TCCAAGGCCACACATCAGGATGCGGTTCTGGAGCTGTTGAAGCCAGGTGATGAAATTAAGCTGACCATTCA
ACACGACCCATTGCCGCCAGGATTTCAGGAAGTGCTACTCAGCAAGGCGGAGGGCGAACGTTTGGGCATGC
ACATCAAGGGCGGCTTGAATGGCCAGCGTGGTAATCCCGCCGATCCCTCCGACGAAGGCGTCTTCGTGTCC
AAAATTAACTCGGTCGGTGCGGCCAGACGGGACGGAAGGCTTAAGGTGGGCATGCGTCTGCTCGAGGTTAA
TGGACACTCGCTGCTGGGCGCCTCGCACCAGGATGCGGTCAATGTGCTGCGCAACGCTGGGAACGAGATTC
AATTGGTCGTCTGCAAAGGCTACGACAAGTCCAATTTAATTCATTCCATTGGCCAGGCCGGCGGCATGAGC
ACTGGCTTCAACTCGTCTGCATCCTGCAGCGGTGGCAGTCGCCAAGGCTCGCGTGCATCGGAAACGGGCTC
GGAACTGAGCCAGAGTCAGAGTGTATCCAGCTTGGACCACGAAGAGGATGAGCGTCTGCGACAGGACTTCG
ATGTCTTTGCCTCGCAGAAGCCAGATGCACAACAGCCAACTGGCCCATCTGTCCTGGCAGCTGCTGCTGCC
ATGGTGCATGGCGCCTCGTCGCCCACACCACCTGCTGCCACCTCCAATATAACTCCCTTACCCACAGCCGC
GGCAGTAGCATCTGCTGATTTAACAGCACCGGACACGCCAGCAACCCAGACCGTGGCGCTCATTCACGCAG
AACAGCAGGCCCATCAACAACAACAGCAGACGCAGCTGGCGCCTTTGGGTCAGGAGAAGAGTACCCAGGAG
AAGGTGCTGGAAATCGTACGCGCGGCTGATGCCTTCACCACCGTGCCACCAAAGTCGCCATCGGAACACCA
CGAGCAGGATAAGATACAGAAGACGACGACGGTTGTCATATCGAAGCATACGCTCGACACGAACCCAACCA
CCCCCACAACGCCGGCGGCGCCTCTTTCCATCGCTGGAGCAGAGTCAGCGAACTCGGCTGGTGCTCCTTCT
CCAGCTGTTCCTGCATCCACGCCCGGCTCAGCGCCAGTTCTTCCTGCCGTGGCCGTGCAGACACAGACGCA
AACGACCTCCACGGAGAAGGATGAAGAGGAGGAGTCGCAACTACAGTCAACACCTGCCAGCAGGGATGGAG
CAGAGGAGCAGCAGGAAGAGGTTAGAGCCAAACCCACTCCGACTAAAGTGCCTAAATCGGTTTCCGATAAA
AAACGCTTCTTTGAGTCAGCCATGGAGGATCAACACAAGCCCACACAAAAGACAGACAAAGTTTTCTCATT
CCTGTCAAAGGATGAAGTGGAAAAGCTGCGACAGGAGGAGGAGAGGAAAATTGCAACATTGCGCCGTGATA
AGAATTCCAGATTACTGGATGCCGCCAACGACAACATTGACAAGGATGCCGCACAGCAGCGGACCAAGAGC
AACAGCAACAGCAGCAGCGGCGACGATAATGACGACAGCGACCAAGAGGAGGGCATCGCTCGCGGGGATTC
CGTTGACAACGCCGCTCTGGGGCATTTCGATGATGCGGAGGACATGAGGAATCCACTCGATGAAATTGAAG
CAGTATTTAGAAGTTAA

***lgl* (LD06034)**

Forward Primer:
5' CGTAGAATTCATGACAACGAGGAAAAAGAAGC 3'

Reverse Primer:
5' CGTGCTCGAGTCATAGAGATTCCTTGGAAGG 3'

Internal Sequencing Primers:
5' CCTGGTGCAATTGAGTCAATCC 3' +550
5' GTACTACTTGAAGAGGAACTCTGC 3' +1039
5' ACAACTTATTGTTGGTGGCACAGC 3' +1566
5' TAGAGGCTCGTTGTGCAGATGACG 3' +2084

ATGTTAAAGTTTATCAGAGGAAAAGGGCAGCAGCCCAGTGCTGACAGACACCGCCTACAGAAGGACCTTTT
TGCTTATCGTAAGACGGCACAGCATGGCTTTCCTCATAAGCCTTCGGCTCTTGCGTATGATCCAGTTTTGA
AACTTATGGCAATAGGGACGCAAACAGGGGCTTTAAAAGTTTTCGGTCAACCCGGAGTTGAATTGTACGGT
CAGCATACTTTGTTAAACAATTCAGCATCGGAGCTTAATGTACAATTACTTGAATGGGTGTATGGAACTGG
TCGCATACTTTCGTTGACGGCAGCGAATCAATTAATTCTATGGGAGCCAGTTGGAGCAACGTTGCTGCCAA
TCAAAACACTACCGTTTGACGGCAAACTTAAAAAAGTTTCATCGCTGTGCTGTTCTCTCAGTAAGGATCTG
CTATGGATTGGAACAGAAGGTGGAAACATCTATCAACTGGATTTACATACATTTACCATTAAGGAGCCTGT
AATTTACCATGACGTTGTGCTAGAGCAGGTGCCACCAGCCTACAAGCTAAATCCTGGTGCAATTGAGTCAA
TCCGCCAACTTCCAAACTCCCCTAGCAAACTTCTAGTTGCATACAATCGCGGCCTTTGTGTTTTGTGGGAT
TTTGAAAGCGCATCTGTCCAGCGAGCATACATAGCCCCTGGACATGGACAGAGCGTTGGTCTTACAGTGAA
CTTCGAAGGATCTGAATTTACCTGGTACCACGCTGATGGTTCATACGCCACTTGGAGCATAGATAACCCAG
AACCGCCGTCGAATGTTAATTATGTGCCTTATGGACCTGATCCATGCAAAAGCATAAATCGACTGTACAAA
GGCAAGCGAAGATCCAACGATGTAATTGTTTTTTCCGGCGGCATGCCACGGTCAGCATATGGTGATCACAA
TTGTGTGTCCGTTCACGCCAGCGATGGACACAAAGTGTGTCTTGACTTTACGTCTAAAGTGATTGACTTTT
TTGTGACCTTTGAAAATAATAGAGATGTCGCTGAAGTTCTTGTTGTACTACTTGAAGAGGAACTCTGCGCT
TACGATCTTACTGACCCTAATATTTGTGCTATCAAAGCGCCATATCTTCACTCTGTCCATGCATCAGCTGT
CACTTGCAATTACCTTGCTTCTGAAGTCGTACAGTCGGTATATGAAAGTATTTTAAGAGCTGGAGATGAAC
AAGACATTGACTATAGCAATATTAGCTGGCCTATCACTGGCGGTACTCTCCCGGATAACTTAGAAGAATCT
GTAGAAGAGGACGCGACTAAGCTTTATGAGATTTTGTTAACTGGTCACGAAGATGGTTCTGTTAAATTTTG
GGACTGCACTGGAGTGTTGCTTAAACCAATTTATAATTTTAAAACTAGCAGCATTTTTGGAAGTGAGTCAG
ACTTCCGAGATGACGCAGCTGCAGATATGAGTGCGGAACAAGTCGATGAAGGAGAACCGCCATTTCGGAAA
TCAGGACTTTTTGATCCTTATTCAGATGACCCTCGTTTAGCAGTGAAGAAAATAGCATTCTGCCCAAAAAC
CGGACAACTTATTGTTGGTGGCACAGCGGGCCAAATAGTTATAGCCGACTTCATAGACTTACCCGAAAAAG
TGTCTTTAAAATACATTTCAATGAATTTGGTCAGCGATCGTGATGGATTTGTGTGGAAGGGTCACGATCAG
TTAAACGTGCGATCGAACTTATTAGACGGAGAAGCAATTCCTACGACGGAACGTGGTGTAAATATATCGGG
AGTACTGCAAGTTTTGCCGCCAGCCAGCATAACATGCATGGCACTCGAAGCAAGCTGGGGCCTAGTATCTG
GTGGGACTGCGCACGGCTTAGTTCTCTTTGACTTCAAAAACTTTGTTCCAGTATTTCATCGCTGCACTTTA
AACCCAAATGATCTTACTGGAGCAGGAGAGCAGCTGTCTCGTCGAAAGTCTTTTAAGAAATCATTGAGGGA
GTCATTTAGAAAGCTTCGCAAGGGTCGATCGACCAGGACCAACCAGAGCAATCAAGTACCAACAACGCTGG
AAGCAAGACCCGTCGAGAGGCAAATAGAGGCTCGTTGTGCAGATGACGGGCTAGGATCCATGGTGCGATGT
TTACTATTTGCCAAAACTTATGTTACTAATGTCAACATAACGTCGCCAACTTTGTGGTCAGCAACAAATGC
CAGTACAGTCTCGGTTTTCCTTCTGCATTTGCCACCAGCGCAGACCGCGGCAACTGCCGTCCCGTCGGCAA
GTGGCAATGCACCACCACACATGCCCCGCCGAATTTCTGCGCAGCTTGCTAAAGAAATACAATTAAAACAT
CGTGCTCCTGTGGTGGGTATTTCTATTTTTGATCAGGCGGGTAGCCCTGTCGATCAGCTGAACGCCGGTGA
AAACGGGAGTCCACCGCATCGTGTACTTATTGCTTCCGAGGAACAGTTCAAGGTGTTTTCACTTCCGCAAC
TAAAGCCGATTAACAAATATAAGCTTACCGCTAACGAAGGTGCTCGGATTCGCCGCATCCATTTTGGTTCG
TTTAGTTGTCGCATATCCCCGGAAACACTGCAGAGTATGCACGGTTGTAGCCCAACTAAGTCCACGCGTTC
ACATGGCGATGGAGAGGCGGATCCTAATATCAGTGGAAGCTTGGCTGTAAGTCGTGGAGATGTATATAACG
AAACAGCATTGATATGTTTAACGAATATGGGCGATATCATGGTTTTATCAGTACCTGAATTAAAAAGACAG
CTGAATGCCGCAGCAGTGCGACGGGAAGACATTAATGGAGTTTCGTCACTTTGCTTTACAAACTCTGGAGA

AGCACTGTATATGATGTCTTCTTCTGAACTGCAGCGTATTGCTTTAGCCACGTCCAGAGTCGTGCAACCCA
CTGGCGTTGTTCCAGTAGAACCATTAGAAAATGAAGAGTCTGTGTTGGAAGAAAATGATGCAGAGAATAAT
AAGGAAACCTACGCATGTGATGAAGTTGTGAATACATATGAAATTAAAAATCCATCAGGCATTTCAATATG
CACAAGGCCTGCAGAGGAAAACGTTGGAAGAAATAGTGTTCAGCAAGTTAATGGAGTCAACATTTCAAATT
CACCTAATCAAGCTAACGAGACTATCAGCAGCTCTATTGGCGATATTACCGTTGACTCGGTGCGCGACCAT
TTAAATATGACGACCACCACTTTGTGTTCTATTAATACAGAGGAAACCATTGGTCGCCTATCTGTACTTAG
CACGCAAACCAACAAAGCCAGTACTACCGTAAACATGAGTGAAATTCCAAATATTAATATTTCTAATTTAG
AGGACTTGGAATCGAAAAGAAATACGACGGAAACGAGTACTAGTTCTGTTGTAATTAAATCTATAATTACA
AACATTTCTCATGAAAAAACGAACGGAGACAACAAAATAGGAACGCCAAAAACAGCGCCTGAAGAAAGCCA
ATTTTAA